VRIJE UNIVERSITEIT

Search for a Strange Phase in Beautiful Oscillations

ACADEMISCH PROEFSCHRIFT

ter verkrijging van de graad Doctor aan
de Vrije Universiteit Amsterdam,
op gezag van de rector magnificus
prof.dr. L.M. Bouter,
in het openbaar te verdedigen
ten overstaan van de promotiecommissie
van de faculteit der Exacte Wetenschappen
op vrijdag 22 oktober 2010 om 11.45 uur
in de aula van de universiteit,
De Boelelaan 1105

door

Tristan Arnoldus du Pree

geboren te Rotterdam

Summary, conclusions, and outlook

To explain the observed matter abundance in the universe, violation of the CP symmetry is required. Violation of this symmetry is incorporated in the standard model of particle physics in the weak interactions, but the amount of CP violation predicted in the standard model is by far too small to explain the size of the matter dominance. Therefore, to explain the observed matter abundance, sources of CP violation beyond the Standard Model are required. One of the goals of B physics is to search for new sources of CP violation, thereby probing models of new physics.

The source of CP-violating processes in the standard model is the irreducible complex coupling in the CKM matrix. Since this phase is opposite for particle and anti-particle decays, their decay rates can differ when this phase contributes to the sum of interfering decay amplitudes. CP asymmetries can be measured by comparing the time dependent decay rates for particle decays and anti-particle decays. This makes it possible to test the complex phases present in the CKM matrix.

The consistency of the different measurements of CP-violating processes can be checked by using the unitarity triangles, of which one angle is $\beta_s = \arg(-V_{cs}^* V_{cb} / V_{ts}^* V_{tb})$. This CP-violating phase is accessible in B_s decays for which both $B_s - \bar{B}_s$ mixing transitions and $b \to \bar{c}cs$ transitions contribute to the total decay amplitude. The small value of the amplitude of the time-dependent CP violation predicted in the standard model, related to $\phi_s = -2\beta_s = -0.04$ rad, can be changed due to contributions of off-shell particles, opening the possibility of finding contributions of heavy particles beyond the standard model.

The decay which offers the best sensitivity to this phase is the $B_s^0 \to J/\psi\phi$ decay. Since this is a decay of a pseudo scalar particle into two vector mesons, the final state is a superposition of states with different angular momentum, and hence of different CP eigenstates. Hence, an angular analysis is required to disentangle the different polarizations. To determine ϕ_s also the flavor of the B_s meson at production needs to be estimated. To suppress background the invariant mass of the final state particles needs to be determined.

An experiment designed to perform a measurement of this CP asymmetry is the LHCb experiment. The LHCb detector is located at the LHC accelerator, where B_s mesons will be produced copiously. The design of the tracking system leads to a proper time resolution of 40 fs, an angular resolution of $20 - 30$ mrad, and a B_s mass resolution of 16 MeV. Using the capabilities to perform particle identification, backgrounds can be suppressed, and a tagging power of 6.2% can be reached.

To reduce the rate of selected events to an acceptable level, the sample of selected events is divided in two samples: a sample of detached events and a sample of prescaled events. The sample of detached events is selected using an online lifetime cut, hereby suppressing background; the sample of prescaled events is selected by applying a prescale factor to

the trigger selection and is used as a control sample. The small set of additional selection criteria is optimized by maximizing a figure of merit $FOM = S/\sqrt{S+\alpha B}$, iteratively adjusting a set of rectangular cuts and estimating $\sigma(\phi_s) \propto \sqrt{S+\alpha B}/S$. When the trigger rate becomes critical, it can be lowered by adjusting the prescale fraction and the lifetime cut in the trigger selection, leaving the other selection criteria untouched.

To perform a measurement of the phase ϕ_s, a multi-dimensional simultaneous fit needs to be performed to the event distributions in the different observables: the proper time, the angular, the tagging and the invariant mass observables. In this thesis methods have been introduced to take into account the inefficiencies, resolutions, and backgrounds introduced by the selection method, the reconstruction algorithms, and the detector acceptance to the distributions in all observables. For the correction of the angular efficiency the usage of an MC sample is proposed, whereas for the other methods control samples are used. For all methods the $B^0_d \to J/\psi K^*$ decay is foreseen to serve as a control channel on which the methods can be validated first.

All methods have been shown to correct for biases in the estimates of the physics parameters on samples of fully simulated MC events. Using the expected experimental effects, resulting from full MC simulations, an estimate has been made of the expected precision of the measurement of the CP-violating phase ϕ_s. For 2.0 fb^{-1} the expected measurement precision is $\sigma(\phi_s) = 24 \pm 1$ mrad.

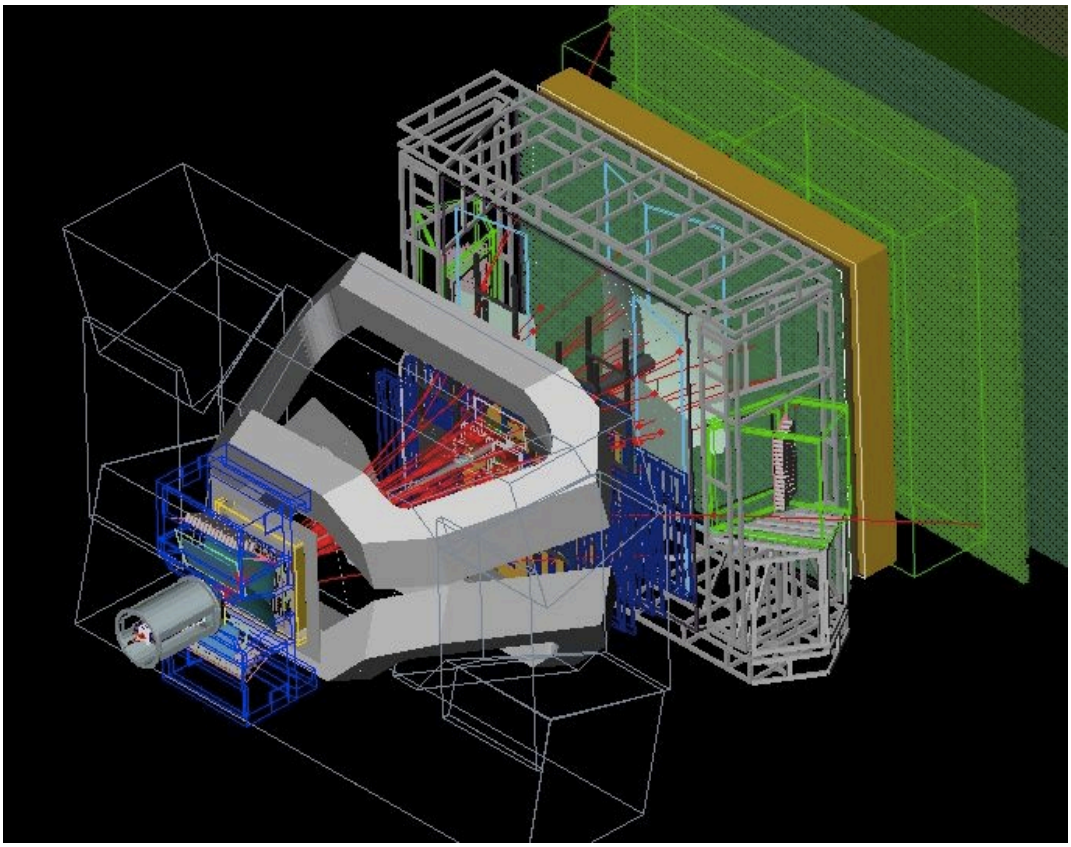

Figure 1: *Display of an event containing a $B^0_s \to J/\psi\phi$ candidate, as reconstructed by the LHCb detector.*

Current status

At the time of writing the first 600 nb^{-1} of data has been recorded at the LHCb experiment. For the decay channels $B^+ \to J/\psi K^+$, $B_d^0 \to J/\psi K^*$, and $B_s^0 \to J/\psi\phi$ candidates have been reconstructed, making it possible to test the predictions based on MC. An example of a $B_s^0 \to J/\psi\phi$ candidate is shown in figure 1.

In figure 2 the proper time and invariant mass of distributions of $B^+ \to J/\psi K^+$ candidates are shown. An abundance of long-living candidates can be seen in the signal region, hinting to reconstructed signal events. A significant invariant mass peak, with a fitted width of $\sigma_m = 23 \pm 2$ MeV/c^2, appears for long-living candidates around the B^+ invariant mass, containing an estimated number of signal events of $N_{\text{sig}} = 198 \pm 16$. As expected, the lifetime of the candidates in the signal region is larger than the lifetime of the candidates in the sidebands. The average proper time resolution is $\langle\sigma_t\rangle = 0.075$ ps.

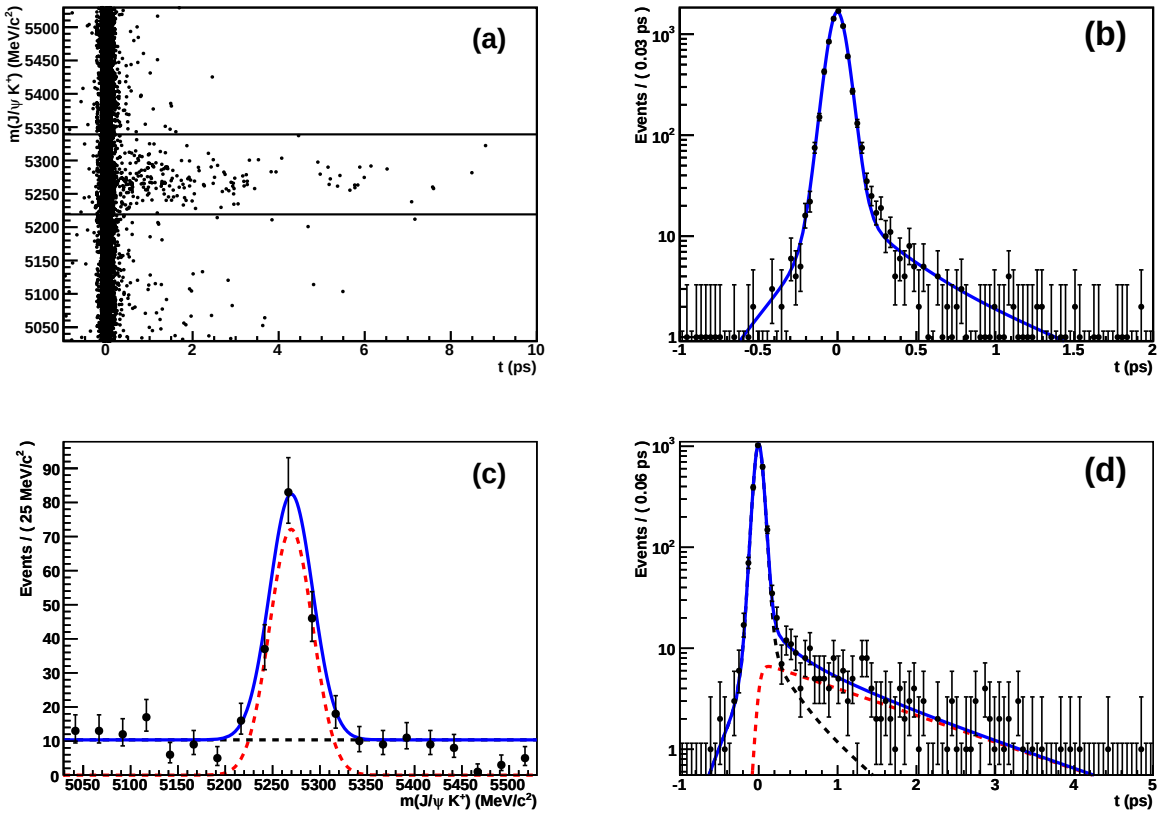

Figure 2: *Invariant mass and proper time distributions of $B^\pm \to J/\psi K^\pm$ candidates, indicating the signal region $|m(J/\psi K^+) - m(B^+)| < 60 MeV/c$ (a). Different projections of the data are shown, with a fit overlaid: the proper time distribution of the candidates outside the signal region (b), the proper time distribution of the candidates inside the signal region (d), and the invariant mass distribution for $t > 0.25$ ps (c).*

In figure 3 the proper time and invariant mass of distributions of $B_s^0 \to J/\psi\phi$ candidates

are shown, using the selection as described in this thesis. An abundance of long-living candidates can be seen in the signal region, hinting to reconstructed signal events. A significant invariant mass peak, with a fitted width of $\sigma_m = 37 \pm 9$ MeV/c^2 appears for long-living candidates around the B_s invariant mass, containing an estimated number of signal events of $N_{\text{sig}} = 23 \pm 5$. As expected, the lifetime of the candidates in the signal region is larger than the lifetime of the candidates in the sidebands. The average proper time resolution is $\langle \sigma_t \rangle = 0.074$ ps.

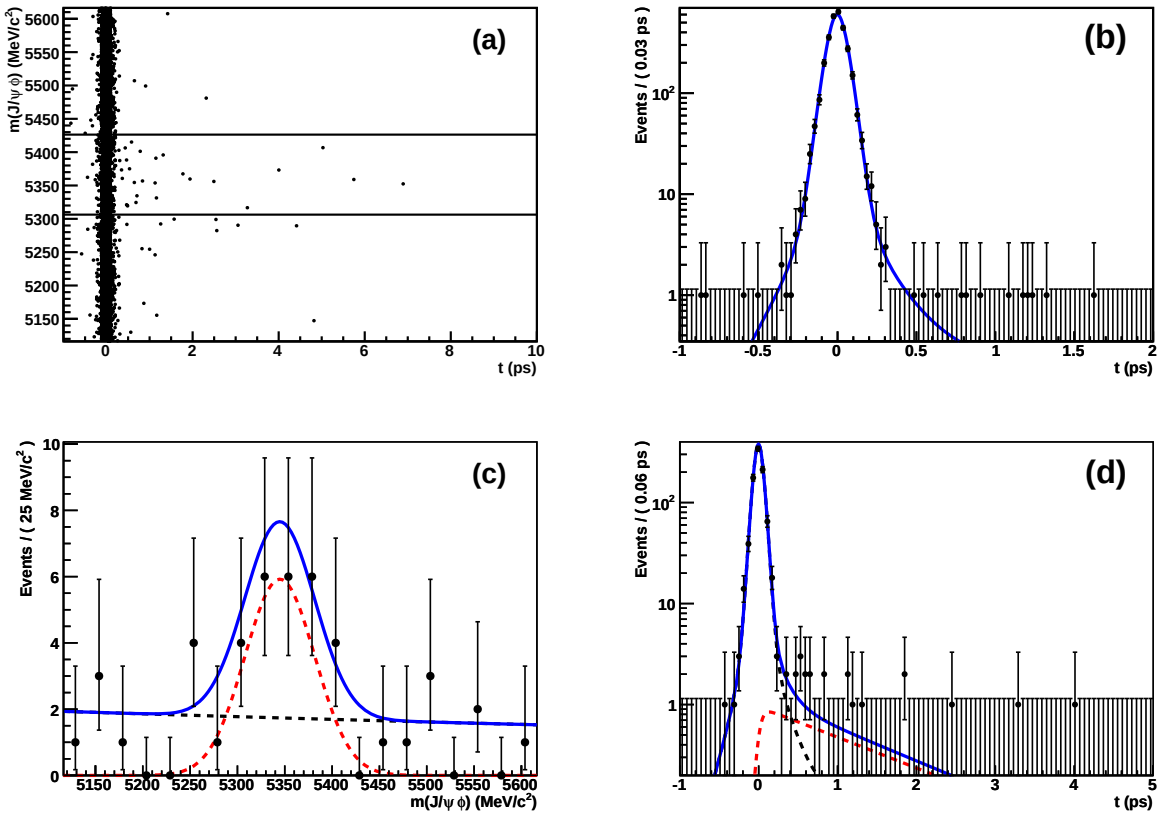

Figure 3: *Distributions of $B_s^0 \to J/\psi\phi$ candidates in the invariant mass and proper time observables, indicating the signal region $|m(J/\psi\phi) - m(B_s)| < 60 MeV/c$ (a). Different projections of the data are shown, with a fit overlaid: the proper time distribution of the candidates outside the signal region (b), the proper time distribution of the candidates inside the signal region (d), and the invariant mass distribution for $t > 0.25$ ps (c).*

From these distributions the following observations can be made. The proper time resolution, which is expected to be $\langle \sigma_t \rangle = 39$ fs based on MC simulations, is found to be a factor 1.9 larger. Since the sensitivity to the CP asymmetry scales as $e^{(\Delta m_s \times \sigma_t)^2/2}$, a maximal worsening of the sensitivity to ϕ_s of a factor two is expected. The mass resolution is, within statistical uncertainties, as large as expected from MC.

To calculate the expected signal yield, a $b\bar{b}$ cross section $\sigma_{b\bar{b}} = (292 \pm 15 \pm 43)\mu b$ at 7 TeV [61] is used and a relative uncertainty of the luminosity of 16% [62] is assumed. In that

case the number of signal events, using the selection described in this thesis, is expected to be 30 ± 7, which is in agreement with the found number of events. Furthermore, the number of events is too small to estimate the tagging performance or determine the polarization amplitudes from the angular distributions.

Hence, given the current situation it can be concluded that there are no limiting factors for the LHCb experiment to proceed to perform a measurement of ϕ_s.

Outlook

At the time of writing, the amount of statistics is too small to apply all analysis methods described in this thesis. When more data is taken, the methods are foreseen to be applied as follows.

The optimization procedure can be repeated using real data. Using pre-selected candidates, the figure of merit can be optimized, possibly adjusting the optimal selection criteria described in this thesis, in order to acquire maximal sensitivity to ϕ_s. As soon as the trigger rate becomes critical, it can be lowered by adjusting the prescale fraction and the lifetime cut in the trigger selection, leaving the other selection criteria untouched.

To test the fit methods described in this thesis, the $B_d^0 \to J/\psi K^*$ decay is foreseen as the control channel on which the methods can be validated. The methods to include inefficiencies, resolutions, and backgrounds in the angular and proper time resolutions can be checked on such a sample first, performing a measurement of mixing and the polarization amplitudes in this channel. When the physics parameters found for this channel are in agreement with the values estimated by the B factories, the same methods can be applied on the $B_s^0 \to J/\psi\phi$ channel, and the mistag fraction can be calibrated using the $B_d^0 \to J/\psi K^*$ channel.

Using the online and offline selection and the fit methods described in this thesis, the performance is expected to be as follows. After 0.1 fb^{-1} of luminosity (at a center of mass energy of 7 TeV), the amount of integrated luminosity expected at the end of 2010, the precision of LHCb should surpass that of the Tevatron for a total luminosity of 18 fb^{-1}, as expected at the end of run 2. After 1.0 fb^{-1} of luminosity, the amount of integrated luminosity expected before the shutdown of 2012, the sensitivity is 48 mrad. After 10 fb^{-1} (at a center of mass energy of 14 TeV) the statistical precision is expected to be 8 mrad, which means that for the SM value of the CP-violating phase, zero CP violation can be excluded at 5σ.

In case the estimated value appears to be different from the SM expected value, the measurement allows not only to discover new particles contributing to the amplitude of the decay processes, but also to determine both the magnitude and phase of the couplings of these new particles.

Searching for the Top

observation of the heaviest elementary particle at the LHC

ACADEMISCH PROEFSCHRIFT

ter verkrijging van de graad van doctor
aan de Universiteit van Amsterdam
op gezag van de Rector Magnificus
prof. dr. D.C. van den Boom
ten overstaan van een door het college van promoties ingestelde
commissie, in het openbaar te verdedigen in de Agnietenkapel
op donderdag 7 juli 2011, te 12:00 uur

door

Alexander Dimos Doxiadis

geboren te München, Duitsland

SUMMARY

By analyzing the collisions at the Large Hadron Collider (LHC) thousands of particle physicists are trying to verify, understand and expand the Standard Model of particle physics. The Standard Model is the model that describes all matter particles and their interactions and governs three out of the four fundamental forces of nature. In this thesis we focussed on the top-quark. The top-quark, which is by far the heaviest of all quarks, has been observed for the first time in 1995 at the Tevatron collider near Chicago, USA. Its production rate, that is how often a top-quark is produced per collision, is known theoretically with great precision (uncertainties of less than 10%). Nevertheless it is one of the most interesting measurements at the LHC that can be performed with early data with the ATLAS detector. The reason for this is threefold: 1. The complex decay of the top-quark makes it a challenging particle to observe experimentally. 2. The measurement of the production rate of the top-quark is a test of the Standard Model. 3. The top-quark plays a special role in many extensions of the Standard Model and observation might provide a first glimpse at beyond Standard Model processes.

Testing the detector

The measurement of the top-quark production rate is an ideal test for the performance of the ATLAS detector. The top-quark is produced in pairs of top and antitop-quarks ($t\bar{t}$) in proton-proton collisions at the LHC. The decay of a pair of top-quarks is characterized in our analysis by three main objects: a muon (the heavier cousin of the electron) with high momentum, four or more regions of high energy depositions in the detector (called jets) and a large amount of 'missing transverse energy'. The latter is found by balancing the measured energy in the detector in all directions and labeling the unbalanced energy 'missing transverse energy'. This missing transverse energy in top-quark pair decays is accounted for by the escaping neutrino, which leaves no trace in the detector. In order to measure the top-quark decay all detector components have to be well understood and calibrated. It is in fact quite amazing that the ATLAS detector has identified and measured the top-quark within the first year of data-taking.

Standard Model predictions

Apart from testing the detector performance, measuring the top-quark pair production rate is also a test of the Standard Model itself. With the LHC we entered a higher energy regime (colliding at a center of mass energy of 7 TeV) and although the top-quark production is well understood, the theory has still to be confirmed at this higher energy. In particle physics the production rate is usually given as a cross section. In Figure 1 we show the measured and predicted production cross section (σ) of top-quarks at different energies. The black points are the measurements performed at the Tevatron at lower energy and the lighter point is the measurement performed in this thesis at 7 TeV. We can see that the experimental data and the theoretical prediction are in great agreement, confirming our Standard Model expectations.

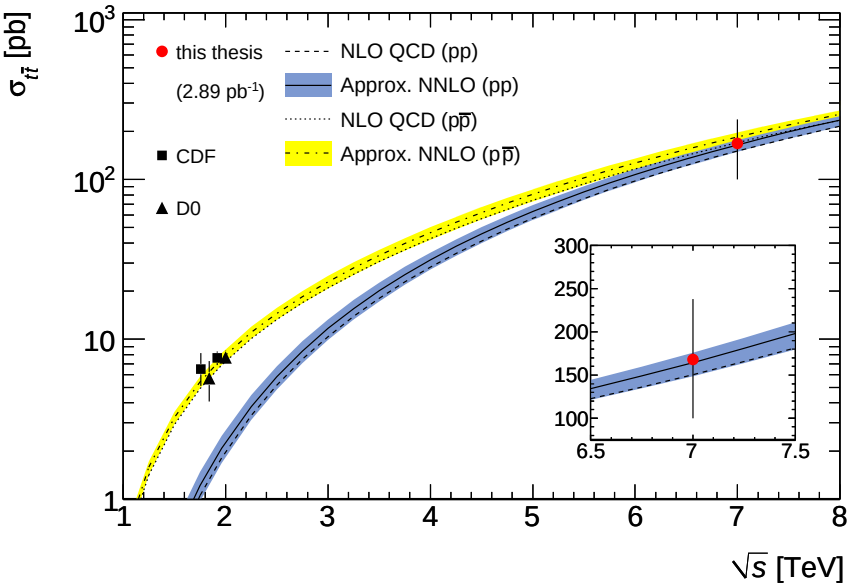

Figure 1: *The measured $t\bar{t}$ production cross section from the CDF and DØ experiments at 1.8 (1.96) TeV and the result presented in this thesis at 7 TeV as a function of the energy ($\sqrt{s}$) compared to the theoretical prediction.*

Extensions of the model

More importantly however and much more tantalizing is the possibility that there is more beyond the horizon than the Standard Model. Many models have been proposed over the years that all try to explain caveats in the existing model that would show up when reaching higher energies. The top-quark plays a special role in many of these models through its large mass and large coupling to the Higgs-field. Any new physics would reveal itself in the top-channel. A measurement of the top-quark production is

essentially a model independent way of searching for new physics. At the moment there is unfortunately not enough data to draw any conclusions about new physics.

Selecting the right events

In order to perform measurement of the production rate, we need to understand the possible background events in the analysis. A background event is an event that is falsely selected as a top-quark event. We have shown that although many different event types are backgrounds to our analysis, there is one kind that is more troublesome than the others: multi-jet events. Most other event types are well understood, but these events can only be simulated with large uncertainties which means that we cannot trust the simulation to tell us how many of these events pass our selection and are thus wrongfully identified as top-quark events. These multi-jet events do not produce any muons directly. Since we select events with a high energetic muons, these events should a priori not pass our requirements. A large fraction of this thesis is therefore dedicated to the study of how these events produce extra muons indirectly and to the analysis of the muon properties. Since we cannot trust our simulation to model the amount of background from these events, we have developed a way of determining the normalization directly from data. We use the knowledge that was gained by studying the properties of these events and exploit finally that they predominantly come from the decay of bottom-quarks. The bottom-quark is the lighter sister of the top-quark and forms bound states (an intermediate clustering with other quarks) that travel on average a few millimeter before they decay. By measuring the distance from where a muon is produced to the primary point of interaction, the muons from top-quark decays (the signal) can be distinguished from the muons from bottom-quark decay (the background). This difference is then the basis to determine the number of multi-jet events that passed all our requirements.

Results

In the final analysis of the first data 19 top-quark pair event candidates have been identified. Of these 19 events we estimated 0.9 ± 0.7 to come from multi-jet background. Although the background seems extremely small, it is important to the measurement to have a solid estimate with well determined error. The $t\bar{t}$ production cross section (as a measure of the production rate) that we extracted from these numbers is $\sigma(t\bar{t}) = 168 \pm 55$ (stat) pb which is in beautiful agreement with the theoretical prediction, see again Figure 1. Note that the total cross section in proton-proton collisions at this center of mass energy is $\sim 10^{10}$ pb. Since the amount of events in the analysis is so low, we cannot rule out new physics models yet, but we can confirm the existence of the Standard Model top-quark. We have also shown that we can deduce the number of background events from data alone (albeit with large uncertainty). Fortunately more data is coming rapidly now and more data means a more precise measurement of the background and hence a more precise measurement of the top-quark production rate. With the full dataset recorded up to now the uncertainties are already of the same order

as the theoretical error. This now means that the era of top-quark physics at the LHC has just begun...

VRIJE UNIVERSITEIT

The Geodesic Deviation Method and Extreme Mass-Ratio Systems

Theoretical methods and application to the calculation of gravitational waves

ACADEMISCH PROEFSCHRIFT

ter verkrijging van de graad Doctor aan
de Vrije Universiteit Amsterdam,
op gezag van de rector magnificus
prof.dr. L.M. Bouter,
in het openbaar te verdedigen
ten overstaan van de promotiecommissie
van de faculteit der Exacte Wetenschappen
op donderdag 15 december 2011 om 09.45 uur
in de aula van de universiteit,
De Boelelaan 1105

door

Gideon Koekoek

geboren te Amsterdam

Summary

This is a thesis about gravity, and a number of the interesting effects it has on the motion of stars when they get in close proximity to each other. Describing such motions turns out to be a complicated problem, and this at first seems to be a remarkable statement. After all, gravity is a force that we human beings are very familiar with from every day experience. It is the force that keeps us with our feet on the ground, makes apples fall from trees, traps the Moon in an orbit around the Earth, and the Earth itself in an orbit around the Sun. The fact that research in gravity is nonetheless challenging, is due to the fact that gravity is conceptually very different from the three other fundamental forces that are known in physics (the electromagnetic force, the strong nuclear force, and the weak nuclear force), which reflects itself in the radically different mathematics involved. It is for this reason that it required the genius of two of the greatest scientific minds in history to provide us with an understanding of how things fall.

Gravity according to Newton and Einstein

Sir Isaac Newton (1642-1727) was the first to provide mankind with an accurate description of gravity. He considered it to be an 'action at a distance', a mysterious and invisible tendency of all matter to pull all other matter in the Universe closer. In 1687 he published a mathematical formula with which the pull could be calculated. This *Universal Law of Gravity* is very successful: for the first time in history, mankind had the means to accurately calculate the trek of the planets around the Sun, to predict solar- and lunar eclipses, and to solve the mystery of the tides. Despite these successes, however, a number of things were not quite exactly described by this theory. For example, very precise measurements on the orbit of Mercury show that the planet orbits the Sun slightly faster than predicted by the Universal Law of Gravity. Also, Newton's theory postulates that gravity is an instantaneous force, by which is meant that there is zero elapse of time between a cause and its gravitational effect. If, for example, the Sun were to magically disappear, the gravitational pull felt on the Earth would vanish at the exact same instant. This would indicate that the effects of gravity traversed the distance between the Sun and the Earth with an infinite velocity. This can not be, as it contradicts the *Special Theory of Relativity*. This is a theory, published in 1905 by Albert Einstein (1879-1955), which states that nothing can go faster than light. Gravity is not allowed to be an exception to this rule, and it thus became clear that Newton's Law of Universal Gravity had to be modified.

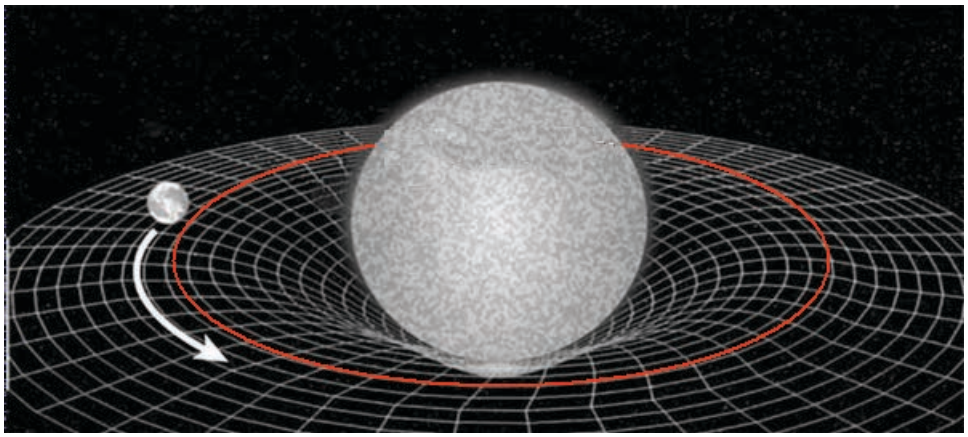

Figure D.1: The curvature of space due to the presence of a star (centre). The planet (left) follows a path that is wrapped around the star due to the curvature of space. The result is a closed orbit.

It was that same Special Theory of Relativity that suggested how this should be done. The theory states that the laws of physics should be the same for all observers moving with a constant velocity with respect to each other. It should therefore be possible to write the equations of physics in such a way that they can be used by all such observers regardless of their relative constant velocity. Einstein realized that this idea should also apply to observers who are *accelerating* with respect to each other, and was able to link this principle to the force of gravity. After all, he argued, if we are standing in an elevator that is accelerating upward, we feel that we are pushed to the floor of the elevator just as we would if there was a force of gravity pulling us down. With this insight, Einstein postulated that the phenomena of acceleration and gravity are fundamentally equivalent to each other, and formulated the *General Theory of Relativity* in 1916.
In the General Theory of Relativity, gravity is described as the curvature of space and time. Just as a meridian deviates from a straight line because the globe is spherically shaped, the path of a mass in motion will not follow a straight line if space is curved; the deviation from the straight line is what we ascribe to gravity. The way that space and time are curved is, in turn, determined by the presence of mass and energy: the more mass is present in space, the more space and time are curved, and the more the paths of masses in motion deviate from straight lines. An example of this is shown in Figure D.1, in which the presence of a heavy star curves space in such a way that the orbit of a planet is wrapped around the star. As a result, the planet follows a closed elliptical orbit instead of a straight line. Einstein published a formula that relates the curvature of space and time to the presence of mass and energy, and showed that when the curvature is not too extreme, the General Theory of Relativity exactly reduces to Newton's Universal Law of Gravity.

Black Holes and Gravitational Waves

The General Theory of Relativity is the most successful description of gravity that we have. It correctly predicts the orbit of the planet Mercury, the deflection of starlight when it grazes the Sun, the slowing down of time due to the presence of mass, and even the expansion of the Universe as a whole. All these predictions have, in a century of experiments, been accurately confirmed by observations. The theory makes two additional predictions that yet await experimental confirmation. The first is the existence of *black holes*: collapsed stars that are so massive that not even light can escape their gravitational pull and where time itself is slowed down to a standstill. Black holes are the most extreme examples of curved spacetime that we know.
The second unconfirmed prediction that the General Theory of Relativity makes is the existence of *gravitational waves*: microscopically small vibrations of space and time that are produced when two large masses move in each other's close proximity. These vibrations travel through the Universe with the speed of light, and we can reveal their presence by closely observing the relative position of two masses. Just as two bobbers will wobble with respect to each other when a little wave of water disturbs the pond, two masses will wobble with respect to each other when a gravitational wave disturbs space and time. The relative motion of the two masses is usually extremely small (the wobbles are typically of the order of a millionth of the size of a proton), and is biggest when the source of the gravitational wave has a very strong field of gravity. The production of the biggest gravitational waves is therefore expected to happen close to a very massive black hole.
Gravitational waves produced in this way contain a treasure trove of information about the black hole and allow us to test the General Theory of Relativity. It is for this reason that measuring gravitational waves is one of the biggest current challenges in physics. At this very moment, experiments such as VIRGO in Italy and LIGO in the United States are working to measure gravitational waves, and plans are in development to continue the effort underground in the upcoming Einstein Telescope, and in space in the upcoming LISA satellite experiment. In all cases, it is of absolute necessity to know in advance the exact shape of the gravitational waves in order to filter out the very small gravitational waves from the data collected by such experiments. This means that these must be calculated using the General Theory of Relativity.

Relativistic Epicycles...

It is not an easy task to calculate gravitational effects close to a black hole, as the mathematics needed to understand the General Theory of Relativity is very complicated. As such, solutions to the formulas are usually found only approximately. One of the ways that researchers do this is by first assuming that the gravitational field around the black hole is weak enough so as to describe it by Newton's Universal Law; the effects due to Einstein's curvature of space and time are subsequently added as corrections to Newton's solutions. A disadvantage of such a method is that it becomes less accurate when the star gets very close to the black hole. After all, it is in that region that the curvature of space and time

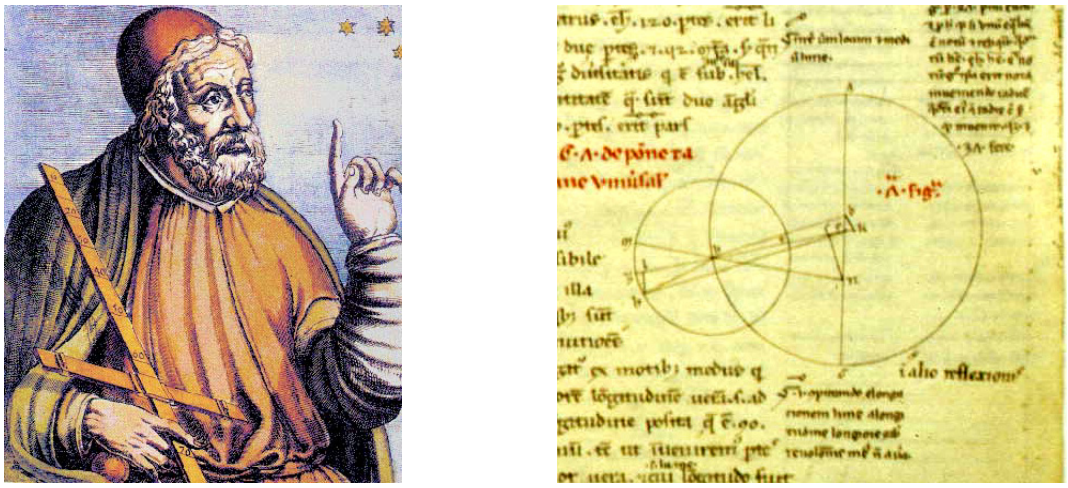

Figure D.2: Ptolemy (left) described the apparent motion of the planets, Sun, and Moon around the Earth by placing circles on top of circles, as is shown on a page (right) from his book *Almagest*.

is the most extreme and Newton's gravity does not suffice anymore. This is unfortunate, as it is also exactly this region where the strongest gravitational waves are produced.
In this thesis we present a novel method to calculate the gravitational waves produced when a star moves in close proximity to a black hole, in which we do not make the assumption that the gravitational field is weak. In our method, we assume instead that the orbit of the star around the black hole is simple enough to be described by a circle. By subsequently adding corrections to this circular orbit, we obtain the equations for more general orbits. The outcome of our calculations turns out to be akin to the system that the ancient egyptian sage Ptolemy (90-168) proposed to describe the apparent motion of the planets, Sun, and Moon around the Earth (which he thought the be at the centre of the Universe). He placed the planets on circles, on top of which he placed smaller circles called *epicycles*, in the manner shown in Figure D.2. Ptolemy's system is, of course, not correct (he made the incorrect assumption that the Earth is at the centre of the Universe, and he had no knowledge of the Theory of Relativity), but our research has shown that the motion of a star around a black hole can be described in a way very similar to Ptolemy's method. In our context, the corrections applied to a circular orbit are not themselves circles, but bear a more complicated shape that we have calculated accurately. We call our model *Relativistic Epicycles*.
In this model we never make any compromise on the strength of the gravitational field of the black hole: we do not assume it to be weaker than it really is. As a result, we expect our predictions for the orbit of the star to be accurate even when the star and the black hole are very close to each other. We found that this is indeed the case: as long as the orbit of the star does not deviate too much from a perfectly circular orbit, our results have an accuracy of more than 99%, and this regardless of how close the star is to the black hole.

...and the resulting gravitational waves

As the orbits of the star around the black hole could be accurately calculated, the next step in our research was to calculate the gravitational waves due to the star's motion in the gravitational field of the black hole. This turns out to be a complicated mathematical challenge: the first steps were already taken in 1957 (half a century ago!), and the final formalism was only published in 2004. This formalism requires that the orbit of the star is known as a function of time, and exactly this is provided by our method of Relativistic Epicycles. The resulting formulas for the gravitational waves we have subsequently solved by using a computer program that we have written ourselves. The gravitational waves we calculated in this way agree very well with the ones that were already known in the literature, and new ones we can calculate effortlessly and rapidly. Here too we found that the accuracy or our method is excellent, with accuracies being of the order of 99% when the orbits do not deviate too much from perfect circles.
Finally, as the last step in our research, we have investigated the limitations of our method of Relativistic Epicycles. The main disadvantage of our method is that we need to assume that the orbit of the star is close to circular; we have indeed found that our results become less accurate when the orbits become more eccentric. However, our calculations have also shown that, as the system sends out gravitational waves, the star's orbit becomes increasingly less eccentric and the predictions of our method are therefore rendered increasingly accurate. This means that the main disadvantage of our method is naturally nullified by the emission of gravitational waves! We therefore conclude that the method of Relativistic Epicycles is very well suited to describe the production of gravitational waves due to the motion of a star around a black hole, even when the star and black hole get in extremely close proximity.

Future research

There are numerous ideas for future research. For example, we could improve the accuracy of the Relativistic Epicycle even more by adding some more corrections on the orbit. Secondly, up to this point we have only taken into account the curvature of space and time due to the presence of the black hole, but it would be in order to also take into account the curvature due to the star. It would also be interesting to investigate whether the calculation of the gravitational waves could be done without invoking a computer, by replacing the outcome of the program by a mathematical formula. Finally, our calculations have shown that the method of Relativistic Epicycles also applies to the situation of electrically charged masses moving around a pulsar (which is a heavy star that is surrounded by a magnetic field that, like a lighthouse, periodically sends out flashes of light). The latter possibility is very interesting, as it allows the study of astrophysical objects by not just looking at the gravitational waves that they send out, but also at their electromagnetics waves. We have already taken the first steps in that direction, which will be the basis for future research.

VRIJE UNIVERSITEIT

Ageing and the Decay of Beauty

Radiation Hardness of the LHCb Outer Tracker and Time-Dependent CP Violation using $B_s^0 \to J/\psi\,\phi$ Decays

ACADEMISCH PROEFSCHRIFT

ter verkrijging van de graad Doctor aan
de Vrije Universiteit Amsterdam,
op gezag van de rector magnificus
prof.dr. L.M. Bouter,
in het openbaar te verdedigen
ten overstaan van de promotiecommissie
van de Faculteit der Exacte Wetenschappen
op maandag 15 oktober 2012 om 13.45 uur
in de aula van de universiteit,
De Boelelaan 1105

door

Daan van Eijk

geboren te Spijkenisse

Summary

This thesis marks the finalization of my PhD research. During the four years of my research, people frequently asked me about my work. I was surprised to notice that especially people from outside the work field of particle physics are very much interested in the work we do as particle physicists. I think their interest originates from questions that everyone asks themselves from time to time, such as 'what is matter made of?' and 'how did the universe begin and how will it end?'. These questions are essentially the motivation for our work. My hope is, that all the people that I have talked to in the last four years can enjoy reading at least parts of my thesis. Therefore, I will first start with a general introduction to particle physics, to explain the research I performed. After this, I will summarize the results of my analyses, guided by the title of my thesis. I will start with time-dependent CP violation using $B_s^0 \to J/\psi\,\phi$ (to be pronounced as *b sub s to jay psi fi*) events and conclude with the radiation hardness of the LHCb Outer Tracker.

Particle Physics and the LHC

The LHC is a particle accelerator that accelerates and collides protons in a circular underground tunnel. It stretches over 27 kilometers and is situated 100 meters below the surface. The protons collide millions of times per second in four distinct points along the LHC ring. Large particle detectors are installed surrounding the collision points to record the collisions or events. In this case, 'to record' means that the information about the passage of particles through the different subdetectors of the experiments is stored on computers. In the early days of particle physics, 'to record' would have meant to take a photograph of the event, as can be seen in Fig. S.1.

I performed my PhD research for the LHCb experiment, one of the four major experiments on the LHC accelerator ring. LHCb is a dedicated B physics experiment, as indicated by the additive 'b'. In B physics experiments, properties of B mesons are studied. To understand what these B mesons and their properties are, it is instructive to first have a look at the so-called Standard Model of elementary particles.

The Standard Model

The Standard Model (SM) describes our current knowledge of elementary particles and their interactions. It can be represented by a mathematical formula, but for the sake of simplicity it can be thought of as the set of all building blocks of nature, as shown in Fig. S.2.

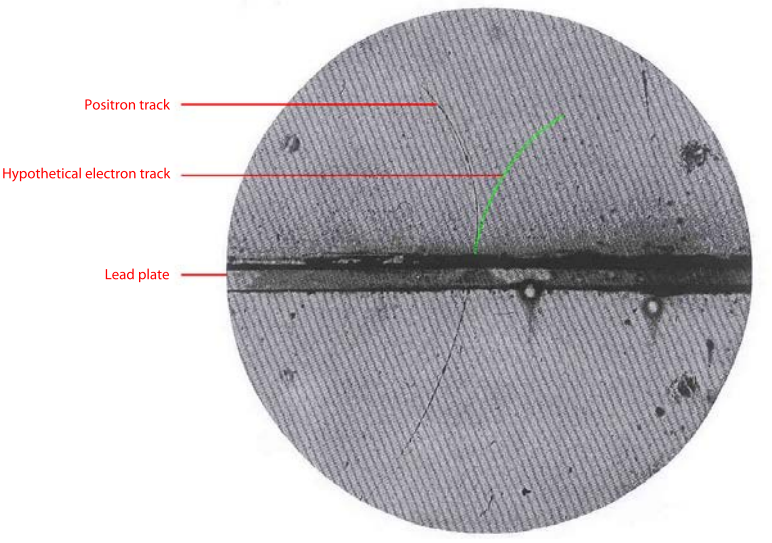

Figure S.1: *Photograph showing the discovery of an anti-electron, a so-called positron, recorded in 1932 by Carl D. Anderson. The identity of the positron is inferred from its direction of curvature, since it is opposite to the direction that is expected for an electron, indicated here by the dashed green line. The lead plate is used to slow down the incoming particle to deduce its direction of motion (upward or downward in the figure) from the difference in the radius of curvature on both sides of the plate.*

The SM is a theory that accurately predicts the many measurements that have been performed during the last decades. However, there are several known problems associated with it. One of these problems is well-known and was one of the reasons the LHC was built in the first place: to prove the existence of the Higgs boson.

Although I did not work on the Higgs search itself, the work that I performed on CP asymmetries is linked to Higgs particles. This is because the so-called Yukawa terms in the SM that express the couplings between the Higgs field and fermions to generate mass, are exactly the terms from which CP asymmetries arise, as explained in Chap. 1. I will now briefly elaborate on the Higgs search, since this puzzle might have been solved very recently.

The Higgs Boson

The Higgs particle was predicted in 1964 by, among others, Peter Higgs and is a necessary ingredient of the SM, since its presence generates mass for all other fundamental particles. It is being searched for in the ATLAS and CMS detectors, which are two other experiments on the LHC ring. July 4 2012 the ATLAS and CMS collaborations announced the discovery of a new boson whose properties are in agreement with the SM Higgs boson. This extraordinary finding was presented in a press conference held at CERN and was broadcasted worldwide

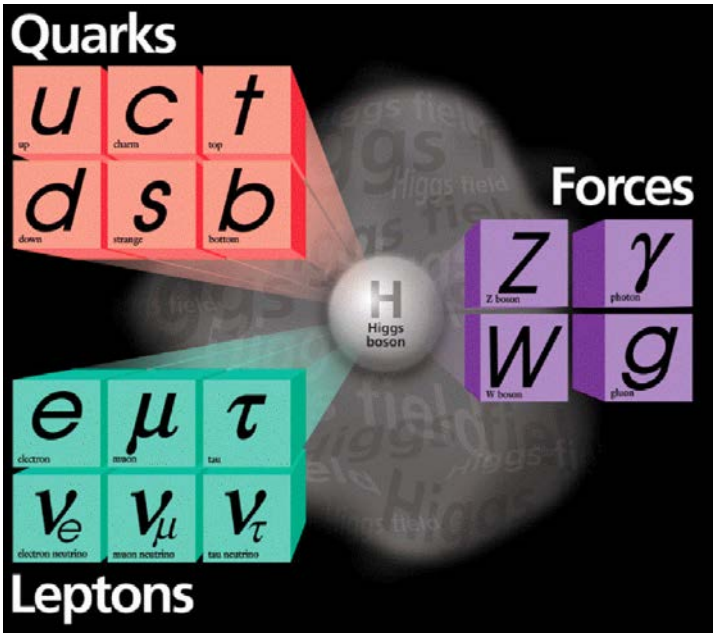

Figure S.2: *Schematic representation of the Standard Model, showing all the fundamental particles currently known. The Higgs boson (or, officially, a boson consistent with the SM Higgs boson) has been discovered on July 4, 2012.*

in the presence of Peter Higgs himself. The goal was not only observing the Higgs boson, but also to determine its mass. The ATLAS collaboration discovered a new boson with a mass of $126.0 \pm 0.6\,\mathrm{GeV}/c^2$ [78], whereas the CMS collaboration independently observed a new boson with a mass of $125.3 \pm 0.6\,\mathrm{GeV}/c^2$ [79]. In the coming years, at the LHC the properties of this new fundamental particle will be studied in order to test the SM. Whatever the results of those studies, the discovery of this new boson marks the end of a longstanding open question in the SM and in particle physics in general.

Fundamental Forces in the SM

The SM describes all elementary particles and their interactions. An interaction of a particle with one of the so-called force-carrier particles (Z, W, g and γ in Fig. S.2) is the manifestation of nature's fundamental forces. There are four fundamental forces in nature. Two of them can actually be observed in daily life. These are gravitation and the electromagnetic force (for example electricity). The two other fundamental forces of nature are the so-called weak force and the strong force. These two forces are less well-known, because their influence is only noticeable on very small (nuclear) scales. The weak force is involved in many radioactive decays, while the strong force acts as the proverbial glue that keeps quarks together to form protons or other bound quark states; so-called hadronic particles. The SM incorporates the strong, the weak and the electromagnetic forces. It does so through gluon particles (g), the

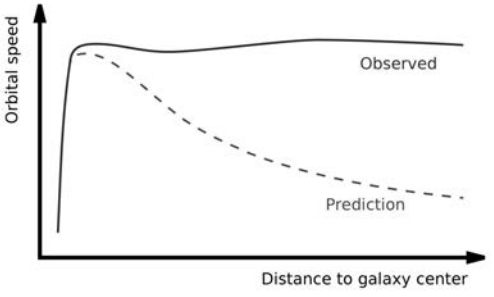

Figure S.3: *Stellar orbital speed as a function of distance to a galaxy center. Newtonian gravity predicts that the orbital speed decreases as a function of distance to the center, but observations prove otherwise. An explanation for this problem is dark matter, an unknown substance that does however feel gravity.*

Z and W particles and photons (γ particles) respectively. However, until now, physicists have been unable to incorporate gravity into the SM.

The Contents of our Universe

I have described two problems with the SM, namely the search for the Higgs boson and the incorporation of gravity. Another striking problem in particle physics deals with the content of our universe itself and arises from cosmological observations. When studying the orbital speed of stars at the outskirts of spiral galaxies, Newtonian gravitation predicts that the orbital speed decreases inversely with the square root of the radius of the orbit. However, observations [80] show that the orbital speed remains almost constant as a function of distance to the galaxy center, as indicated qualitatively in Fig. S.3. The best explanation so far is that there is some sort of invisible matter (here, 'matter' is a substance that is subject to gravity) in addition to visible matter, like that in stars. The ratio of known visible matter to this unknown so-called dark matter can be derived from the orbital-speed observations and amounts to a stunning one to five. Within the SM, there are no particles that can explain dark matter. Thus, the SM can account for only 20% of all the matter in the universe.

New Physics

To solve part of the problems associated with the SM mentioned above, theoretical physicists are trying to devise new mathematical models that incorporate and extend the SM. Such New Physics (NP) models make predictions for new types of particles, like dark matter candidates and new types of interactions. The experiments at the LHC are a unique environment for scientists to search for these new particles and interactions. These searches can be performed both in a direct way and in an indirect way. The former approach is used by the ATLAS and CMS detectors, by searching for the hypothetical particles in the decay products from the proton-proton collisions. In LHCb, however, the search for NP is performed indirectly, as

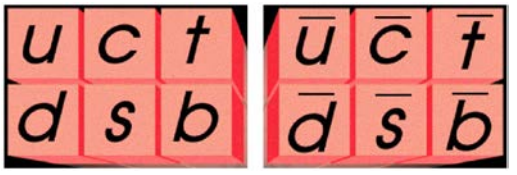

Figure S.4: *In 1928, Paul Dirac predicted that every fundamental particle has its own antiparticle associated with it. This is illustrated here for the six different types of quarks. For example, the up quark u, indicated on the left, has the anti-up quark as its associated antiparticle, indicated on the right by $\overline{u}$.*

LHCb measures parameters that are affected if new particles contribute to certain processes. When a significant deviation from the SM prediction is found, this could be an indication of New Physics. The measurement of such a parameter is the subject of my thesis and is denoted symbolically as ϕ_s. To explain what this parameter represents, another ingredient is needed: antimatter.

Antimatter

The schematic picture of the SM depicted in Fig. S.2 is actually incomplete. In 1928 the physicist Paul Dirac predicted the existence of so-called antimatter on mathematical grounds. This implied that every particle in the SM should have an antiparticle partner, as indicated for the quarks in Fig. S.4. Dirac was proven right in 1932, when the positron was discovered. A positron is the antiparticle of the well-known negatively charged electron, which means that it carries a positive charge. The photograph in Fig. S.1 shows one of the first positrons ever observed. Its identity was deduced from the direction of curvature in a magnetic field, since this was opposite to the direction that was expected for an electron, as indicated in the picture. When matter and antimatter particles meet, they 'destroy' or annihilate each other, producing photons. In the next paragraph I will explain B mesons and anti-B mesons, what CP violation means and how this relates to the parameter ϕ_s.

B mesons, CP Violation and ϕ_s

Mesons are quasi-stable particles that consist of two quarks. B mesons are mesons that contain one b or $\overline{b}$ (this denotes an anti-b) quark. These b quarks are sometimes called beauty quarks and, correspondingly, B mesons are occasionally referred to as beauty mesons. Here, since I have studied the decay of a beauty meson, we have arrived at the title of my thesis: The Decay of Beauty. The quark content of a B_s^0 meson is $(\overline{b}s)$, while the decay products in $B_s^0 \to J/\psi\,\phi$ decays are the J/ψ meson $(c\overline{c})$ and the ϕ meson $(s\overline{s})$, as indicated in Fig. S.5.

The final ingredient that is needed to explain the parameter ϕ_s is a property of B mesons called mixing. Mixing means that B mesons can oscillate back and forth to their own antiparticle. This happens at an incredibly high frequency, roughly 18 trillion times per second. When two protons collide in LHCb, B_s^0 mesons and their antiparticles, $\overline{B}_s^0$ mesons, are produced in equal amounts. Due to mixing, the decay to the state $J/\psi\,\phi$ can take

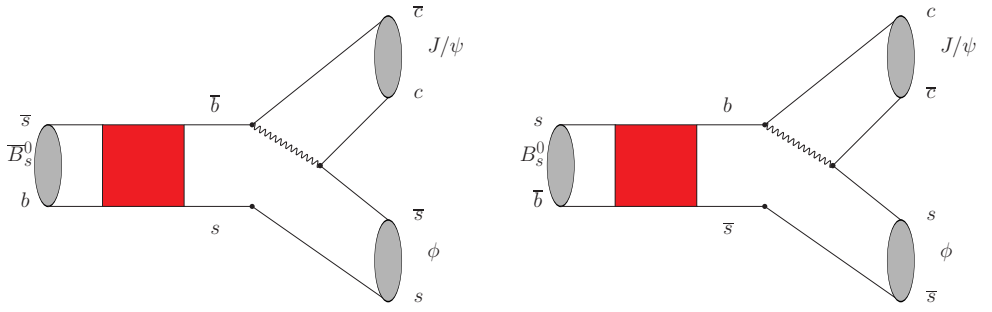

Figure S.5: *Left: schematic representation of a $\overline{B}^0_s$ meson oscillating to a B^0_s meson (a process indicated by the red box) before decaying into the final state $J/\psi\,\phi$. Right: schematic representation of a B^0_s meson oscillating to a $\overline{B}^0_s$ meson (again indicated by the red box) before decaying into the final state $J/\psi\,\phi$. Depending on the decay time of the B meson that was produced in the proton-proton collision, there is a possible difference in the decay rate of these two processes, which would be an indication of CP violation. The amount of CP violation is measured by ϕ_s and can be enhanced with respect to the SM prediction by NP processes in the red boxes.*

place at a moment when the parent particle was a B^0_s particle, a $\overline{B}^0_s$ particle or even a quantum-mechanical superposition of the two.

Depending on the decay time of the B meson, there could be a difference in decay rate between decays where the originally produced particle was a B^0_s meson and where the produced particle was a $\overline{B}^0_s$ meson. This effect is called time-dependent CP violation[1], represented graphically in Fig. S.5. The parameter ϕ_s is a measure of the amount of time-dependent CP violation in $B^0_s \to J/\psi\,\phi$ decays. In the SM, ϕ_s is predicted to be very small, whereas NP models can enhance its value. Therefore, any significant deviation in ϕ_s from the SM prediction could be an indication of a New Physics discovery. In the next section, I will present the results of my ϕ_s measurement.

The Decay of Beauty: Time-Dependent CP Violation using $B^0_s \to J/\psi\,\phi$ Decays

In the SM, ϕ_s is predicted to be $\phi_s = -0.036 \pm 0.002$ [17]. Any significant deviation from this prediction is an indication of New Physics. The value I measured is $\phi_s = 0.00 \pm 0.10\,(\text{stat.}) \pm 0.02\,(\text{syst.})$, which is in perfect agreement with the value as predicted by the SM. The result of my analysis can be presented and compared to earlier experiments by drawing contours in the $\phi_s - \Delta\Gamma_s$ plane as shown in Fig. S.6, where $\Delta\Gamma_s$ is the lifetime difference between two types of B^0_s mesons. The smaller these contours, the more precise the measurement, therefore the measurement presented here is currently the most precise.

[1]The 'C' and 'P' in CP violation stand for charge and parity respectively. For more information, see Chap. 1.

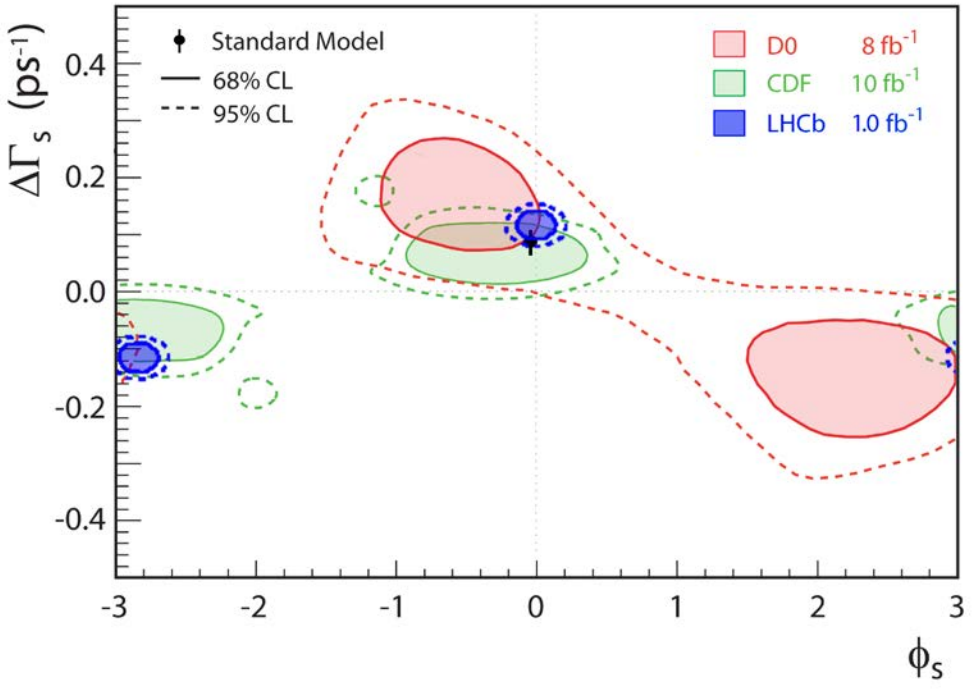

Figure S.6: *Two-dimensional confidence contours in the $\phi_s - \Delta\Gamma_s$ plane for the D0 collaboration [59] (red), the CDF collaboration [72] (green) and the values found in this analysis (blue). The black square indicates the SM point ($\phi_s = -0.036 \pm 0.002$, $\Delta\Gamma_s = 0.087 \pm 0.021\,\mathrm{ps}^{-1}$).*

Although the measured value for ϕ_s is in agreement with the SM, it is important to continue this analysis by adding more data and different decay channels that are sensitive to this parameter. This will reduce the uncertainty on the measurements and allow the observation of possible deviations from the SM. In the next section, I will summarize the second part of my thesis, which is related to the radiation hardness of the LHCb Outer Tracker.

Ageing: Radiation Hardness of the LHCb Outer Tracker

The Outer Tracker (OT) is one of the subdetectors of the LHCb experiment. It is used to reconstruct the trajectories of charged particles through the detector originating from proton-proton collisions. To detect a traversing particle, the OT uses straw tubes filled with an ionization gas that act as cathodes with a central anode wire. It consists of three detection stations and each station comprises 4 detection layers. The OT has a modular design, meaning that it consists of 432 modules of 128 straw tubes, leading to a total of roughly 55 000 straw tubes in the entire OT. The modules are constructed by glueing the

straws to the module panels.

After construction and prior to installation of the modules in the LHCb experiment, laboratory tests [30] proved that outgassing of the glue that was used in the module construction reduced the performance of the detector modules. In the context of particle detector technology, effects that gradually reduce detector performance, such as outgassing, are collectively called ageing effects.

The modules that were installed in the LHCb cavern were subjected to several treatments to reduce or prevent ageing effects [41, 30, 42]. My thesis summarizes the results of tests that monitor the behavior of the OT modules after installation in the LHCb cavern. The effects of the beneficial treatments were tested by deliberately irradiating and scanning modules using a dedicated scanning setup which is installed in front of the modules. Before adding an oxygen component to the counting gas, several modules showed severe radiation damage after relatively small received dose, although large module-to-module variations were observed. After adding O_2 to the OT gas mixture, few to no radiation damage was observed.

To monitor the behavior of the OT modules after the startup of the LHC in 2009, two methods were devised. The first method uses the same scanning setup as described above to regularly perform reference scans of a subset of the modules. These scans are performed manually in the LHCb pit and can therefore only be performed during technical shutdowns of the LHC. The second method uses charged particle tracks produced by LHC collisions to study hit efficiency as a function of the amplifier threshold of the OT electronics. These so-called threshold scans are performed while the LHC is operational and producing collisions with tracks in the LHCb detector.

Both methods to monitor the performance of the OT modules were applied in my research. In this thesis, I conclude that neither method has shown any significant gain loss in the OT so far. Both types of tests are and will continue to be performed regularly to monitor the radiation hardness of the OT.

Effective Theories in Cosmology

ACADEMISCH PROEFSCHRIFT

ter verkrijging van de graad van doctor
aan de Universiteit van Amsterdam
op gezag van de Rector Magnificus
prof. dr. D.C. van den Boom
ten overstaan van een door het college voor promoties
ingestelde commissie,
in het openbaar te verdedigen in de Agnietenkapel
op dinsdag 24 september, om 10:00 uur

door

Sander Johannes Nicolaas Mooij

geboren te Haarlem

Summary

I take it as a great privilege that for four years and a half already I have been around in this "Big Bang business". On these pages I would like to clarify what this has been about for me: from a general introduction to cosmology to the research described in this thesis. Every now and then some corners are cut short, but then again I do not intend to keep the reader busy with this for four years and a half...

Man in an expanding universe

As we cannot simply step out of it for a second, the universe should be studied from within. In this first paragraph I want to explain briefly how man, despite its modest place in the universe, manages to extract quantitative information from the night sky.

First of all we need a method to determine distances in the cosmos. In everyday life we perceive depth when our brain compares the separate images caught by our left and right eye. The so-called "parallax method" applies this same principle in astronomy. Two measurements, with an interval of six months, are made of the angle that a star makes with the horizon. In these six months the earth changes its position: she completes half of her orbit around the sun. Just like we do not see exactly the same with our left and right eye, the two measurements of the position of the star yield two different results. From their difference follows the distance to the star.

A second method makes use of the brightest light source we know in the universe: type IA supernovas. These are enormous explosions that occur in some binary systems (two stars orbiting each other). They are perfect to be used as lighthouses in the cosmos as, to a very good approximation, they are all equally bright. That is to say: if they had all been equally distant. By comparing a supernova's brightness with those of another supernova whose distance to us we know, we find the distance to the first one.

Apart from the distance to a star we would also like to measure its velocity relative to us. This can for example be done by employing the Doppler effect. Anyone who has ever seen a fire truck passing knows this phenomenon. When the truck is approaching us the distance between two consecutive sound waves shrinks, and we hear the siren at a higher tone then the firemen do themselves. Once the fire truck has passed, its sound of waves reaching us are somewhat stretched out, and we perceive a lower tone.

This same effect also happens in the light waves that a star emits. When the star is moving towards us, its light waves seem to be closer to each other. When she is moving from us, we measure a larger distance between two consecutive wave fronts. By comparing a star's emitted pattern to what we would measure had she been at rest, we find its velocity.

In this same way Edwin Hubble measured the distances and relative velocities of many stars in the

'20s of the last century. He found not only that all stars are moving from us, but also that their velocities are proportional to their distances from us. A star that is three times further from us than another one, is moving three times as fast from us. How is that possible? Hubble thought and concluded "Because they all started in the same point!" The Big Bang theory had been born. Everything began at the same point in space and time. Had this one star not been moving three times faster, it would not have got three times further from us. We are observing the consequences of a cosmic explosion: after 13.8 billion years pieces are still flying around.

The background radiation

After Hubble the picture of the expanding, cooling universe has been refined much further. Increasingly precise measurements have yielded an ever more accurate model. This section is about one of the most important observations, indispensable for this thesis: the cosmic microwave background (CMB) radiation. When the universe was about 380,000 years old, the temperature decreased such that free electrons could no longer exist. Instead they got caught inside protons to form hydrogen. As a consequence, travelling light particles (photons) did no longer scatter off electrons, and their (straight) path through the cosmos was no longer disturbed. These photons are still travelling and produce a signal that we know as the CMB. It was discovered in the '60s by Penzias and Wilson in the US. Looking for something totally different, they tried their very best to get rid of this "noise" signal. They even checked their telescope for pigeon droppings, but the signal persisted to be there. At this point they were made aware of the work by George Gamow, who was the first to speculate about the CMB. By chance Penzias and Wilson turned out to have made a Nobelprize-worthy discovery: a baby picture of the universe. As the photons in the CMB have travelled freely to us since 380,000 years after the Big Bang[1], they contain a lot of information about the early universe.

Symmetry on large scales...

Then what do we see in the CMB? In two words: complete symmetry. The CMB's temperature is 2.73 Kelvin ($\approx -270°$C), in all directions. This is a very surprising result. Two photons reaching a telescope on earth from opposite directions, were very distant from each other when they began their journey. In 13.8 billion years such a photon travels 13.8 billion light years (not even taking into account the expansion of the universe). At the start of their straight flight they were therefore more than 27 billion light years apart. Now, Einstein prescribes that information can not travel faster than the speed of light. When the CMB was emitted, the universe was about 380,000 years old. At that moment we expect that information (like a temperature) can have travelled over 380,000 light years at most. It is therefore very surprising that two photons that were more than ten thousand times further apart, still had managed apparently to adjust to the same temperature.

The uniform CMB temperature fits in well with our general picture of the universe on large scales. (Note that by "large" we here mean cosmologically large: length scales of 10^{24} meter and larger.) At such scales the visible universe looks the same everywhere and in all directions. Again the question rises: what caused all that homogeneity and isotropy?

[1]Note that the CMB was produced everywhere in the universe. Therefore there is no end to the CMB-bombardment. A CMB photon that arrives on earth today was simply produced a bit further away than one that was detected last year.

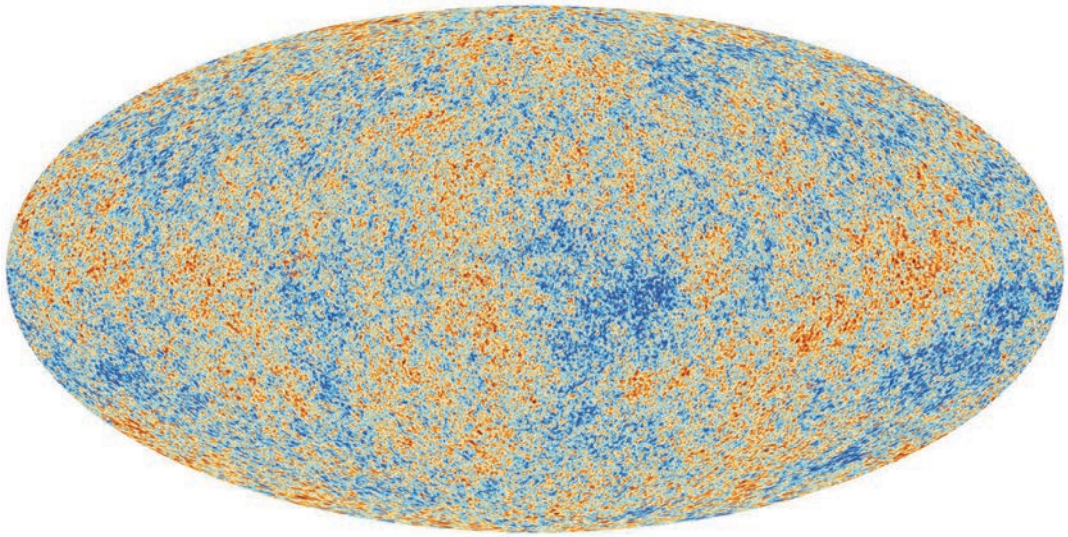

Projection of the temperature of the CMB. Red areas are a fraction warmer than the general background temperature of 2.73 Kelvin, blue areas are somewhat colder. The difference between the warmest and coldest spots is one thousandth of a degree. (esa.int/planck)

... perturbations on small scales

On smaller scales the universe is of course not at all that homogeneous. The closer we look, the more "perturbations" of the cosmological equilibrium situation manifest themselves: from star clusters to this booklet. This leads us to a second interesting question: what causes these perturbations? How do the first lumps come about in the originally perfectly symmetric primordial soup? The answer is partly in the background radiation. It turns out that on top of the universal background temperature of 2.73 Kelvin there exist tiny temperature fluctuations: a photon from the one area is just one thousandth part of a degree colder than a photon from another area. This indicates that when the CMB was emitted gravity in such an area was just a tiny bit stronger than the global average[2]. At such a place the soup gets pulled a bit more and a little clump is formed, which in turn pulls the rest a bit harder. With this principe the structures in the current universe can be explained quite easily.

This answer to the question how structure formation begins instantly points to a new one: what causes the temperature fluctuations in the CMB? How come that already when the universe was only 380,000 years old, gravity was not totally homogeneous anymore?

Cosmological inflation

The paradigm of cosmological inflation, proposed by Alan Guth in 1980 and further developed by (among many others) Slava Mukhanov and Andrei Linde, solves both of the problems sketched above in one go.

[2]A stronger gravitational force at some place attracts more particles and therefore leads to a higher temperature. However, it takes more energy now for a photon to escape. This is a stronger effect. The net result therefore is that we measure a somewhat lower temperature.

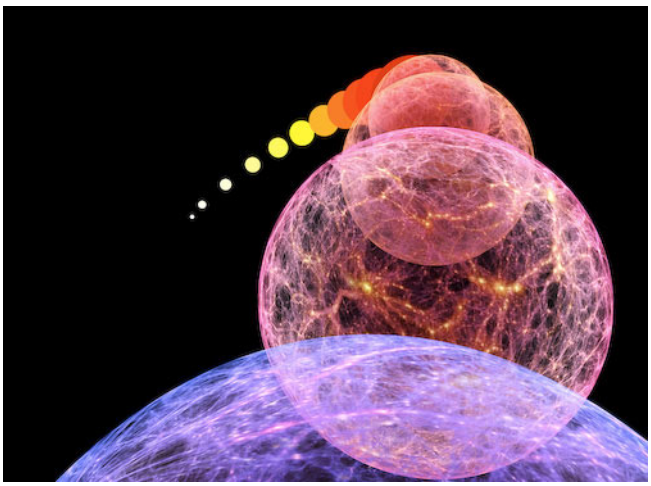

Cosmological inflation: an explosion of space itself. This artist's impression shows what an "observer outside the universe" would see. (scienceblogs.com)

Or better: in one explosion. The hypothesis is that when the universe was (much) younger than one second, it has undergone an enormous expansion. This adds to the "standard" expansion measured by Hubble. Guth demonstrated that if in a fraction of the first second the universe increases its size by a factor of 10^{26} at least[3], we can explain why it looks so homogeneous. According to Guth initially the universe does not have to be that homogeneous. The consequence of the enormous expansion (inflation) of the universe is that everything that we can see today, was confined to a very small space before inflation took place. At such small scales it is not difficult to imagine homogeneity.

To understand how inflation solves the problem of structure formation as well, a bit more background knowledge is needed. Einstein has shown by his famous formula $E = mc^2$ that to create a particle with mass m out of nothing, one needs an amount of energy of mc^2. At the other hand there is quantum mechanics stating that on the smallest length scales (the order of the size of an atom, about 10^{-10} meter) there is always some uncertainty in the amount of energy. Even in the vacuum there can be some energy for some short time. And where there is energy, there can be particles! Merging Einstein's (special) relativity with quantum mechanics shows that even in the vacuum two particles can be created out of nothing, which after a short time collide and disappear in thin air again. The vacuum therefore is not really empty. It is more like a boiling pot, with bubbles of the size of an atom.

The work done by Mukhanov has shown that during inflation this process of particle creation and annihilation is hampered. Because of the very rapid expansion of the universe, both particles do not get back to each other anymore. The bubbles in the vacuum do not disappear anymore, but are blown up to sizes that exceed quantummechanical scales and that can influence the "big" world. In his famous calculation, partly sketched in chapter 1, Mukhanov showed that blown up quantum bubbles precisely form the seeds that (over the next 380,000 years) grow into the tiny temperature fluctuations in the CMB. Ultimately all structure that we know originates from a pot of primordial soup that is boiling over!

In the last 30 years hundreds of models of inflation have been proposed. The most influential model builder is probably Andrei Linde, who is also co-author of article [5] on which this thesis is based. Every

[3]This expansion is faster than the speed of light, but there is no violation of special relativity. It is space itself that is expanding, there is no information travelling faster than light through space.

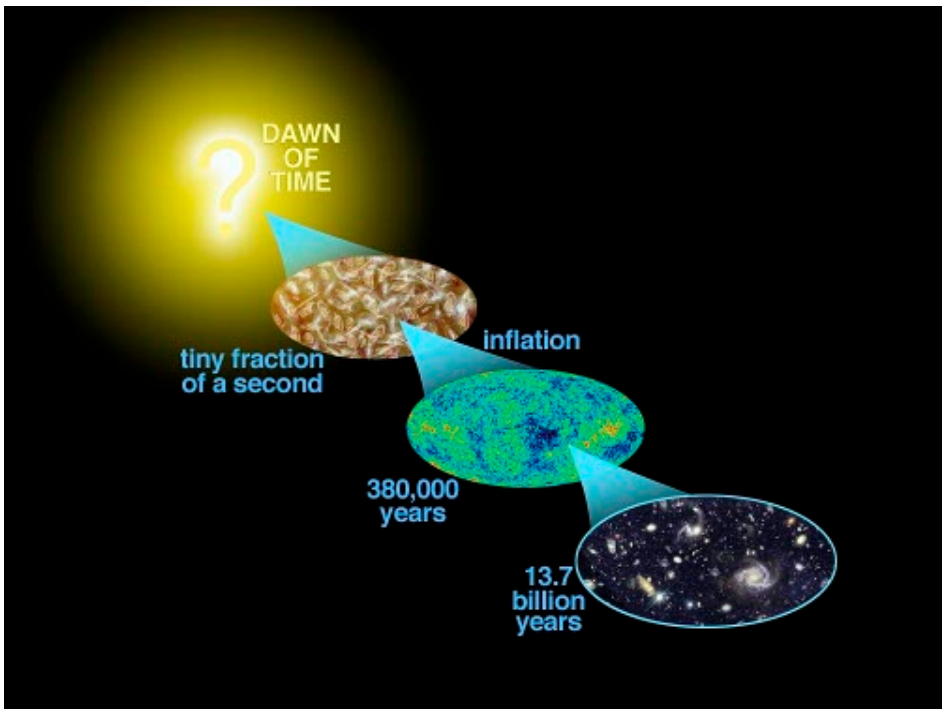

The history of the universe. Before (and during) the Big Bang we know nothing. Inflation blows up a small, causally connected part of space thereby generating the homogeneous universe that we observe. Quantum bubbles (of the inflaton field) are stretched out and lead to the temperature fluctuations in the background radiation. These evolve further to all structures we observe in the universe today. (scienceblogs.com)

model is characterized by the properties of the "inflaton" (the particle that causes inflation to happen) and the forces that act on it. This leads to precise predictions of the statistical properties of the CMB fluctuations that can be tested experimentally.

Inflation with the Higgs field

Recently there has been much attention for models that make the Higgs particle (discovered at CERN in Geneva last year) responsible for inflation. This has the advantage that there is no need to postulate a new particle (all other known particles are fundamentally incapable). Therefore the number of new parameters to be determined experimentally is minimal. Even better: by combining the results of the LHC (like the mass of the Higgs particle) with cosmological measurements of the CMB, the theory can really be tested. At the moment the Higgs mass seems a tiny bit too small for the model to work. However there are still too many issues not well understood, theoretical as well as experimental, to be able to draw a definitive conclusion.

The chapters 3 and 4 of this thesis describe our research of one of these not well understood elements of Higgs inflation. When the Higgs particle is used in the early universe as an inflaton, it has more freedom of movement than when it is measured at CERN. The vibrations of the quantum field associated to the Higgs particle follow a pattern that is more dynamical. That is why the usual Higgs theory needs to

be generalized. In a simplified model we have precisely shown what are the consequences of these extra dynamics, and shown how the theory is still "gauge invariant" (invariant under modification of certain parameters).

Superinflation

Since the early '70s there has been a lot of interest for supersymmetry, supergravitation and superstring-theory. These "supertheories" have in common that, by proposing (many) new particles, some theoretical shortcomings of the current standard theorem can be overcome. The ultimate goal: a theory that describes gravity on quantum scales, has still not been found. However, the validity of standard theorems can be stretched out to higher energy scales. Experimentally, however, no postulated new "superparticle" has been found. Another problem is that the huge number of unknown parameters in these new theorems drastically reduces their predictability.

The chapters 5 and 7 of this thesis describe how inflation can work in such a "super context". Chapter 5 tries to decouple the dynamics of inflation as much as possible from the model's other dynamics. In this way inflation's predictability can be maintained, even if there is so little quantitative information available about the other (super)particles in the model. Chapter 7 shows how an existing model of inflation can be made compatible with superstringtheory. This last theory requires the existence of extra spatial dimensions, which are only observable on extremely high (experimentally unaccessible) energy scales. Still these extra dimensions have some indirect influence on the physics on lower energy scales, and we have shown under which conditions these new effects do not spoil inflation.

Particle production during inflation

Chapter 6 looks at a model in which during inflation extra particles are produced. It follows from adding one new particle and one new coupling (between that particle and the inflaton) to the most standard model of inflation. The question is now: which observable quantity is most sensitive to this new coupling, and can therefore be used to constrain it? We have pointed out that, contrary to what was claimed in literature, for once this observable was not to be found in the CMB. It turns out that the very limited presence of a certain type of black holes in the universe puts the most stringent pressure on this proposed coupling. We show as well how these same models can still work in an "superenvironment" (embedded in a model of supergravitation).

Future research

So what is next now? I know more than four years and a half ago, but I have more questions as well. At this point my first goal is to work out the model of Higgs inflation in much further detail. Different research groups have different opinions on the theory's precise predictions, and I first of all want to work out how the effects studied by us further influence this debate. But there is so much more to do, also because the new measurements of the PLANCK satellite constrain the existing models ever further. Less than a hundred years after Hubble's discovery cosmology has become a precision science. I am happy that I will have three more years at least to work on that, at a place where the sun shines in daytime and the stars light up at night...

The color of X-rays

Spectral X-ray computed tomography using energy sensitive pixel detectors

ACADEMISCH PROEFSCHRIFT

ter verkrijging van de graad van doctor
aan de Universiteit van Amsterdam
op gezag van de Rector Magnificus
prof. dr. D.C. van den Boom
ten overstaan van een door het college voor promoties ingestelde commissie, in het openbaar te verdedigen in de Aula der Universiteit
op vrijdag 5 december 2014, te 15:00 uur

door

Enrico Junior Schioppa

geboren te Rome, Italië.

Summary

The retina of the eye is quite insensitive to these rays: the eye placed close to the apparatus sees nothing.

W. C. Röntgen, 1895 [62].

Professor Röntgen calls these rays "X-rays", as he says, *for the sake of brevity* and probably to emphasize that, apart from the observation that *bodies behave to the X-rays as turbid media to light*, he knew very little about the nature of this phenomenon. To such an extent that he did not have any trouble in placing his own eyes just in front of what seems to have been a rather powerful radiation source if *Platinum 2 mm thick allows some rays to pass.* Today, we are well aware of the dangers of such an action, and radiation protection teams work hard in order to avoid such occurrences.

Apparently however, professor Röntgen was the first who, unwillingly, attempted to detect X-rays with an energy sensitive pixel detector: the human retina. Of course he could not see anything, because the retina is not at all sensitive to X-rays. The technology required to realize energy sensitive X-ray artificial retinas has become available only 100 years later. These detectors are made by connecting a semiconductor pixel sensor to an energy resolving readout chip and can be employed to achieve color, i.e. material resolved, X-ray imaging.

The principle of color vision in the retina relies on the presence of three types of "pixels", the cone receptor cells, each having its sensitivity peak at a different wavelength. The incoming light spectrum is filtered by each receptor and the image is decomposed onto a basis of three colors (red, green and blue, see figure 7.1a).

Following a different concept, spectroscopic pixel readout chips for semiconductor X-ray detectors are able to separate an incoming radiation spectrum into multiple energy channels, at the level of single pixels. Compared to the retina principle, where three images in different color channels are obtained at the expense of spatial resolution (one out of three receptors are used to form each image), energy sensitive X-ray imaging devices allow for the formation of multiple simultaneous images with no resolution loss (figure 7.1b).

We are able to see more "colors" in X-rays than in visible light. The question that remains open is: what is color for X-rays?

In a similar way as different types of surfaces exhibit different reflection properties of visible light, different materials are characterized by different X-ray transmission properties. The X-ray spectrum reaching the detector pixel thus bears information on the material traversed by the radiation along its path from the source to the pixel.

Until recently, this information was completely lost, because X-ray detectors were only able to measure one integral value, be it the total deposited energy or, more recently, the total number of photons (the beam intensity). On the contrary, spectroscopic X-ray detectors give the possibility to measure the full energy spectrum, even if just coarsely binned, at single pixel level, which provides a handle to extract more significant knowledge on the material content of the sample than the one encoded in a simple grayscale radiograph.

Spectral information can be used to identify different materials and their distribution in the sample. If different colors are assigned to each material, color X-ray imaging is achieved.

The set of 3D X-ray imaging techniques exploiting energy information is called spectral Computed Tomography (CT). Spectral CT is a relatively new field, due to the fact that energy sensitive X-ray imaging detectors only appeared recently.

The main challenge in spectral CT is to answer the following question:

> What is the best way to process spectral information from a set of two-dimensional radiographs and realize color (i.e. material resolved) X-ray three-dimensional imaging?

The aim of this thesis has been to answer this question for a specific set of detectors, i.e. silicon sensors connected to the spectroscopic readout chips of the Medipix family. The work needed to reach this goal not only involves the

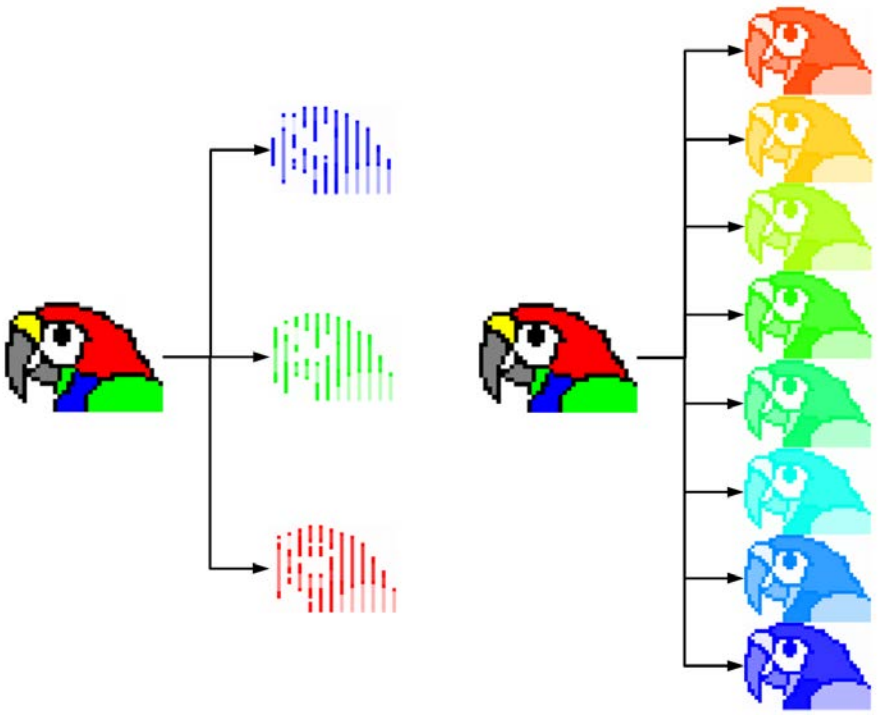

(a) **Human retina.** (b) **Medipix3 spectroscopic mode.**

Figure 7.1: **Image decomposition into color bases.**

implementation of dedicated image reconstruction algorithms capable of handling the spectral information measured by these detectors, but it also requires a precise characterization of the properties of the silicon sensor. This knowledge is necessary in order to implement the detector response in the reconstruction phase.

In the first place, a calibration method is developed, needed in order to define the detector energy scale. As monochromatic reference sources, the method exploits fluorescence X-ray radiation emitted from elements that are excited by the primary beam of an X-ray tube. A fitting procedure is designed to achieve an efficient calibration of single pixels, which is crucial to correct for variations

due to inter-pixel mismatches and to reach an equal response of the full detector.

To understand how an incoming X-ray spectrum is distorted due to detector effects, the energy response function of the sensor has to be known. The strategy adopted in this thesis is to reach this result with a fully measurement based approach, in order to avoid biasing errors from the introduction of physics constants and to avoid the need to calculate the electric field configuration, which would require the precise knowledge of the doping profile of the sensor.

The measurement of the detector response function has been performed through a test beam with relativistic charged particles and a synchrotron test beam. Charged particles are used to study the transport properties of the sensor. Exploiting the energy information provided by the pixel readout, the energy deposition as a function of different positions in the pixel volume is determined. This information is used to extract the evolution of the charge profile as a function of the drift distance. The particle beam is thus used as a micro-probe to look at charge diffusion at microscopic level.

This information is exploited to implement a numerical framework for the calculation of the detector energy response function. The synchrotron test beam is needed to determine the values of the parameters of this model by comparing the calculations with measurements. Using monochromatic synchrotron radiation at different energies, the energy response function of the detector is measured directly over a wide spectral range.

The energy response function is used to calculate the detected spectrum, given an input spectrum coming from the transmission of an X-ray beam through an object. This step is crucial for the implementation of a spectral CT reconstruction algorithm suited for data taken with Medipix based silicon detectors.

As a proof of principle, an algorithm is derived by extending a conventional iterative method in order to incorporate spectral information. The algorithm, as formulated at this stage, is only applicable to a limited subset of sample geometries. Nonetheless, the results not only show an example of material resolved X-ray CT, but they also show the benefits arising from spectral CT with respect to conventional CT. The quality of the reconstruction improves as beam hardening artifacts are eliminated, which typically appear if spectral information is not accounted for.

To obtain a more efficient implementation, a statistical reconstruction algorithm is developed, based on a maximum likelihood principle. First results on simulated data show the validity of the method and hint at the necessity to further develop this research line in order to exploit the full potential of the Medipix chip (and similar technologies) in X-ray imaging applications. The algorithm is implemented using tools developed for the statistical treatment of

large amount of data from high energy physics, thus giving a demonstration of how fundamental research can be exported to applications in other fields.

Although the results are derived only for a very specific type of detector operated in a specific state (a 300 μm silicon sensor read out by a Medipix chip and operated at 100 V bias) these devices, at these operating conditions, are standard for the majority of the applications. The results, and especially the methods, have thus a more general validity. First applications in several fields, including medical, are not far away. The general belief is that once fully understood and established, spectral CT will surely have a considerable impact in the field of X-ray imaging.

Enrico Junior Schioppa
Amsterdam
30 November 2014

The Higgs Boson

ACADEMISCH PROEFSCHRIFT

ter verkrijging van de graad van doctor
aan de Universiteit van Amsterdam
op gezag van de Rector Magnificus
prof. dr. D.C. van den Boom
ten overstaan van een door het College voor Promoties ingestelde
commissie, in het openbaar te verdedigen in de Aula der Universiteit
op vrijdag 26 juni 2015, te 11:00 uur

door

Stefan Gadatsch

geboren te Hachenburg, Duitsland

Summary

The Standard Model of Elementary Particle Physics (SM) provides a fundamental description of all established elementary particles, their dynamics and interactions, except gravity. Fermions of half-integer spin form all matter in nature. The interactions between the fermions are interpreted as exchange of force-mediating bosons of integer spin. Symmetries play an essential role in constructing the SM, making it an remarkably elegant theory. However, the particles embedded into the theory are a priori massless, unlike the observed particles. Thus, a mechanism must be introduced to give the particles mass in the theory.

The W and Z gauge bosons can acquire their mass through breaking of the electroweak symmetry, referred to as electroweak symmetry breaking (EWSB). In the SM, the complex Higgs scalar field induces a spontaneous breaking of the electroweak gauge group when it acquires a non-vanishing vacuum expectation value. The mechanism is commonly referred to as the Brout-Englert-Higgs mechanism. The Higgs field picked up its vacuum expectation value through the so-called electroweak phase transition when the early universe cooled down and expanded after the Big Bang. The underlying dynamics of this process are not known. Spontaneous symmetry breaking also gives mass to the fermions, yet the concept differs from the mechanism gauge bosons acquire their mass. The fermion mass terms are generated in the SM by gauge invariant Yukawa interactions between the Higgs field and the fermion fields. The Brout-Englert-Higgs mechanism postulates the existence of one real scalar field, identified as the Higgs boson. In 2012, the discovery of a new particle with a mass near 125 GeV in the search for the SM Higgs boson [4–6] provided the first hint at the mechanism of EWSB. Elucidating the mechanism of EWSB and the origin of elementary particle masses is among the principal quests of the CERN LHC physics program.

This manuscript presents comprehensive precision measurements of the Higgs particle's properties, in particular of its mass, production and decay rates, and coupling strengths. The results are based on the samples of proton-proton collision data recorded by the ATLAS and CMS detectors at the LHC in Run 1. The analyzed samples correspond to an integrated luminosity of approximately 5 fb^{-1} and 20 fb^{-1} at a collision energy of 7 TeV and 8 TeV, respectively, for each experiment.

At the LHC, multiple inelastic proton-proton interactions may occur at the same time. Understanding this complex environment is essential for any analysis at the LHC. The event reconstruction algorithms, in particular those associated with the ATLAS Inner Detector (ID),

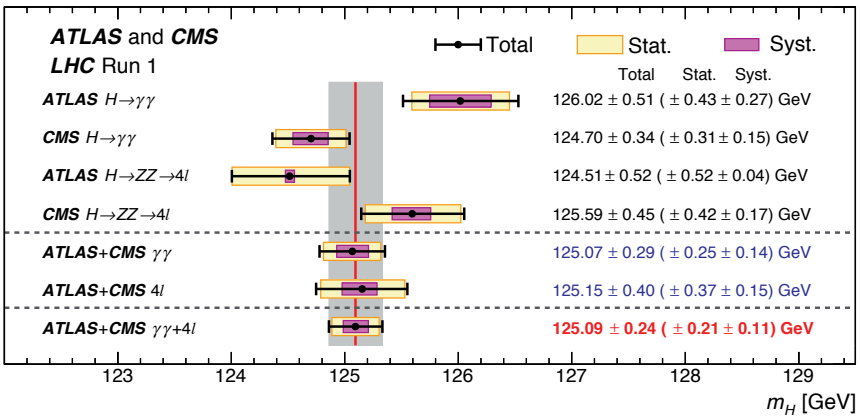

Figure 1: Summary of Higgs boson mass measurements from the individual analyses of ATLAS and CMS and from the combined analysis presented here. The systematic (narrower, magenta-shaded bands), statistical (wider, yellow-shaded bands), and total (black error bars) uncertainties are indicated. The (red) vertical line and corresponding (gray) shaded column indicate the central value and the total uncertainty of the combined measurement, respectively.

are studied in terms of physics and detector performance and computational efficiency. Optimizing the early stages of the pattern recognition yields a 30 % faster ID reconstruction, while maintaining the reconstruction efficiencies and resolutions for all physics objects in a high occupancy environment [19].

In the SM, the Higgs boson mass is not predicted by the theory. Instead, it must be determined experimentally from data. Prior to the turn-on of the LHC, Higgs boson masses below 114 GeV and in the range of 158 GeV to 175 GeV have been excluded by direct searches at LEP [1] and Tevatron [2], respectively. Global fits to precision EW data implied an upper limit on the Higgs boson mass of 158 GeV [3]. Combining the $H \to \gamma\gamma$ and $H \to ZZ^* \to 4\ell$ channels, in which the mass of the Higgs boson can be explicitly reconstructed from its decay products, and using the full LHC Run 1 collision data sets of the ATLAS and CMS experiments, the mass is now – virtually independent of SM assumptions – determined to an accuracy of 0.2 %. The measurement is summarized in Fig. 1. The total uncertainty is dominated by the sample statistics of the analyzed data set. The systematic uncertainty is dominated by effects related to the photon, electron, and muon energy or momentum scales and resolutions [22].

Having established the Higgs boson mass, all properties of the SM Higgs boson, such as its production cross section and partial decay widths, are predicted by the SM. This then allows to test the predictions against the recorded collision data. As an example, the sequential Higgs boson decay $H \to WW^* \to \ell\nu\ell\nu$, with the Higgs boson produced through gluon fusion

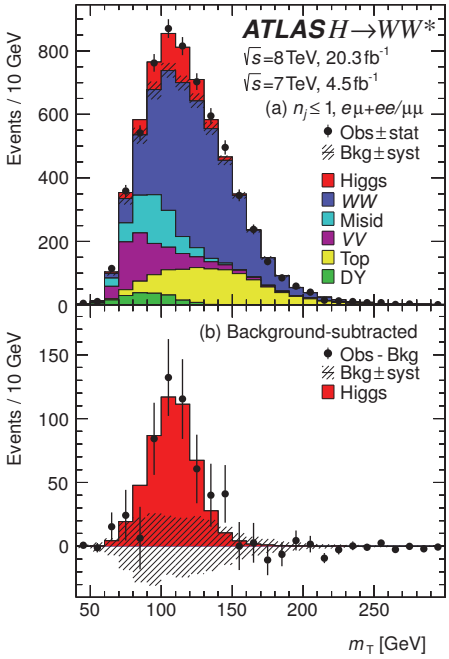

Figure 2: (a) Cumulative m_{T} distribution integrated over all lepton-flavor final states and $n_j \leq 1$ categories of the 7 and 8 TeV data sets after profiling all nuisance parameters. (b) Residuals of the data with respect to the total estimated background, compared to the predicted m_{T} distribution of a SM Higgs boson with a hypothesized mass of 125 GeV and scaled by the measured inclusive production strength. Although the reconstructed transverse mass m_{T} is not identical to the invariant mass m_H of the Higgs boson due to the unknown longitudinal momenta of the neutrinos in the final state, it has a kinematic bound at the true Higgs boson mass, smeared by the detector resolution.

(ggF) or vector boson fusion (VBF), is studied. For a Higgs boson with a mass of approximately 125 GeV, the decay mode is relatively abundant in the SM. The neutrinos produced in the signal process escape detection so that the final state can not be reconstructed fully, unlike $H \to \gamma\gamma$ and $H \to ZZ^* \to 4\ell$. To extract the Higgs boson properties, the categories enriched in signal events from gluon fusion employ a three-dimensional discriminant. The categories enriched in Higgs boson candidates produced through vector boson fusion make use of a Boosted Decision Tree (BDT), combining information about background rejection, the VBF topology, and the $H \to WW^* \to \ell\nu\ell\nu$ decay topology. To reduce the influence of simulation uncertainties of the many background processes on the signal estimate, the signal selections are augmented with control samples. The statistical data analysis is designed to estimate (almost) all background processes from data in regions that are kinematically close to the phase space enriched in signal events. These control selections have been optimized to simultaneously minimize the statistical uncertainty on the background estimate and the systematic uncertainties associated with the extrapolation of the background rates in the control samples to the signal regions. Figure 2 illustrates the results of the analysis. The local significance of the observed excess of events in data with respect to the background hypothesis is 6.1 standard deviations. The reported signal strength, $\mu = 1.09^{+0.23}_{-0.21}$, is the most precise measurement of its kind in a single decay channel, to date [30], despite the inability to explicitly reconstruct the Higgs boson invariant mass from its decay products.

Statistical data analysis is an important element of all physics analyses. In this context, a key part of the effort is the construction of probability models that can be fit to the data, where predictions are based on simulated data. Possible deformations of these distributions associated to known systematic uncertainties are introduced in these models through a technical procedure called template morphing. In this thesis a new non-linear moment morphing method is presented. It is fast, numerically stable, allows for the morphing of both binned histogram and continuous templates, has proper handling of both horizontal as well as vertical shifting distributions, and is not restricted in the number of input templates, the number of model parameters, or the number of input observables [20]. These features are of increasing importance for complex probability models with many systematic uncertainties. Moment morphing is applicable to many problems in modern particle physics and beyond because modeling of systematic uncertainties on distributions is a common issue in statistical analyses. The statistical analysis of the $H \to WW^* \to \ell\nu\ell\nu$ channel is among the first ones exploiting this new interpolation technique: in the absence of an analytical prediction of the probability density functions (p.d.f.s) used in the statistical data analysis at the LHC, the dependence on the Higgs boson mass is modeled continuously through moment morphing. The analysis of Higgs boson decays to four leptons ($H \to ZZ^* \to 4\ell$) by the ATLAS collaboration is an example for the use of moment morphing to model the variations of systematic uncertainties [24]. Moment morphing of n-dimensional distributions is also used in the context of Higgs boson spin and parity measurements in diboson final states by the ATLAS collaboration [33].

To shed light on the mechanism responsible for EWSB in the SM, precise measurements of all Higgs boson properties are required. Every theoretical extension of the SM alters the scalar sector of nature and exhibits distinct features that probe specific aspects of the SM. For the best possible analysis, a joint likelihood model is built. It comprises the detailed likelihood models of each of the individual channels, taking into account all systematic correlations. The statistical interpretation of the data combines knowledge of the phenomenology of Higgs boson production and decays, state-of-the-art advances in theoretical calculations, as well as a detailed understanding of all reconstructed physics objects used by the experiment.

The simplest model to describe the joint data is a variant of the SM that allows a different global signal strength of Higgs boson production, while keeping all other properties identical to the SM. The global signal strength relative to the SM expectation is measured to be $\mu = 1.18^{+0.15}_{-0.14}$, compatible with the SM hypothesis, and asymptotically corresponding to a significance of more than 10 standard deviations. Other interpretations of the data that allow different signal strengths for all known production mechanisms result in a strong evidence for Higgs boson production through vector boson fusion with a significance of 4.3 standard deviations. The analysis also supports the SM predictions of the Higgs boson production in association with a vector boson or a pair of top quark with a significance of 2.6 and 2.4 standard deviations, respectively [31].

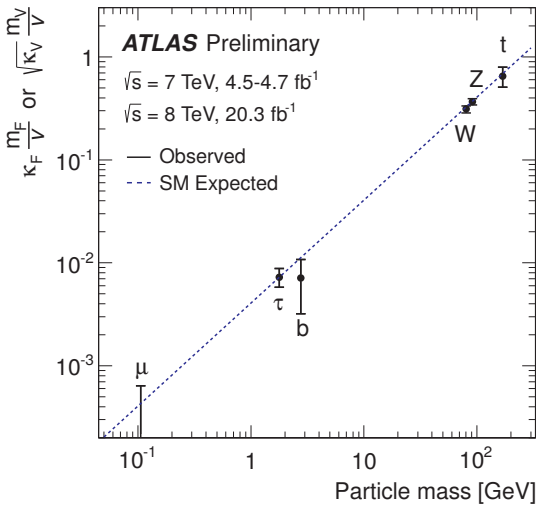

Figure 3: Fit results for the reduced coupling strength scale factors $y_{V,i} = \sqrt{\kappa_{V,i}\frac{g_{V,i}}{2v}} = \sqrt{\kappa_{V,i}}\frac{m_{V,i}}{v}$ for weak bosons and $y_{F,i} = \kappa_{F,i}\frac{g_{F,i}}{\sqrt{2}} = \kappa_{F,i}\frac{m_{F,i}}{v}$ for fermions as a function of the particle mass, assuming a SM Higgs boson with a mass of 125.36 GeV. The dashed line indicates the predicted mass dependence for the SM Higgs boson.

Beyond rate measurements of Higgs boson production modes, the observed production and decay rates are also interpreted in terms of modified Higgs boson coupling strengths, where the allowed modifications are parametrized following the degrees of freedom allowed in the leading order processes for Higgs boson production and decay [31]. This treatment allows to disentangle the effects of modified couplings in the production and decay, which occur in varying admixtures in the probed channels. The compatibility of the Higgs boson coupling strengths with the SM expectation is tested for a wide range of benchmark scenarios, building up on symmetries of SM. A variety of (physics-motivated) assumptions on the Higgs boson total decay width is studied. Depending on the choice of assumptions, the upper limit at 95 % confidence level (CL) on the branching fraction for invisible or undetected Higgs boson decays varies from 13 % to 68 %. Loop induced processes are used to indirectly search for new charged or colored particles. The effective coupling strengths associated with these processes are determined to an accuracy of approximately 10 % to 20 %, depending on the benchmark scenario. No significant deviations from the SM predictions are found. Under the considered benchmark models and for a wide range of assumptions, the compatibility of the data with the SM hypothesis is 29 % to 99 %. As an example, Fig. 3 shows the Higgs boson coupling strengths to μ and τ leptons, b and t quarks, and W and Z-bosons as function of the respective particle mass and illustrate the salient feature of the Brout-Englert-Higgs mechanism: the measured coupling strengths of particles to the Higgs boson are proportional to the observed masses of these particles.

Although the measured properties of the Higgs boson support the SM, and the SM is a viable perturbative description of physics phenomena up to the Planck scale, several fundamental questions are not answered satisfyingly. Among these are for example the hierarchy problem regarding the naturalness of the Higgs boson mass, the nature of dark matter, or the

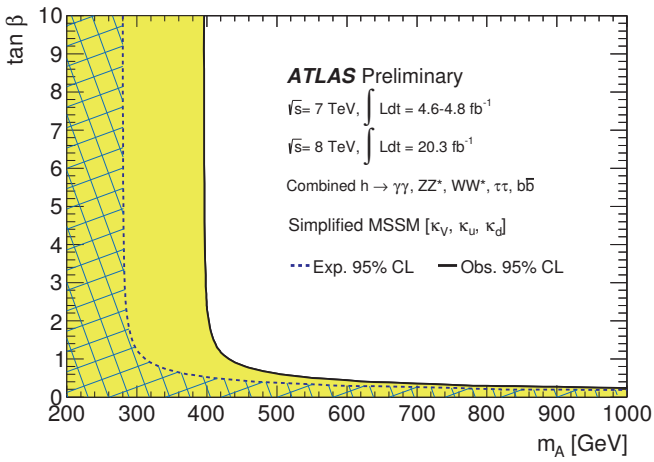

Figure 4: Regions of the hMSSM parameter space that are indirectly excluded at 95% CL or greater from a combined measurement of the Higgs boson production and decay rates. The regions expected to be excluded in case the scalar sector would be as predicted by the SM, are overlaid. The light shaded and hashed regions indicate the observed and expected exclusions, respectively. The indicated confidence intervals are constructed under the assumption that the test statistic $-2\ln\Lambda(m_A, \tan\beta)$ asymptotically is distributed as a χ^2 distribution with two degrees of freedom. The SM decoupling limit is at large m_A.

dynamical origin of EWSB. Many of the proposed solutions for these open questions have implications at the current energy frontier and predict modifications or extensions of the minimal scalar sector that is embedded in the SM. Some of the promising scenarios with fundamental physics beyond the SM are composite Higgs models, theories with two Higgs doublets, supersymmetry, and other models with a dark matter candidate. All these models make explicit predictions how the couplings of the observed 125 GeV Higgs boson deviate from the SM expectation. Tests with these model specific parametrizations are performed. Under certain assumptions, stringent limits on the model parameters associated with new phenomena are set [38]. These results possibly guide future direct searches for fundamental physics beyond the SM towards a discovery.

An example of a new physics theory that is constrained by measurements of properties of the observed Higgs boson is the Minimal Supersymmetric extension of the Standard Model. In this extension of the SM the scalar sector is represented by two doublet fields rather than one, which manifest themselves as five scalar particles: h, H, A, and $H^{\pm}$. In a simplified version of the theory [271, 272] the coupling properties of the light h boson depend only on two parameters: the mass of the heavy A boson and the mixing angle β of the light h and heavy H fields. Assuming the observed Higgs boson is the light state h of this theory, Fig. 4 shows the constraints on m_A and $\tan\beta$ that follow from the observed coupling properties of the Higgs boson in this simplified model.

Finally, the physics potential of the ATLAS experiment at the HL-LHC for measuring the Higgs boson production and decay rates and coupling strengths is studied. By the year 2022 the data sample recorded by the ATLAS detector is expected to correspond to an integrated luminosity of $300\,\text{fb}^{-1}$ at a collision energy of 14 TeV and increases to $3000\,\text{fb}^{-1}$ by 2035. The precision on the measured parameters is expected to significantly improve with increasing integrated luminosity, though advances both in the theoretical calculations and in the understanding of the detector are required to fully benefit from the upgrade program [52]. The possible synergies of the Higgs physics programs at the HL-LHC and the ILC are also studied. The two facilities are expected to complement each other with the HL-LHC having advantages in measuring decay modes with a low rate and other rare processes, and the ILC being ideally suited for determining the absolute Higgs boson coupling strengths.

university of groningen

Discovery of rare B decays

First observation of the $B_s^0 \to \mu^+\mu^-$ decay,
first evidence of the $B^0 \to \mu^+\mu^-$ decay

PhD thesis

to obtain the degree of PhD at the
University of Groningen
on the authority of the
Rector Magnificus Prof. E. Sterken
and in accordance with
the decision by the College of Deans.

This thesis will be defended in public on

Friday 8 April 2016 at 14.30 hours

by

Siim Tolk

born on 16 March 1987
in Tallinn, Estonia

Chapter 11

Summary and outlook

Modern physics successfully describes the structure and the processes of the microscopic world. According to the established theory of the microscopic world, The Standard Model (SM), the ordinary matter in the universe consists of six quarks and six leptons, and its dynamics is dictated by the forces between these constituents. In the SM, these forces are described by an exchange of force carriers, called bosons.

Even though successful in general, the SM does fall short in answering some important questions: little is known about the matter that constitutes the majority of the mass of the universe or why we live in a matter rather than anti-matter dominated universe. In search of these answers, physicists have come up with many clever solutions. The successful SM could be extended by postulating yet unseen New Physics (NP). For instance, these NP models can be built by postulating supersymmetric partners of the observed particles (SUSY), or additional Higgs-boson-like particles.

The NP models must be compatible with the verified SM predictions, while they may predict new measurable but yet unverified effects. Particle physics experiments look further than the already verified SM domain in various ways: reaching for higher collision energies, devising new more precise measurements of already observed processes, or searching for yet unobserved processes; in all cases, the effects in which the NP predictions can differ from the SM ones are of interest. The rare B_s^0 and B^0 meson decays into two muons (i.e. $B_{(s)}^0 \to \mu^+\mu^-$ in short) are a good example of a search for yet unobserved processes.

The results from the Large Hadron Collider (LHC) experiments at CERN have taken us closer to solving the big open problems. Perhaps the most memorable results of 2011 and 2012, the so called "Run 1", were the discovery of the Higgs boson [4, 5] and the first evidence of B_s^0 meson decays to two

muons ($B_s^0 \to \mu^+\mu^-$) [118], which were both long searched for. At the same time, several hints of discrepancy with the SM hold promises of new exciting results in the years to come.

The history of $B_{(s)}^0 \to \mu^+\mu^-$ searches over 30 years is shown in Fig. 11.1. This dissertation describes the $B_{(s)}^0 \to \mu^+\mu^-$ searches at the LHC. It explains why $B_{(s)}^0 \to \mu^+\mu^-$ decays are interesting from the theoretical perspective, how these decays were looked for in the LHCb experiment and what was found [58], and how the $B_{(s)}^0 \to \mu^+\mu^-$ analysis results from the LHCb experiment were combined with the $B_{(s)}^0 \to \mu^+\mu^-$ analysis results from another experiment, CMS. The parts to which the author has contributed personally are discussed in greater detail. In particular, these include improving the trigger efficiency estimation (Ch. 5), constructing the LHCb likelihood model (Ch. 6), normalising the LHCb signal yields (Ch. 7), fitting it to the data to obtain the results (Ch. 8), combining the LHCb and CMS likelihood models and obtaining the combined results (Ch. 10). As is shown in Sec. 10.3, the combination of the results leads to the first observation of the $B_s^0 \to \mu^+\mu^-$ decay and the first evidence of the $B^0 \to \mu^+\mu^-$ decay [43].

The rate at which the decays proceed is expressed through the branching fraction ($\mathcal{B}$). The $B_s^0 \to \mu^+\mu^-$ (or $B^0 \to \mu^+\mu^-$) branching fraction into a dimuon final state is the fraction of $B_s^0 \to \mu^+\mu^-$ (or $B^0 \to \mu^+\mu^-$) decays with respect to all the possible B_s^0 (or B^0) decays. The SM processes contributing to the $B_{(s)}^0 \to \mu^+\mu^-$ decays are well understood. In the SM, $B_{(s)}^0 \to \mu^+\mu^-$ decays are suppressed by the GIM mechanism and proceed through higher order loop diagrams (see Ch. 1 and Fig. 1.3). The SM B_s^0 and B^0 meson branching fractions to two muons are precisely predicted [41, 43]:

$$\mathcal{B}(B_s^0 \to \mu^+\mu^-) = (3.66 \pm 0.23) \times 10^{-9}, \tag{11.1}$$

$$\mathcal{B}(B^0 \to \mu^+\mu^-) = (1.06 \pm 0.09) \times 10^{-10}. \tag{11.2}$$

With these very low expected SM rates and loop processes dominating the transition, it is likely that NP, especially in models with extended Higgs sectors or additional bosons, significantly alters the $B_{(s)}^0 \to \mu^+\mu^-$ decay probability.

The main results of the LHC $B_{(s)}^0 \to \mu^+\mu^-$ searches are the measurements of the B_s^0 and B^0 meson branching fractions [43]:

$$\mathcal{B}(B_s^0 \to \mu^+\mu^-)^{LHC} = \left(2.78\,^{+0.66}_{-0.60}(\text{stat})\,^{+0.27}_{-0.18}(\text{syst})\right) \times 10^{-9} \quad (6.2\sigma), \tag{11.3}$$

$$\mathcal{B}(B^0 \to \mu^+\mu^-)^{LHC} = \left(3.94\,^{+1.58}_{-1.41}(\text{stat})\,^{+0.31}_{-0.24}(\text{syst})\right) \times 10^{-10} \quad (3.2\sigma). \tag{11.4}$$

The branching fractions and the significances are extracted from the combined CMS and LHCb likelihood model, shown together with the data in

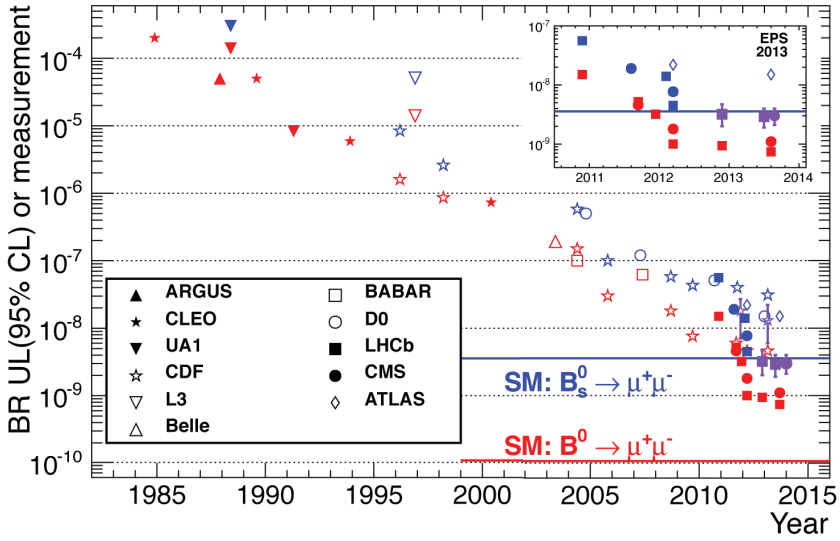

Figure 11.1: The long history of $B^0_{(s)} \to \mu^+\mu^-$ searches. The blue and red marks denote the results of the $B^0_s \to \mu^+\mu^-$ and $B^0 \to \mu^+\mu^-$ searches, respectively. Upper limits, set by various searches throughout the years, are shown together with the latest measurements by CMS and LHCb.

Fig. 11.2. The main contribution to the uncertainties is of statistical nature and can be reduced in the coming years. Compared to the total uncertainty, the systematic uncertainty amounts to 35% and 18% in the $B^0_s \to \mu^+\mu^-$ and $B^0 \to \mu^+\mu^-$ branching fractions, respectively. It arises from the signal normalisation, the mis-identified background yield estimation, and the di-muon mass model. The uncertainty in the measured hadronisation fraction ratio (f_s/f_d) from Ref. [113] is the dominant systematic uncertainty.

The impact of the $B^0_{(s)} \to \mu^+\mu^-$ measurements can be seen by comparing the excluded parameter space of various NP models before and after the LHC Run 1 results (see Fig. 11.3): with the results from LHC, a large part of the parameter space is excluded. Given the still large uncertainty, the current measurement is compatible with the SM predictions. However, the NP models tend to have complex parameter spectra and they can seldom be excluded by the measurement of a single observable. Sizeable NP contributions can still be present in other observables even if the measured $B^0_s \to \mu^+\mu^-$ branching fraction is close to the SM value. Therefore, future efforts have to be directed on one hand to improve the precision of the branching fraction measurements and on the other to measure additional observables.

The observation of the $B^0_s \to \mu^+\mu^-$ decay and the evidence of the $B^0 \to \mu^+\mu^-$ decay are the culmination of 30 years of experimental $B^0_{(s)} \to \mu^+\mu^-$

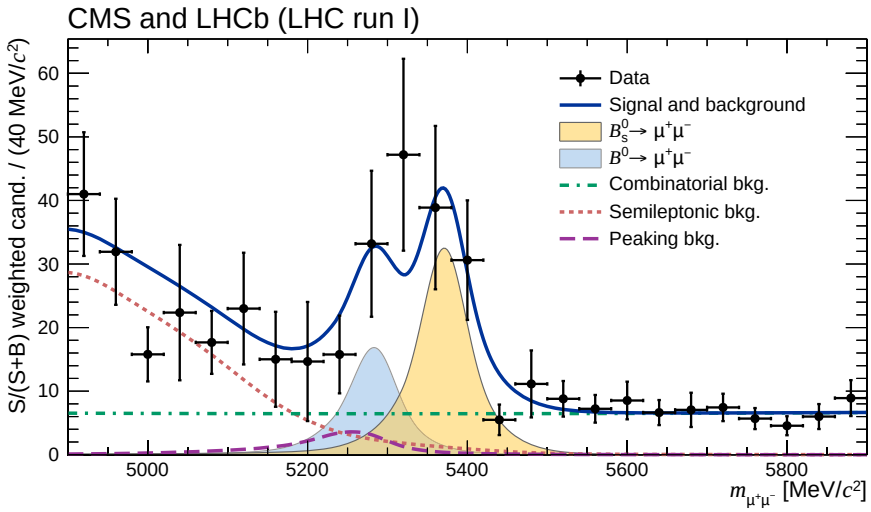

Figure 11.2: Di-muon invariant mass distribution of the $B^0_{(s)} \to \mu^+\mu^-$ candidates in the combined CMS and LHCb analysis. Superimposed on the data points (black dots) are the combined fit (solid blue line) and its components: the B^0_s (yellow shaded peak) and B^0 (light-blue shaded peak) signal components; the combinatorial background (dash-dotted green line); the sum of the semi-leptonic backgrounds (dotted pink line); and the peaking backgrounds (dashed violet line).

searches, and open the possibility of precise measurements of these channels. As pointed out in Ref. [129], the $B^0_s \to \mu^+\mu^-$ decay is a theoretically clean probe for the Wilson coefficient C^R_{10}. A more precise determination of this coefficient is mandatory in the light of several tensions in other decays involving $b \to s$ transitions, such as $B^0 \to K^{*0}\mu^+\mu^-$ [130], and $B^+ \to K^+\mu^+\mu^-$ and $B^+ \to K^+e^+e^-$ [131]; more stringent constraints on C^R_{10} are necessary in order to identify NP contributing to other Wilson coefficients, such as C^R_9. Moreover, the current best $B^0 \to \mu^+\mu^-$ branching fraction measurement is more than three times higher than what the SM predicts. This excess needs to be investigated and measured with a better precision.

More precise measurements will already be possible in the LHC Run 2. At the time of writing, the LHCb has recorded $0.32\,\text{fb}^{-1}$ of proton-proton collision data at $\sqrt{s} = 13\,\text{TeV}$ (equivalent to $0.5\,\text{fb}^{-1}$ at $\sqrt{s} = 8\,\text{TeV}$). The expected uncertainties for the future LHCb analysis are shown in Fig. 11.4. Two possible near-future scenarios for the $B^0_{(s)} \to \mu^+\mu^-$ studies in LHCb are shown in Fig. 11.5. Assuming the current analysis sensitivity, detector performance, and the measured $B^0 \to \mu^+\mu^-$ branching fraction, the LHCb experiment has

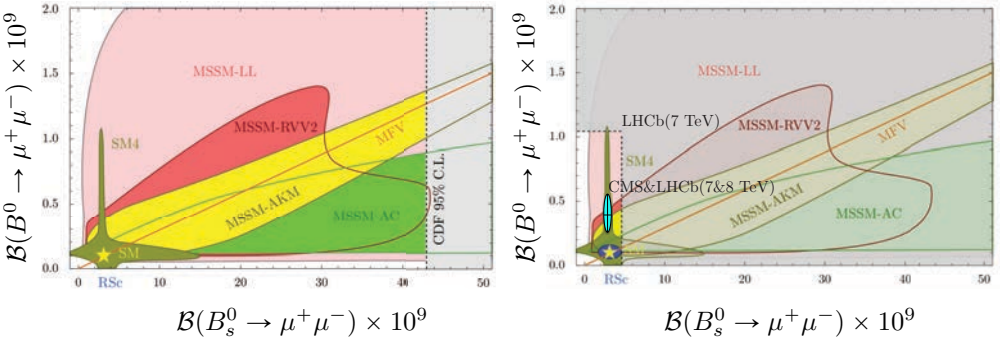

Figure 11.3: Allowed $B^0 \to \mu^+\mu^-$ and $B_s^0 \to \mu^+\mu^-$ branching fractions values on the $\mathcal{B}(B^0 \to \mu^+\mu^-)$ and $\mathcal{B}(B_s^0 \to \mu^+\mu^-)$ plane in different New Physics models. The Standard Model prediction is shown as a star. The shaded grey area on the left figure denotes the region experimentally excluded before the LHC results, the shaded grey are on the right figure denotes the region experimentally excluded by the LHCb $B_{(s)}^0 \to \mu^+\mu^-$ analysis with 2011 data [125]; the light blue ellipse on the right figure denotes the latest combined CMS and LHCb measurement [43].

a good chance to measure an evidence for a non-SM $B^0 \to \mu^+\mu^-$ branching fraction value! The possibility of an NP enhanced $B^0 \to \mu^+\mu^-$ branching fraction makes the $B^0 \to \mu^+\mu^-$ measurement the most awaited result of the next LHCb $B_{(s)}^0 \to \mu^+\mu^-$ analysis.

The impact of the $B_s^0 \to \mu^+\mu^-$ measurements has also been studied in models with tree-level contributions from different types of new particles [28, 29]. Such contributions could arise from new heavy vector bosons, as predicted in various Z' and Little Higgs models, or from new scalar or pseudo-scalar particles, as predicted in different types of two-Higgs doublet (2HDM) models (see Sec. 1.4, Fig. 1.8).

The current situation can be considerably improved by measuring an additional observable, the mass-eigenstate asymmetry in $B_s^0 \to \mu^+\mu^-$, $\mathcal{A}_{\Delta\Gamma}^{\mu^+\mu^-}$. At this moment, the size of the still allowed parameter space suggests that the pseudo-scalar Higgs (A^0) and scalar Higgs (H^0) dominated 2HDMs are less favoured by the measurement, and that models with new heavy gauge bosons, such as Z', are less constrained by the measurement. Together with a more precise $B_s^0 \to \mu^+\mu^-$ branching fraction measurement, the $\mathcal{A}_{\Delta\Gamma}^{\mu^+\mu^-}$ measurement will be an important future step in the $B_{(s)}^0 \to \mu^+\mu^-$ analyses. As suggested in Ref. [27], $\mathcal{A}_{\Delta\Gamma}^{\mu^+\mu^-}$ can be extracted from the lifetime distribution

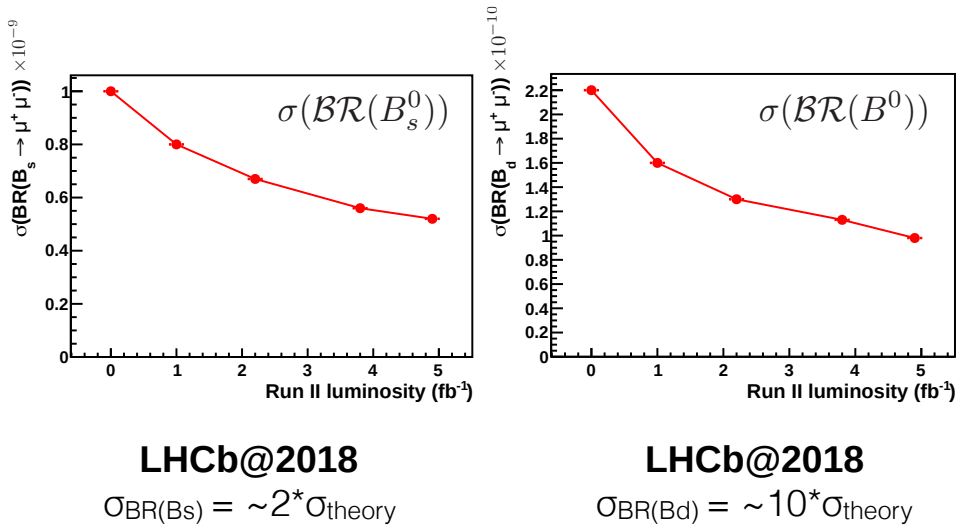

Figure 11.4: The expected uncertainties in the $B_s^0 \to \mu^+\mu^-$ (left) and the $B^0 \to \mu^+\mu^-$ (right) branching fractions, shown as a function of the pp collision data expected in the LHCb Run 2. The studies assume SM branching fraction values, and Run 1 analysis sensitivity and detector performance.

of the $B_s^0 \to \mu^+\mu^-$ decays. Depending on the result, a measurement of $\mathcal{A}_{\Delta\Gamma}^{\mu^+\mu^-}$ could distinguish between scalar, pseudo-scalar, and gauge boson exchange in $B_s^0 \to \mu^+\mu^-$ [27, 28].

In summary, the results of the $B_{(s)}^0 \to \mu^+\mu^-$ branching fraction measurements presented in this dissertation, have had a significant impact in the search of NP, reducing a large part of the parameter space of NP models. The improvement in the measurements expected in the coming years, as well as the possibility of measuring new observables such as $\mathcal{A}_{\Delta\Gamma}^{\mu^+\mu^-}$, hold promises of new exciting results and will be a strategical goal of the LHCb experiment.

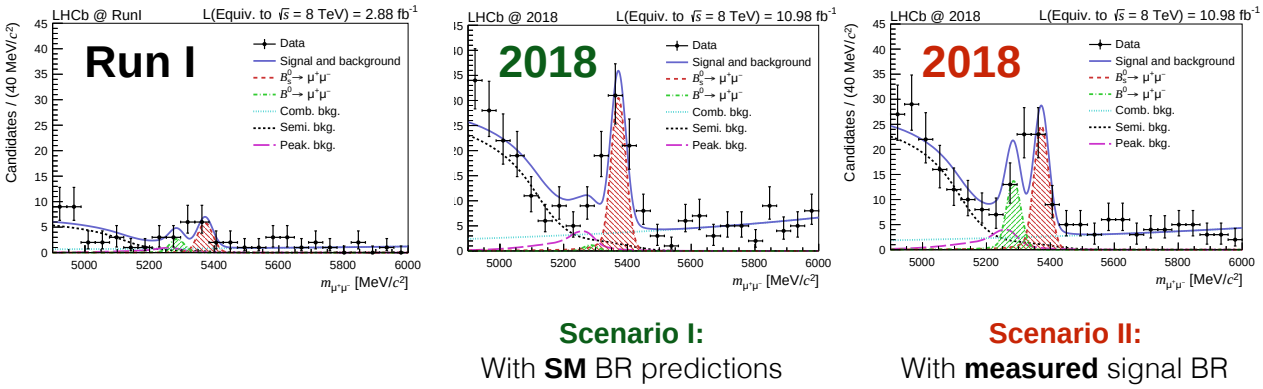

Figure 11.5: The invariant di-muon mass distribution in the LHCb $B^0_{(s)} \to \mu^+\mu^-$ analysis on Run 1 data sample (left), and on the simulated data samples expected to be collected by the LHCb at the end of 2018, shown for the SM $B^0_{(s)} \to \mu^+\mu^-$ branching fraction hypothesis (middle), and the measured branching fraction hypothesis (right). The simulated data samples include the Run 1 sample, and assume the Run 1 detector performance and analysis sensitivity.

Character Profile of the Higgs Boson

ACADEMISCH PROEFSCHRIFT

ter verkrijging van de graad van doctor
aan de Universiteit van Amsterdam
op gezag van de Rector Magnificus
prof. dr. ir. K.I.J. Maex
ten overstaan van een door het College voor Promoties ingestelde commissie,
in het openbaar te verdedigen in de Aula der Universiteit
op vrijdag 22 september 2017, te 11:00 uur

door

Lydia Brenner

geboren te Utrecht

S Summary

Elementary particle physics describes and measures the properties of the smallest, most fundamental particles that make up the universe. The Standard Model of elementary particle physics (SM) provides a fundamental description of particles, their dynamics and interactions. The particles embedded into the theory are, a priori, massless, while observed particles have mass. In order to explain the origin of the elementary particle masses, the Brout-Englert-Higgs mechanism is introduced. The complex Higgs field introduces a spontaneous breaking of the electroweak (EW) gauge group when it acquires a non-vanishing vacuum expectation value. The Brout-Englert-Higgs mechanism introduces the existence of one real scalar field, with the Higgs boson as excitation, however it does not predict its mass. To verify that the Higgs mechanism is the origin of elementary particle masses is one of the main goals of the Large Hadron Collider (LHC) programs at CERN.
Before the start of the LHC, there was no experimental evidence of the existence of the Higgs boson, and limits on the Higgs boson mass were set by the Large Electron-Positron Collider (LEP) [1] and Tevatron [2]. The Higgs boson masses below 114 GeV and in the range of 158-175 GeV have been excluded by these experiments. The first run of the LHC (Run 1), which collected data between 2010 and 2012, discovered a new particle of a mass around 125 GeV in 2012 [3, 4]. Precision measurements of the Higgs boson properties are ongoing in the second run of the LHC (Run 2) with an increased beam energy.

This thesis gives an overview of the precision measurements of the Higgs boson properties, with reinterpretations of the Run 1 results, results of the ongoing Run 2 and prospects for the full second run and the High Luminosity LHC (HL-LHC).

With the measured mass of the Higgs boson, all other properties of the SM Higgs boson, such as its production cross section and decay widths, are predicted by the SM. In the ongoing second run of the LHC (Run 2) the couplings of the Higgs boson are further studied, including the production cross sections and decay widths. The measured total $pp \to H$ cross sections measured in Run 1 and Run 2 are summarised in figure S.1. No significant deviation from the Standard Model predictions is observed.

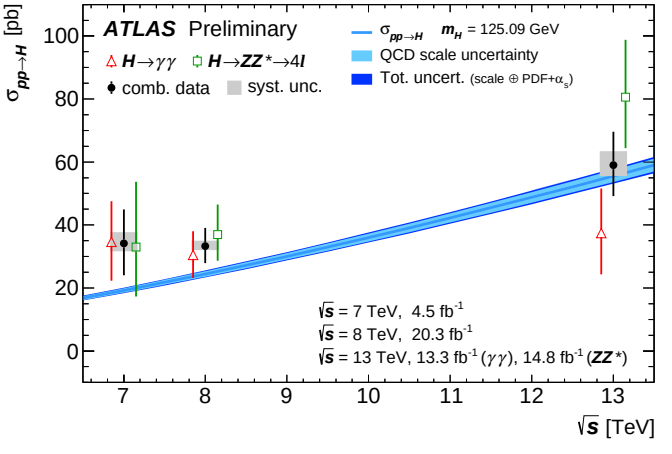

Figure S.1: Total $pp \to H$ cross sections measured at different centre-of-mass energies, compared to SM predictions at up to N^{3}LO in QCD. The grey bands on the combined measurements represent the systematic uncertainty, while the black lines are the total uncertainties. The light blue band represents the QCD scale uncertainty and the dark blue band represents the total uncertainty on the theory prediction, assuming a Higgs boson mass of 125.09 GeV.

The expected improvement on the measurement of the coupling of the Higgs boson to vector bosons, κ_V, and the coupling to fermions, κ_f, is shown in figure S.2. The improvements at high luminosity compared to Run 2 are a factor of 2-3, particularly without the inclusion of the current theoretical systematic uncertainties. The scenario without systematics is included as a benchmark, since systematic uncertainties are expected to improve in the future, but no firm prediction exists on the expected rate of improvement.

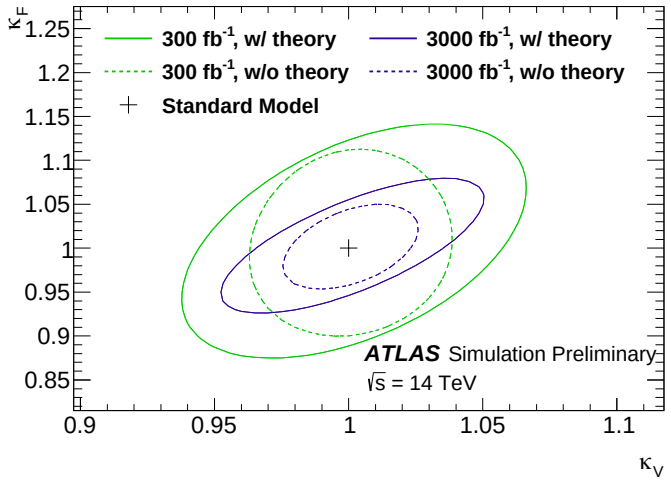

Figure S.2: 68% CL expected likelihood contour for κ_V and κ_f in a minimal coupling fit at 14 TeV for an assumed integrated luminosity of 300 fb^{-1} and 3000 fb^{-1}.

Even with the discovery of the Higgs boson, the SM is not a complete theory of nature, as it does not answer several fundamental questions satisfactory. Proposed solutions for open questions often predict modifications or extensions of the minimal scalar sector that is embedded in the SM. Models with fundamental physics beyond the SM, such as composite Higgs boson models, theories with two Higgs doublets, Supersymmetry (SUSY) and models with a dark matter candidate, make predictions for modified couplings of the observed Higgs boson with a mass around 125 GeV. Data coming from the detectors of the LHC can be compared with these Beyond the Standard Model (BSM) theories.

The studies of the tensor structure of the Higgs boson couplings to gauge bosons are based on signal models including at most one or two beyond-the-standard-model couplings contributing at a time, with all remaining Beyond the Standard Model (BSM) parameters set to zero. For Run 2, it is envisioned to have signal models which depend on a larger number of coupling parameters simultaneously considered. These coupling parameters in the Higgs coupling to SM particles change the predicted cross section, as well as the shape of differential distributions. In this context, it is necessary to revise the existing signal modelling methods that only modify signal rates and provide alternatives which are better suited to describe both signal rate and shape changes in a n-dimensional parameter space. For this purpose, a morphing method has been developed and implemented. It provides a continuous description of arbitrary physical signal observables such as cross sections or differential distributions in a multidimensional space of coupling parameters. The morphing-based signal model is a linear combination of a minimal set of orthogonal base samples (templates) spanning the full coupling parameter space. The weight of each template

is derived from the coupling parameters appearing in the signal matrix element. A simplified illustration of the morphing procedure is shown in figure S.3.

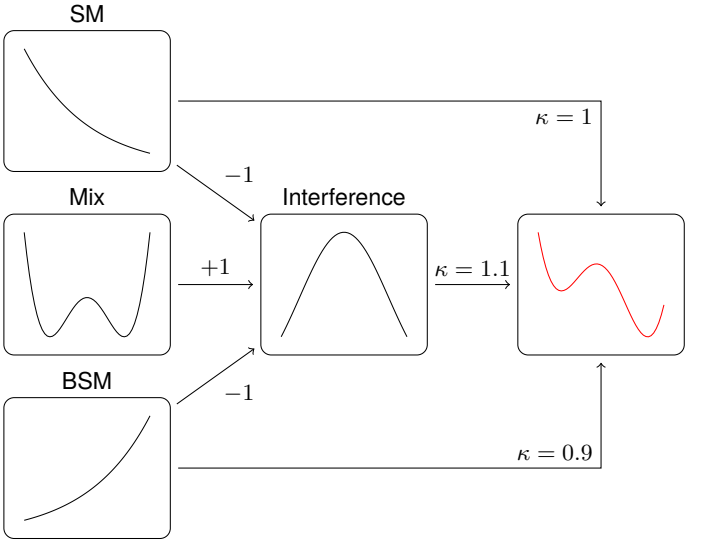

Figure S.3: Illustration of the morphing procedure in a simple showcase.

The morphing method has been shown to perform as expected using generator-level and reconstruction-level distributions. In addition, a preliminary study on the impact of BSM coupling parameters in the context of VBF Higgs boson production has been performed, acting both as a proof-of-concept for elaborate studies using this method and as a showcase for the performance of the morphing method. This method is capable of continuously morphing signal distributions and rates based on a minimal orthogonal set of independent base samples. Therefore it allows to directly fit for the coupling parameters that describe the SM and possibly non-SM interaction of the Higgs boson with fermions and bosons of the SM.
A method for optimising the sample basis has been proposed which could reduce the error arising from statistical precision of the input samples.

Within the Standard Model (SM) the Higgs must be a CP even scalar, a spin 0 particle. However, many BSM theories predict the existence of additional Higgs bosons which can be CP even, CP odd, or, as a result from the superposition of CP eigenstates, partially violating the CP symmetry. With the data collected at the ATLAS detector during Run 2 of the LHC it is possible to measure the CP properties of the coupling of the Higgs boson to top quarks for the first time. To reveal the CP structure of the Higgs boson coupling to top quarks, CP sensitive observables have to be considered to perform a direct measurement. Due to the conservation of angular momentum, a particularly promising CP sensitive observable is the azimuthal angle between two final state jets ($\Delta\Phi_{jj}$). As a result gluon-gluon fusion accompanied by two jets will be a very promising channel in which the CP structure of the Higgs boson coupling to top quarks can be measured [162]. Using the morphing method described in this thesis, a direct measurement is performed on the sensitivity of mixing angle α between a CP even and a CP odd Higgs boson. The expected result of this measurement is shown in figure S.4.

Higgs boson coupling measurements from the combination of multiple production and decay channels have been used to indirectly search for new physics. The results are based on up to 4.7 fb^{-1} of pp collision data at $\sqrt{s} = 7$ TeV and 20.3 fb^{-1} at $\sqrt{s} = 8$ TeV recorded by the ATLAS experiment at the LHC. No significant derivation from the SM expectation is found in the observables studied, which are used to constrain various models of new phenomena. Projections have been derived for 300 fb^{-1} and 3000 fb^{-1} of pp collision data at $\sqrt{s} = 14$ TeV expected to be collected by the ATLAS experiment, assuming the data follows the SM expectation. Figure S.5 shows as an example the region of the parameter space of a two Higgs doublet model that can be excluded with 300 fb^{-1} and 3000 fb^{-1} of data, assuming the data follows the expectation of a standard model Higgs boson.

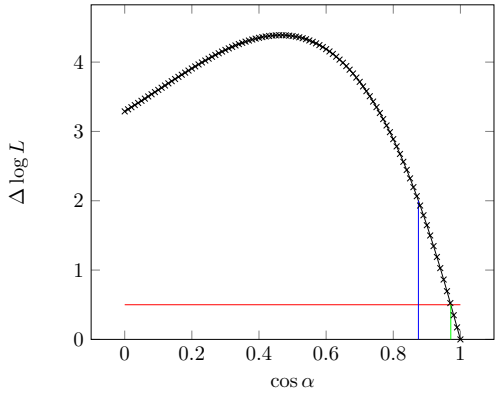

Figure S.4: Scan of the mixing angle, $\cos\alpha$, for an Asimov dataset created for a SM CP even Higgs boson. The mixing angle, $\cos\alpha$, mixes between a CP even and CP odd Higgs boson of the coupling of the Higgs boson to top quarks.

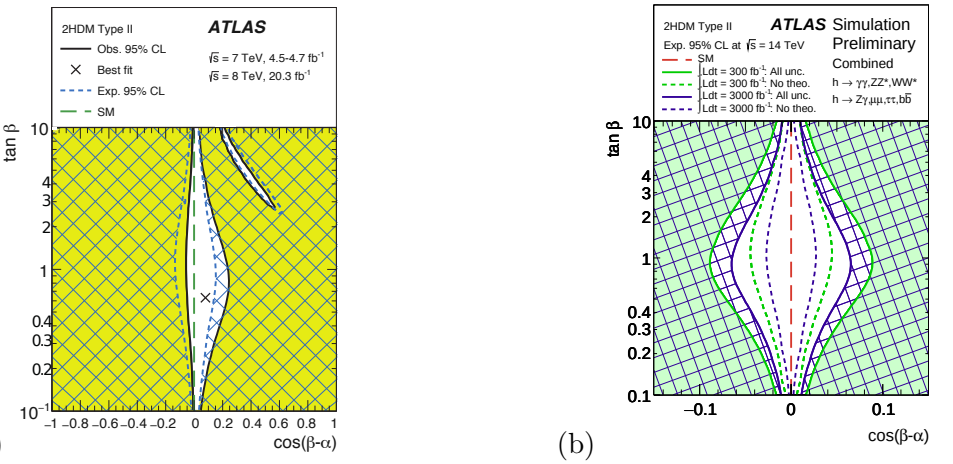

Figure S.5: Regions of the $(\cos(\beta-\alpha), \tan\beta)$ plane of a model with an additional Higgs doublet, where α is the angle between a CP even and CP odd Higgs boson and β is the ratio of the vacuum expectation values of the two Higgs boson. (a) Shows the excluded region by fits to the measured rates of Higgs boson production and decays and (b) shows the expected region to be excluded by fits to the measured rates of Higgs boson production and decays. The confidence intervals account for a possible relative sign between different couplings. The expected likelihood contours where $-2\ln\Lambda = 6.0$, corresponding approximately to 95% CL (2σ), are indicated assuming the SM Higgs sector. The light shaded and hashed regions indicate the observed and expected exclusions, respectively.

Higgs physics at the ATLAS detector has reached an exciting new phase of precision measurements, but the analyses are still mostly set up for conducting searches. The research shown in this thesis has provided measurements in the Higgs sector, placed limits on new physics, and, with the Analytic Lagrangian Morphing tool, opened the door for precision measurements of Higgs physics at the LHC. Searches for extensions to the standard model can be performed with this tool, and will provide accurate possible predictions for any Standard Model and beyond the standard model parameters. Whilst this technique for analytic morphing is becoming widely accepted within the ATLAS Higgs group and was included in the recommendation in the Handbook of LHC Higgs Cross Sections (Yellow Report 4) [6], it can also be used within searches for BSM contributions to top-quark physics, precision measurements of EW processes and for measurements of processes such as triple gauge couplings. An exciting, interesting and productive new phase of precision measurements in Higgs physics at the ATLAS detector has started.

Running in the early Universe

UV sensitivity of single-field inflationary models

Academisch Proefschrift

ter verkrijging van de graad van doctor

aan de Universiteit van Amsterdam

op gezag van de Rector Magnificus

prof. dr. ir. K.I.J. Maex

ten overstaan van een door het College voor Promoties

ingestelde commissie,

in het openbaar te verdedigen in de Agnietenkapel

op donderdag 25 oktober 2018, te 12.00 uur

door

Jacopo Fumagalli

geboren te Cremona, Italië

Summary

In the next lines I will try to explain why I dedicated almost 4 years of studies to a phenomenon that presumably lasted 10^{-33} (zero comma thirty-two zeroes and then a one) seconds,[1] and that we think happened 13.8 billion years before this thesis was written.

Panku the giant

"[...] his sweat became rain and dew, meanwhile, all the stars in the sky were born from his hair. In this way, Panku, the giant, made the World."

(Chinese creation myth)

Since cultures exist, Homo Sapiens has always wondered what's behind the origin and the appearance of the Universe in which he ended up. In every civilization, myths served to this need. They contained the answers to these questions.

The difference between the last hundred years and the previous 70 thousand is that in the last century these questions can be answered scientifically. This means that we first have to admit our ignorance. Then we start building a story about our Universe based on equations and mathematical models. The story usually makes some predictions on what telescopes and satellites are going to observe. Every time an observation confirms a small piece of the story, we start to trust it a little bit more. Ultimately we have a theory which represents our most up-to-date version of reality (but which is still falsifiable).

Let us consider the theory of Big Bang. In 1927 a Belgian priest and astronomer, Georges Lemaitre, applied the equations of the new theory of gravity (general relativity) to the entire Universe. The result was surprising: the Universe might

[1] The exact values are model dependent but the orders of magnitude are always similar.

be expanding.[2] Two years later Edwin Hubble, an American astronomer, finalized a series of observations from which he concluded that all the galaxies are moving away from us. Remarkably, he noted that the further the galaxy the higher was its recession velocity. The observations made by Hubble led to a simple and possible conclusion: the Universe is expanding. It is not hard to understand why. Consider a panettone, an Italian Christmas "cake" which contains raisins. The panettone is the Universe while the raisins are the galaxies (see picture). Consider three raisins A,B and C. At a given time A and C are separated by a length which is two times the distance between A and B. If after an hour the panettone has rises doubling its dimensions, than A and C will move apart with a speed which is two times the velocity with which A and B are separated.

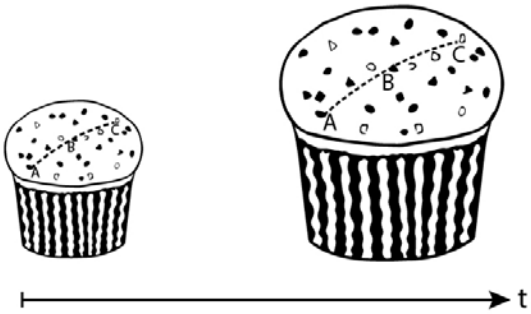

A panettone as an expanding Universe. The three raisins A,B and C are three galaxies.

An expanding Universe has a logical consequence: there should be a moment in the past where everything was close and packed into a small volume with high density and temperature, the so called Big Bang.

Today, the notion of a Universe that is expanding from a point with high density is taken for granted. In order to understand why the result was completely unexpected at that time we have to look back and think as an astronomer at the beginning of the twentieth century. If you were born at that time, everybody around you, from the priest to the most respected scholar, once questioned on the issue, would have replied that the Universe was something static. In the end, by contemplating every day and every year the same celestial dynamics you would have agreed. For two thousand years, Aristotle's view prevailed that the Universe was eternal and immutable, with no beginning. Even if scientists had overcome most of Aristotle's ideas, they were still happy with an eternal Universe. This

[2] In his original paper (in French), Lemaître collected the few data available at that time which roughly supported his idea. Laimatre himself chose to omit them from the translated English version after the publication of the more complete results of Hubble.

saved them from speculating about what causes its beginning. Even those who believed that the Universe had a beginning were still persuaded that from the creation onwards nothing had been changed. Einstein himself, not exactly a conservative, after realizing that his theory led to an expanding Universe decided to introduce an additional term to his equations, the so called cosmological constant, in order to obtain a static Universe aligned with his beliefs. Later on Einstein declared this was one of his worst mistakes.[3] In short, the Hubble's revolutionary observations had a counterpart in Lemaître's theoretical derivation. Is this enough to conclude that we are still observing the consequences of a Universe that has started is expansion from a very hot and dense state?

No. A scientific theory able to explain one observation can be easily replaced by an alternative description (for example the "steady state model" was popular at that time). This is true in particular if the world view offered by the theory is in contrast with all beliefs of its epoch. The moment in which scientists started to take seriously the Big Bang hypothesis is when they realized that the same description had new implications that could be tested. In 1948, physicists Alpher and Gamow showed that the abundance of hydrogen and helyum could be explained by the Big Bang hypothesis. Moreover, together with another physicist, Herman, they made a new prediction: if the Universe evolved from a primordial hot and dense state, the expansion and subsequent cooling led to an inescapable fact: it must exist a ubiquitous radiation, the so called *Cosmic Microwave Background* (CMB). The observation of the CMB is now considered the biggest evidence in favour of the Big Bang as well as fundamental for the work of this thesis.

When the Universe was about 380 thousand years old, the temperature had decreased enough such that free electrons in the primordial plasma were caught by the protons to form hydrogen atoms. As a result, photons, the light particles, no longer scattered with this sea of electrons anymore, but they were allowed to propagate freely for the first time. Some of these photons reach our Earth today after a journey 13.8 billion years long. This is the Cosmic Microwave Background. It is as if the Universe was permeated by a dense fog in the past. At a given time the fog disappeared and the light started to travel freely from every point and in all directions. Photons coming from regions close to us have reached us in the past while the ones further away reach us today. Thus, these photons show us how the Universe looked like when the "fog" disappeared 380 thousand years after the Big Bang.

[3] Recently (1998), from the observations of type Ia Supernovas, it has been discovered that our Universe is undergoing a phase of accelerating expansion. This can be explained by adding the cosmological constant to Einstein's equations. Thus, it seems that Einstein was meant to introduce futuristic concepts even when he made mistakes.

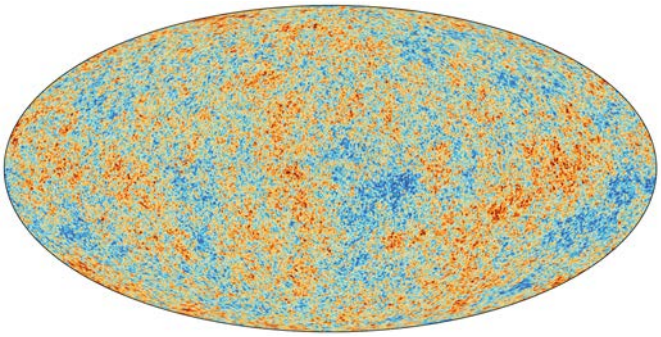

The CMB is the oldest light reaching our telescopes. It surrounds us as a sphere at the edge of our observable Universe. The figure shows the projection of this sphere where temperature fluctuations have been highlighted. These correspond to regions of slightly different densities at the time the Universe was 380 thousand years old.

In 1964 in New Jersey, two physicists working for a telecommunications company, Arno Penzias and Robert Wilson, were experimenting with an antenna to capture astronomical radio signals. In the same way as one tries to tune to a radio station but an annoying noise mumbles in the background, there was an interference bothering their apparatus. They tried everything to get rid of this noise, they even cleaned up the excrements of some pigeons who nested on the antenna. After a year of attempts they called their colleagues in Stanford. Their perseverance has led them to a Nobel prize worthy discovery: the noise captured was the Cosmic Microwave Background.

The CMB bombards us from all directions with photons of the same temperature. Today we know with high precision that the CMB temperature is 2.73 K (about -270 ° C) plus or minus tiny variation of the order of 0.000001 K.[4] We will get back to those fluctuations later. If different regions share the same information (in this case the temperature), it is reasonable to assume that there was a moment in the past where they have interacted. Two photons reaching the Earth from two opposite directions traveled 13.8 billion light years each. Without taking into account the expansion of Universe, this means that these two photons were separated by a distance greater than 27 billion light years when they start their journey. The contradiction is clear. How is it possible that regions so widely displaced could have interacted if the Universe was only 380 thousand years old at the time the CMB was emitted?

One could argue that, maybe, at the beginning of its expansion the Universe was

[4] As a consequence of the expansion of the Universe, these photons reach us after loosing most of their energy.

A tiny fragment of the primordial Universe inflated resulting in our observable Universe.

already in a homogeneous state. This is an assumption or a tweak (fine-tuning) on the initial conditions that physicists do not like to consider. I will use a metaphor to persuade the reader that this is more than a whim. Suppose that in an exam with a huge number of participants, let us say[5] 10^{60}, everybody gets the same score. Would you think that the attendants received a common hint before the exam or that the result is just a coincidence?

An impressive expansion

In 1980 Alan Guth, an American cosmologist, proposed a simple solution to solve the homogeneity puzzle: well before reaching its first second of life, our Universe underwent an exponential expansion, growing by a factor 10^{26} within a fraction of a second. In order to appreciate this number one can think that in proportion it is as if the Universe expanded, in a fraction of a second, from the dimensions of a bacteria (10^{-6} m) to 100 times the dimensions of our galaxy (the Milky Way has a diameter which is roughly 100 thousand light years $\approx 10^{20}$ m).

This impressive expansion, called *cosmic inflation*, inflated a tiny fragment of the primordial Universe to what now is our observable Universe, which is thus homogeneous. Still, it is legitimate to ask whether this is enough to be confident that the first second of our Universe has been characterized by such an impressive expansion? Most likely, this would have not been enough to explain the great popularity the theory has today. Even if inflation was introduced to solve the problem mentioned above, its big success lies in the fact that a period of inflation can explain, in a simple and elegant way, another observation: our Universe has

[5]The number is obviously bigger than the world population, but these are the number of causally disconnected regions with the same temperature in the CMB.

small inhomogeneities such as our galaxy or our planet.

Let's back up. Thanks to the contribution of different satellites today we know that the CMB temperature is *almost* homogeneous. Remember the tiny variation of the order of 0.000001 K? It means that, at the time the CMB was emitted, some regions were slightly colder than the average. This implies that in these regions gravity was a little bit stronger than the average. Over there, matter starts to accumulate growing little by little under the effect of gravity. The subsequent evolution creates the structures we observe in the Universe today.
But how is this all related to inflation?

Well, a period of inflation provides a mechanism that explains in a rather surprising fashion, how the tiny temperature variation of the CMB originates. In order to have an idea of how this mechanism works we introduce a couple of concepts that will also be helpful later on. Thus, the patience of the reader will be rewarded twice. Quantum mechanics, the branch of physics that studies the microscopic world (sizes comparable to atomic distances), teaches us that there is always an unremovable uncertainty in the amount of energy present in a system. From this uncertainty and from the famous Einstein formula $E = mc^2$, two particles can be created out of the vacuum for a short period of time. Thus, it is advantageous to picture the vacuum not just as empty space, but as if it is full of particles continuously arising and annihilating. During a period of exponential expansion like inflation, these fluctuations are stretched and amplified until scales able to influence the gravity of the macroscopic world. Mukhanov, Starobinsky and Hawking first showed independently how the fluctuations generated during inflation have a counterpart in the tiny temperature variations of the CMB. Therefore, the inflationary hypothesis provides us with the exciting possibility to relate what we observe in the sky with what could have happened a fraction of a second after the Big Bang.

Everything looks beautiful so far, however, we are still not able to bring a satisfactory answer to the following question: who or what was responsible for such an impressive expansion? Since inflation was introduced hundreds of models and possible scenarios have been proposed. Each model describes the dynamics of the inflaton, the particle (or more general, the physical mechanism) responsible for inflation. This provides precise predictions for the properties of the CMB (such as the size and the distribution of the temperature fluctuations) that can be tested by observations.[6]

The approach mainly considered in this thesis is based on Ockham's razor. In order to be the inflaton a particle needs to have a certain intrinsic property. The only

[6]The equations describing this mechanism have been briefly summarized in chapter one.

particle with this property, that has been proved to exist, is the Higgs boson which was discovered in 2012 at the particle accelerator of CERN in Geneva (LHC). A minimal approach suggests the Higgs boson as a candidate to be the inflaton and models in this direction have been proposed. Despite that the energy scales at the LHC are high (of the order of thousands of electron-volts), these are still ten orders of magnitude lower than the typical energy scale relevant during the inflationary era. The question now arises: If we know only the properties of the Higgs boson at low energy, how can we describe its behaviour at the inflationary scales and make reliable predictions about the CMB?

Running in the early Universe

The motivation behind this thesis is to relate what we observe in telescope and with satellites (the properties of the CMB) to the Higgs parameters measured at CERN. These parameters, called coupling constants, are the equivalent of the electric charge for an electron.

Let us remember what we have just learned: given an inflationary model this provides predictions for the features of the CMB. However, we cannot simply describe the dynamics of inflation with the parameters measured at low energy for a reason that might seem counterintuitive: the value of the parameters change with the energy. The coupling constant are not really constant!

In order to understand this concept consider the electric charge. This parameter measures the repulsion strength between two electrons. Approximately, we can think to measure this charge by shooting an "electron probe" towards another electron and observe the following bounce. Do you remember that the vacuum is not exactly empty? The same is true for the space surrounding the electron. It is more like a boiling pot with particles and antiparticles (with opposite charge) that are created and disappear. These restless vacuum fluctuations form a cloud around the electron that "screens" the electric charge. In our experiment, the higher the energy of the probe electron is the "more deeply" it will penetrate in the cloud. In this way it will "feel" a different charge.

To be able to make predictions about the CMB, the Higgs parameters are the ones that we would have liked to determine during the period of inflation (at high energies), but since we were not in a position to do so at that time, we have to find a way to derive them from our experimental results found at lower energies. One of the main goal of this thesis has been to understand how the parameters change by increasing the energy, in physical language they *run*, until the typical energy scales of the primordial Universe. Thus, we have studied the *running in*

the early Universe.

In particular, in chapter 3 we analyzed in detail the most popular model in which the Higgs is the inflaton, so-called Higgs inflation. We asked if the predictions of this model for the CMB are consistent with a rigorous study of the running of the parameters. In computing how the parameters run across many orders of magnitude another aspect has to be carefully taken into account. Well above the energy tested in our experiments new particles or new phenomena that we do not know at the moment (in short we refer to them with the name *new physics*) may turn up (remember $E = mc^2$). This new physics will participate as well in the "dance" of the vacuum fluctuations. As a consequence, the running of the parameters can be affected. Thus, it has been necessary to properly parameterize the effects of new physics. What we have discovered is that, surprisingly, the predictions are independent of the contribution of new physics and in perfect agreement with the observations of the Planck satellite.[7]

In chapter 4 we have extended the previous result to a broader class of inflationary models. Setting aside Ockham's razor for a moment, we show that the mathematical structure of these models (of which Higgs inflation represents a particular case) guarantees the robustness of their predictions once the running of the parameters is taken into account.

Finally, in chapter 5, we have considered an alternative to Higgs inflation, simply labeled as new Higgs inflation, which does not belong to the class studied in chapter 4. By tracing back the history of our Universe, we show that the predictions of this model are sensitive to the running of the couplings. This weakens the predictivity of this model but also shows its sensitivity to new physics which thus can be probed. The main goal of this last chapter was to show that in general the running of the parameters is fundamental to sensibly compare a model to the data.

It is interesting to note that the main motivation behind building Higgs inflationary models was the request for minimality: to avoid introducing in our theoretical model additional physics and particles. However, as our analysis shows (as well as other studies on the subject), the introduction of new physics is somehow unavoidable to consistently explain how present-day particle physics is related to the physics of inflation. For physicists this is not necessary bad news. Usually we are happy when we realize that what we know is not everything there is to know.

Is it not true that by admitting our ignorance this story has begun?

[7] More precisely, unless the effect is so strong that a period of inflation is precluded, the predictions for Higgs inflation remain stable against the contribute of new physics. That's the reason for the title "UV (in)sensitivity of higgs inflation".

VRIJE UNIVERSITEIT

Substantiating the void

Strong-field tests of general relativity
with the first direct detection of gravitational waves
and
Fast likelihood evaluations for future tests

ACADEMISCH PROEFSCHRIFT

ter verkrijging van de graad Doctor aan
de Vrije Universiteit Amsterdam,
op gezag van de rector magnificus
prof.dr. V. Subramaniam,
in het openbaar te verdedigen
ten overstaan van de promotiecommissie
van de Faculteit der Bètawetenschappen
op woensdag 7 februari 2018 om 11.45 uur
in de aula van de universiteit,
De Boelelaan 1105

door

Jeroen Meidam

geboren te Oss

The common thread of the research presented in this thesis is performing tests of the strong-field dynamics of the theory of general relativity using gravitational waves. The main goal of this summary is to make sense of the previous sentence.

I will explain these concepts to the interested reader that does not have background in physics and perhaps for those who simply wish to refresh their memory. The theory of general relativity can be rather counter-intuitive and I will only be able to skim its 4-dimensional surface, so please forgive me for being brief on such a widely fascinating and complex topic.

Relativity

Before we get into general relativity (GR) we should first refresh our knowledge of the theory of relativity itself; a theory that everyone is familiar with whether they realize it or not.

First we will need to get some terminology out of way. When I speak of a frame of reference (sometimes I will just say "frame"), think of it as an observer performing his or her physics experiment. A frame of reference is always indicated by 3 spatial coordinates, a time coordinate and possibly some velocity or even acceleration. A frame of reference could for example be a moving car, an elevator, or a stationary room. Certain physical processes may appear differently when observed from different frames of reference. A simple example would be a balloon in a car: The balloon will behave differently in an accelerating car than it does in a parked car. An important special frame of reference is the inertial frame; a frame that is not accelerating. An inertial frame moving at some velocity is said to be in uniform motion. To make sure the laws of physics make sense to any observer, we need rules to transform from one frame to another. When some description of a physical process changes when we do this it is said to be invariant under this particular transformation.

The principle of relativity is not a novel concept in physics. Galileo Galilei already proposed that for the laws of mechanics there is no preferred state of motion for any particular inertial observer. This means that the laws of mechanics are the same for any inertial frame of reference regardless of its velocity. This can easily be made intuitive: Consider opening a bag of cookies upside down, surely you expect the cookies to fall to the ground approximately vertically. Now suppose you are standing in a high speed train travelling at a smooth constant speed of 300 km/h. Once again you clumsily open the bag of cookies upside down. Now, surely you do not expect the cookies to fly in your face at 300 km/h. This is the concept of relativity that is intuitive to us and it is often referred to as Galilean relativity.

In this principle of relativity, absolute velocities are not measurable. Consider once more that you are the observer in the train. If you are unable to look outside and thus unable to see the landscape moving past, you have no way of determining whether you are moving or not. Movement can only be measured relative to other frames of reference or when uniform motion is interrupted. When the train enters a sharp bend or when the tracks are no longer smooth, you are no longer in an inertial

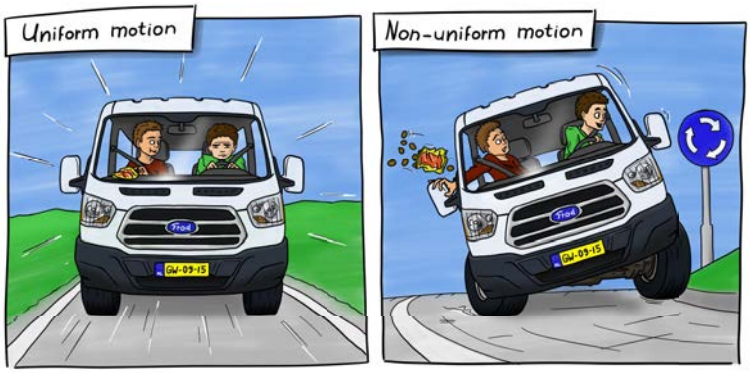

Figure 6.1: left: A car traveling toward us in uniform motion. **right:** The same car going around a bend, exhibiting noticeably non-uniform motion.

frame and this can be measured. Fig. 6.1 demonstrates the difference with a car, and for completeness, another bag of cookies. What you experience is force and Newton describes force to be a result of acceleration and not mere motion. Newton states that as long as an object is not accelerating, no matter how fast it moves, no force acts upon it.

So far we only considered the laws of mechanics (how stuff moves). Things get more interesting when electromagnetism is taken into account. Newton thought that light was made of particles moving at some velocity and following the same laws of mechanics as everything else. Early in the nineteenth century however it was shown that light behaves as waves. This lead to the assumption that light must travel through some medium like sound waves through the air or ripples on the surface of a pond. Another important observation was that James Clerk Maxwell's equations that accurately describe electromagnetism, were not invariant when going from one moving frame of reference to another. Even at low velocities the electric and magnetic fields become messy and nonphysical when we try to do this. Hendrik Lorentz devised a transformation under which Maxwell's equations do behave. His transformation works by deforming the medium through which light was thought to propagate.

The existence of a medium through which light propagates, called the Ether, was later disproved by an experiment performed by Michelson and Morley. This resulted in another significant discovery. Scientists were able to prove that the speed by which light propagates must be the same for all observers: The speed of light (in vacuum) is a constant!

This is where Einstein comes in. He was rethinking the way space and time behave starting with two assumptions: 1) The speed of light is constant for all observers and 2) the laws of physics must be the same for all inertial observers. The second can be rephrased a bit more technically by stating that the laws of physics must be invariant under a transformation between inertial frames. He already knew that the Lorentz transformation was required to achieve this for electromagnetism. Einstein then realized that the one transformation that worked with electromagnetism implied

that the laws of mechanics too must hold under the Lorentz transformation. What followed was what we now know as the special theory of relativity. In the special theory of relativity all the laws of physics hold under a single transformation by allowing not some Ether, but space and time itself to deform.

What makes the theory special is that it only applies to special frames of reference, namely inertial frames. It only applies to observers moving at constant velocities. Einstein realized this and set out to make his theory general. He came up with a brilliant thought experiment.

Consider the following thought experiment: You are standing on a high diving board, as anywhere else on Earth, you notice gravity is pulling you down. Now you step off the diving board and let yourself fall. Suddenly, the sensation of weight, the telltale sign that gravity is pulling you toward the Earth has vanished (forgetting for a moment that you can see you are falling). Of course, the Earth's gravitational pull is still present and people did not suddenly start floating as you stepped off the edge of the diving board (consider the alternative in Fig. 6.2).

Figure 6.2: When you dive off a diving board you lose the sensation of weight, yet gravity remains. The alternative would result in a strange universe indeed.

Einstein realized how the world must work when he performed a similar thought experiment (his involved someone walking off a roof). He realized that the behaviour of objects in the presence of gravity is indistinguishable from them being in an accelerated frame of reference. This may be a big leap, but as illustrated in Fig. 6.3, it basically comes down to an astronaut not feeling the difference between standing still at the launch site or being accelerated though empty space at $9.8\,\mathrm{m/s^2}$ (roughly the gravitational acceleration at the Earth's surface).

Special relativity already tells us that space and time are connected and should really be described as space-time as a whole. This equivalence between accelerating frames of reference and the presence of gravity is know as the equivalence principle. Putting together the special theory of relativity and the equivalence principle allowed Einstein to formulate the general theory of relativity.

In the general theory of relativity, space-time can be considered as a fabric that twists and bends under the influence of matter and energy. All matter follows the

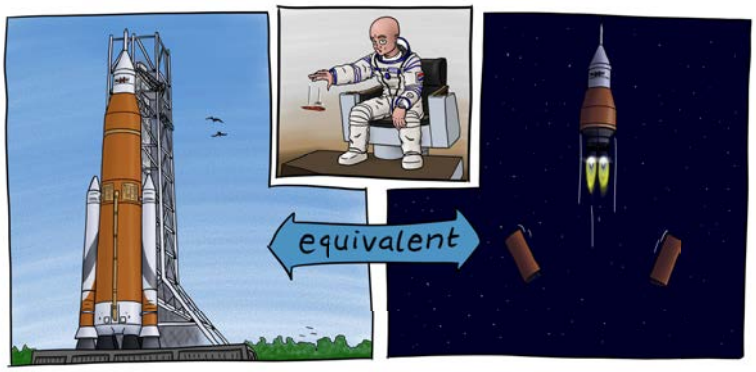

Figure 6.3: An astronaut dropping a pen in two equivalent situations. **left:** In a rocket waiting at the launch site. **right:** In the same rocket, but this time in empty space under acceleration $g = 9.8\,\mathrm{m/s^2}$. The astronaut will find that the pen falls to the floor in precisely the same way in both situations.

curvature of space-time and force is only experienced when something is prevented from doing so. What we experience as gravitational force on Earth is a result of space-time bending under the influence of the mass of the Earth. We follow the curvature but our path is obstructed by the earth itself and we experience force. When stepping off a diving board, we are in free fall and we can follow the curvature of spacetime unimpeded. As soon as we hit the water, our sensation of weight returns as the water now prevents us from following the curvature of spacetime.

Einstein's theory is remarkably elegant (everything it predicts is written in a single short equation) and especially in 1915 when he first presented it to the Prussian Academy of Science, it was unorthodox. Of course, as is the way of science, the theory had to be tested.

First tests of general relativity

General relativity predicts that everything in free-fall – only influenced by gravity and nothing else – follows the curvature of space. Let's use an often considered example to provide an idea of how this works: Imagine a trampoline with a heavy ball at the center. The fabric curves around the ball. This trampoline fabric can be thought of as the fabric of space-time curving under the influence of the mass of the sun, represented by the ball. Now roll a small marble into the pit without hitting the center ball. Its path will be curved. If you roll it just right you can even make it circle around the large ball. The marble can be thought of as the Earth revolving around the sun. Of course, unlike the marble, the Earth will not crash into the sun. In the case of the marble, friction reduces its velocity causing it to spiral into the pit. So Earth follows the curvature of space around the sun and because it has just the right velocity, it keeps going in circles.

Light is also just another form of matter obeying the curvature of space-time. Think back to the trampoline experiment. As long as we give the marble a high enough velocity it will not fall into the gravitational well. Instead, when going really fast, it will bend slightly and zoom past it. As light is no exception, it too will curve very slightly and change direction when passing the sun closely.

This effect – the fact that matter can curve the path of light – is the first prediction of GR that could be tested. Astronomers around the globe set out to be the first to confirm or disprove Einstein's prediction. They observed the apparent change in position of stars as their light bends under the influence of the sun.

Performing these observations was no easy task, but the principle of how they could prove Einstein's predictions can be demonstrated with a few sketches as in Fig. 6.4. As light from a distant star moves past the sun toward us, it bends slightly and the apparent position of the star shifts. Fig. 6.4 shows the positions of a few stars when the sun is not present in the left panel. The middle panel shows how light from a distant star would deviate under the influence of the sun and the right panel shows how this changes our observations of the same stars. The effect is tiny and was only measurable for stars that appeared very close to the edge of the sun. Indeed, under normal circumstances, distant stars cannot be seen right next to the blazing brightness of the sun itself and the observations had to be done during a total solar eclipse. Eddington was the first to provide observations that confirmed the predicted apparent deviation of the positions of the stars by observing them during a solar eclipse.

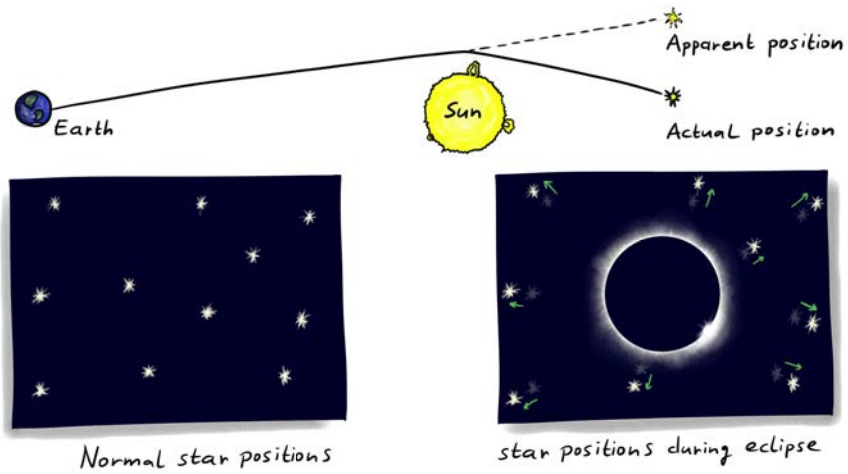

Figure 6.4: An illustration of how the bending of light around a massive object was observed. The top illustration illustrates the path of a light beam originating from a star far away. The bottom left panel shows the positions of a few stars in the night sky. The right panel shows how the position of the stars seem to have shifted when looking at them during a total solar eclipse.

And so general relativity passed its first test. The angle of deviation predicted

was also observed, many times over.

GR has been tested across a wide range of physical processes with great precision and has passed each and every one with flying colors. However, what has been covered so far is only the tip of the proverbial iceberg. Before we get to the part where that makes sense, we first need to take a small detour into the life of a star.

A bit of stellar evolution

As mentioned once or twice, space-time curves under the influence of matter. The more matter, the stronger the curvature. Let's consider that for a moment. Turning back to the trampoline example, we know that when we roll a marble past the central mass at a certain distance, it is its velocity that determines whether it will fly past, orbit, or plunge into the pit. At this point we can leave the trampoline behind and consider a mass forming a gravitational well at which we hurl all sorts of test objects. Fig. 6.5 illustrates a few situations.

If there is more mass at the center, the well will be steeper and an even larger velocity is required to make an object pass it at the same distance. We also know that the same goes for light; it too will follow the curvature of space. In fact, when the mass at the center is sufficiently large, even light, the fastest stuff in our universe can plunge toward the object and never come out. Such an object is called a black hole.

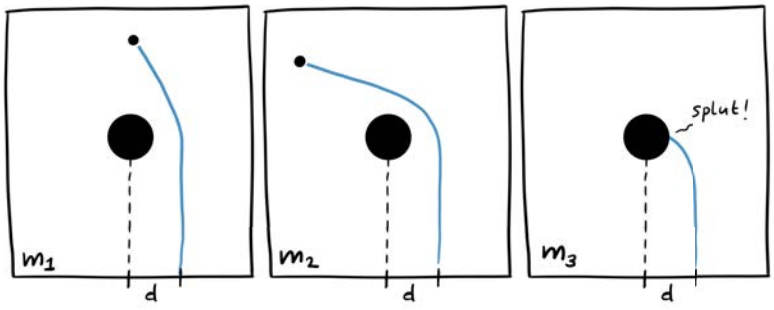

Figure 6.5: Demonstration of the effect of mass on an approaching object. The approaching object moves at the same initial velocity in each picture and passes at the same distance (d). The mass of the central object is different in each panel, getting heavier from left to right. At some point the approaching object does not pass fast enough to escape the central object's gravitational attraction.

Black holes are quite weird. Their masses range from a few times the mass of the sun, to billions of times as much. At the "surface" of the black hole, the escape velocity (the velocity it takes to fly away from the object) is the speed of light. This means that no light can be emitted from it, hence its blackness. To form a black hole, enough mass needs to be compressed into a small enough volume. This is where stellar evolution comes in. It tells us that if a star is massive enough, it will eventually collapse and form a black hole.

Our sun shines because the hydrogen it is predominantly made of, is compressed so much by gravity that the atoms are smashed into each other at the core, producing energy. The energy that is released by this fusion generates an outward pressure. In the sun, and any other star, there is a balance between inward pressure caused by gravity and outward pressure caused by the energy release of fusing atoms (see Fig. 6.6).

Fusion of light elements such as hydrogen, creates heavier elements such as helium and releases energy. These heavier elements can in turn be fused together to produce even heavier elements such as carbon. This chain of fusing elements into heavier elements goes all the way up to iron at which point fusion no longer releases energy, but requires energy. This fusion process therefore ends at this point; a star, such as the sun eventually runs out of fuel[1]. When the sun, or any star, runs out of fuel the outward pressure will be gone and only gravity remains: The star collapses.

There are different forms of collapse depending on the star's mass. A star such as the sun will not collapse all the way and form a compact ball of carbon and oxygen. Heavier stars, around twice the mass the sun will collapse in something that is even more compact: A neutron star. These are balls of matter roughly the size of Amsterdam, but twice as massive as the sun! A drop of this matter would weigh around one billion kilograms. So what about stars that are even more massive?

Given enough mass, in a small enough volume, the density will be so high that no form of matter we know of can counter the gravitational force it produces. Stars exceeding five times the mass of the sun inevitably collapse into a black hole. At this point light can no longer escape its surface. It is interesting to note that for such an object the exact nature of the central mass is hidden from us. Anything happening outside the black hole is described by pure general relativity: Black holes are the ideal laboratory to study GR as no complicated descriptions of matter are required to describe the surrounding space-time.

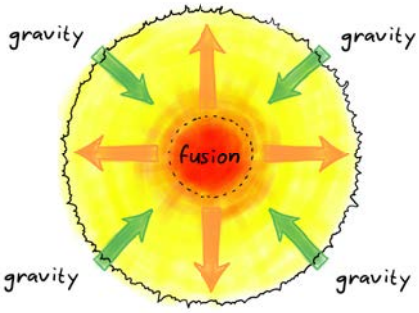

Figure 6.6: The two forces playing in a star: Nuclear fusion generates outward pressure while gravity causes inward pressure. The two balance each other as long as there is fuel for the fusion process.

Weird as they may be, there is strong evidence for the existence of black holes. For example, at the center of our galaxy we can see stars whizzing around some dark

[1]Don't worry we still have a reasonable 4 billion years left before the sun runs out of fuel.

center that must have the mass of a billion suns confined in a small volume.

The reason we only have indirect evidence for the existence of black holes is because these are objects that cannot directly produce electromagnetic radiation (radio, infrared, x-ray, etc...). Yet our ideal laboratory is not completely unobservable: It turns out that GR predicts a form of information that can escape even the deepest gravitational wells.

Gravitational waves

Space-time is dynamic, it can be stretched by a stationary mass, but an accelerating mass will create waves in space-time! We spark our imagination one last time with an analogy closer to home: The surface of a pond. We can also deform the surface of water by placing a little ball on it. Again, the ball represents a mass that is curving space-time, which in turn is represented by the surface of the water. Now move the ball around a bit and you create waves.

Waves on a surface happen when the surface needs time to adjust to changes. When we suddenly remove the ball out of the water, we see an expanding circular wave. The dip in the surface will not disappear instantly. It is said that the surface has a certain stiffness: The stiffer the surface, the faster the wave will travel and the faster the surface adjusts itself to changes.

Something similar happens in the fabric of space-time. When some mass excellerates, the gravitational well it produces follows it along. Of course the place where the object used to be no longer has a well since the mass is now gone. However, like the surface of the pond, space-time has a certain stiffness and its shape can not instantly change from curved to flat. So accelerating masses generate waves in space-time, which we call gravitational waves. Space-time turns out to be incredibly stiff. A lot of mass and energy is required to generate some decent waves and they travel at the speed of light.

Strong evidence supporting the existence of gravitational waves was already found in the 1970s by Russell Alan Hulse en Joseph Hooton Taylor. They observed two neutron stars revolving around each other for many years. They found that the separation between the two objects decreased precisely according to what general relativity predicts. The reason according to GR, is energy being carried away from the system through the emission of gravitational waves.

Recall that a marble on a trampoline could not sustain a perfect orbit due to friction. These two neutron stars revolving around each other are dragging their way through spacetime. So even in empty space such a system experiences something analogous to friction. At some point they will fall into each other. The Earth-Sun system moves much too slow for this to be a serious effect, but the neutron stars in the Hulse-Taylor binary orbit each other every eight hours! Even so, the gravitational waves leaving this system are still too weak to directly see with our gravitational wave detectors on Earth.

The strong-field dynamical regime of GR

The fate of this system of neutron stars – something we call a binary neutron star – is inevitable collision. So what does the future of such a system look like until that moment?

Gravitational waves carry energy away from the system causing the two objects to move closer to each other. This in turn increases their orbital velocity. Now that they are revolving around each other even faster, the system generates stronger waves and loses energy faster. So as a result the objects move into tighter orbits and their velocities increase even more, et cetera. In fact this happens exceedingly fast, resulting in a runaway effect until the two neutron stars merge into a single object. For a system like the Hulse-Taylor binary this will still take about three hundred million years and unfortunately the waves will only be strong enough to detect on Earth for the last minute or so (unless in three hundred million years we are able to just fly there and enjoy the show locally).

Even though we all hope to soon detect gravitational waves originating from such a system, I will focus here on an even more extreme binary system: A binary black hole (BBH), a system where two black holes revolve around each other.

For quite some time already BBH systems were believed to exist, but it was very difficult to estimate how many there would be as there is really no way of seeing them directly. It was an exciting surprise to detect gravitational waves originating from a merging BBH system on September 14th 2015.

Each black hole in this system had a mass of around thirty suns. We witnessed the last ten orbits the black holes made before plunging toward each other releasing an enormous amount of energy as they collided and formed a single black hole. The event that we were able to observe by detecting its gravitational waves has proven to be the most powerful event ever observed by mankind. Space-time was violently stretched, twisted and turned during these final ten orbits in only a fraction of a second. These final moments of such a massive system are unveiling the nature of GR under the most extreme circumstances.

As I mentioned before, black holes are the ideal laboratory to test general relativity and a binary black hole merger shows off all that GR has to offer. Never before have we had such an opportunity.

The first tests of the genuinely strong-field dynamics of general relativity

All tests of GR that we have been able to perform so far have been in either a regime where fields are weak (only subtle curvature in space-time) or where there are only small dynamical aspects (slowly moving and evolving systems).

Particles in close orbit around black holes could be described by approximating GR as the more complex effect in GR are too subtle to notice. Even though these particles are moving in a very strong gravitational field, the system is still static; the mass producing the field is just sitting there. The Hulse-Taylor binary is not static

and does provide a more interesting test of GR, but even in such a system only small corrections to Newtonian mechanics can be measured. The effects of GR in such systems are still subtle and we can not use them to confirm if all the complicated dynamic aspects of GR are also correct.

Before September 2015 we have never been able to observe the strong-field dynamics of GR. But there is a deeper reason behind wanting to observe and investigate these illusive waves: Nature is telling us there is something fishy going on with our current understanding of the universe. GR explains the large aspects of the universe to unprecedented precision, while quantum mechanics shines in explaining the very smallest of things. But here's the funny thing: These two theories are not compatible with each other. GR does not feel comfortable at the quantum scale and quantum mechanics has nothing to say at large scales. Something must be missing. If there is something missing in GR, our only hope to observe it is in its currently unexplored strong-field dynamics!

This is the main topic of this thesis as the subtitle – not so subtly – states. In the remainder of this section I will explain how we have accomplished this with the first detections of gravitational waves.

The shape of a signal

I shall skip the method of detecting gravitational waves as the focus of this thesis is not the detection itself, but rather what physics can be extracted from detected signals. What I do need to mention is that the shape of a wave passing a detector is never clean. Detecting a gravitational wave is done by measuring extremely tiny length differences (a fraction of the size of an atom) in two perpendicular vacuum tubes, typically a few kilometers long. Unfortunately not only the stretching of space-time results in measuring such length differences. Many other sources of vibrations such as tremors in the earth cause the detector's output signal to be messy. The resulting undesired signal that is not caused by gravitational waves is called noise. In Fig. 6.7 I illustrate what a short piece of data from a detector can look like.

We are capable of finding tiny signals buried in all this noise. When a signal is found buried in the noise, we can start working on the stretch of data containing the signal. As mentioned above, such a signal is buried in noise and gets distorted. In order to find it we need to have a pretty good idea of what a signal can look like.

General relativity predicts precisely what a gravitational wave (GW) signal passing our detectors should look like, depending on the type of source that created it. In Fig. 6.8 the shape of such a signal originating from two black holes is illustrated. The two black holes will revolve around each other, slightly getting closer each orbit while their velocity is increased. This increase in velocity means a higher GW frequency. This process continues to pick up the pace. The GW frequency will rise faster and faster as the black holes move toward each other. The GWs will gain strength so the amplitude increases as well. Finally they will plunge into each other forming a single deformed black hole. This remnant black hole will then ring for a while (very much like a bell does when hit with a hammer) until it has settled down and it no longer emits any waves.

The shape of the signal looks simple to the eye, but to accurately describe it,

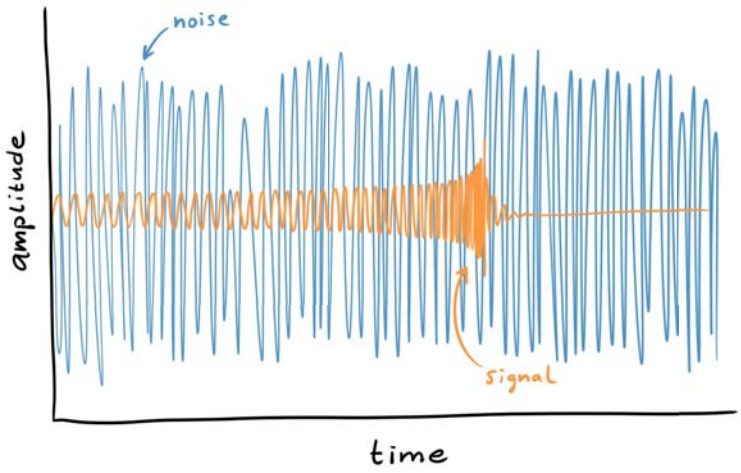

Figure 6.7: A small stretch of what data from a detector would look like containing a signal. The blue messy lines are noise resulting from all sorts of things like seismic vibrations and the tiny red wiggle is a gravitational wave.

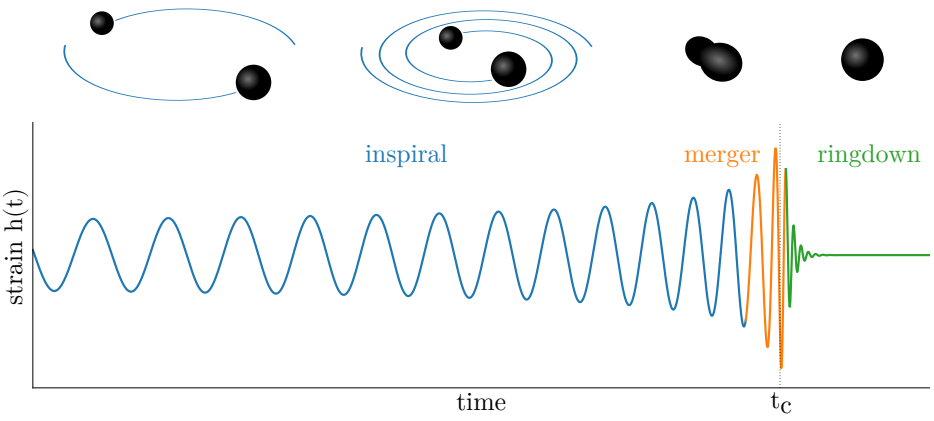

Figure 6.8: The shape of a gravitational wave resulting from two objects revolving around each other closer and closer. Highlighted in blue, orange and green are the three regions that are often referred to as inspiral, merger and ringdown. The time t_c, is roughly where the two objects merge into a single one.

the full complexity of GR is required. Also, the signal will be different for different sources. In fact, its shape depends – in the case of black holes – on the two masses of the black holes m_1 and m_2, and the way they spin around their own axis described by six spin-components that give the direction and how fast they are spinning. Change any of these numbers a bit and the signal will change as well.

Estimating the source parameters

When we analyze the signal and try to measure what parameters the source must have had, we keep tweaking the masses and spins until our tweaked waveform matches the signal in the data. Noise in the data will have distorted the signal, so we can never know precisely what the true masses and spins were, but we can find a range in values that fit the signal best. This range in possible values is a probability distribution for the parameters, based on the data. As this is rather a mouthful I will refer to these as "posteriors".

This range in possible values is called a posterior distribution and is illustrated in Fig. 6.9. The width of this posterior distribution tells us how certain we are about our best match. The wider the distribution, the larger the grain of salt we must take with the most likely value at the top.

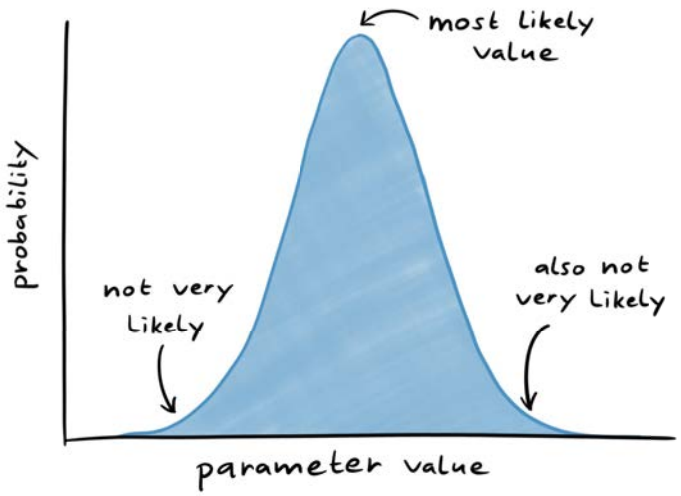

Figure 6.9: The distribution of possible values for a particular parameter after performing parameter estimation on the signal. The distribution, called a posterior, is highest at the most likely value. The width indicates our uncertainty about the most likely value. Values in the tails are unlikely to be the true value of the source.

So for each parameter we have a control knob, we turn them back and forth while we note at each setting how much the tweaked waveform matches the signal. Thankfully we do not have to do this by hand and can use clever algorithms and lots of computing power.

How we performed the tests of GR

The tweaked signal that we keep using is in fact calculated using GR. If GR is the true underlying theory, the only parameters that can change the signal are indeed the masses and spins. If GR is however not correct, it is the theory itself and not only the parameters of the source we should change to get a good match with the signal. There are quite a few theories that try to extend or change GR in some way or another and in principle we could repeat the tweaking process for each of these models and see which one works best. In this thesis however, we do not assume we have any idea where GR may or may not fail. We introduce testing parameters that work very much like the tuning knobs for the source parameters, only these will tweak certain aspects of GR itself.

So if GR is not correct, we should need to tweak it along with the source parameters to properly fit the signal. To do so we add a few testing parameters which we give some fancy labels: $\delta\hat{\varphi}_1$, $\delta\hat{\varphi}_2$, et cetera. These testing parameters are special, as they should all be zero if GR is the correct theory.

We now perform the parameter estimation exercise again, this time also tuning the testing parameters. As we did with the source parameters, we obtain posterior distributions.

These distributions are the main result of this thesis as their implications are significant. As with the posteriors of the source parameters, the width tells how certain we are of our measurements. There are two things we need to be mindful of here: 1) The posterior should overlap with zero for GR to be an acceptable theory to describe the signal and 2) the width of the posterior tells us how much room for error there still is in GR. In other words if the posterior is narrow for parameter $\delta\hat{\varphi}_3$ and its peak is roughly at zero, we are very confident that the part of GR that $\delta\hat{\varphi}_3$ represents is pretty accurate.

The testing parameters are cleverly chosen and in the tests we performed they roughly represent different physical processes that appear in GR. Let's take $\delta\hat{\varphi}_3$ for example. This parameter represents interactions between the spins of the black holes. Only the strong-field dynamics of GR are able to reveal its secrets in the way of gravitational waves. The width of our posterior on that parameter means that we were able to place a bound on its value: This particular effect that GR describes still stands strong. If an alternative theory for gravity is thought up, it has to fit between the bounds we place.

Finally, if we take the posteriors for the testing parameters, put them on their side and show them all next to each other we get Fig. 6.10: The actual results of the first ever tests of the genuinely strong-field dynamics of GR! From these figures alone we can conclude that once again general relativity prevails.

Fig. 6.10 shows some nice constraints for some of the parameters, but others still have a lot of wriggle room. A lot of the posteriors are still rather wide, but these will get narrower as more detections are made and more information is combined. GR is still within the range of acceptable models (all posteriors overlap 0), but this wriggle room could perhaps accommodate a slight change in GR that would make it work at the quantum scale as well.

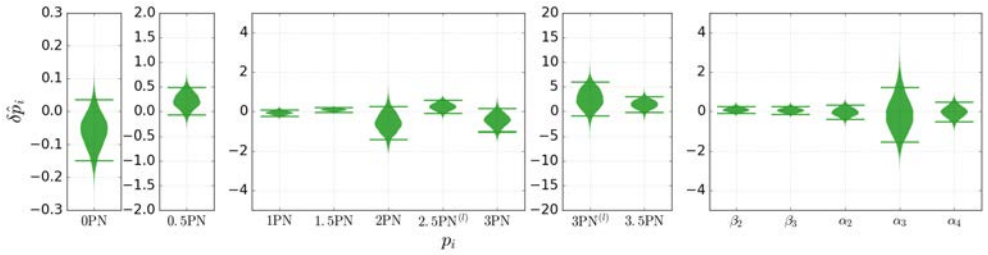

Figure 6.10: These are the posteriors (turned sideways and mirrored) we obtained from tweaking the various testing parameters. The numbers on the vertical axis show fractions; 0.1 means a 10% difference from GR and 0.0 is GR exactly. The results I show here are in fact the combined results from the first two detections. Each posterior shows how certain we can be about how much wriggle room there still is for changes in GR. For example the posterior labelled with 1.5PN is the parameter representing spin interactions between the two black holes as mentioned in the text. We show that this particular effect is pretty well described by GR, there is no more than about 3% room for error anymore. Note that *all* posteriors overlap with zero meaning that our measurements are still consistent with GR!

Speeding things up

In the previous sections I explained that we need to calculate many different waveforms for many values of source parameters and testing parameters to obtain posteriors. This requires a lot of computation. In some cases it took a month of continuous calculation on a super computer to obtain the results. This is a severe bottleneck in performing our tests of GR.

In my thesis I present a method to significantly increase the speed at which we calculate waveforms and evaluate how well they fit the signal. Although the core concept of how this can be done is not new in the field of gravitational waves, it is a challenging task to get it to work with extra testing parameters.

The process by which we can speed up the calculations is actually by being lazy; we only calculate what we absolutely have to. Pretend for a moment that a gravitational wave is determined by only the masses of the two objects that are generating the wave. If we want to find the masses that best fit the signal we see in the detector, it looks like we need to calculate a waveform for every imaginable combination of masses. Maybe the best value for one of the masses is 10, then again it could also be 10.1, or 10.0001. You can probably also imagine that if we calculate the waveform for a mass of 10.0001, we probably will not need to calculate it again for 10.0002. At some point, there is no way to tell the difference.

So clearly we do not need to calculate all possible waveforms, which is a good thing as there are infinitely many possible values for the masses. It turns out that we can cleverly choose a few values for the masses, evaluate their waveforms and use them as a basis for calculating a waveform for any other combination of masses. It is a little bit like a cooking recipe; a few ingredients can be combined into many different meals

depending on the amounts we use for example. The ingredients are the basis of the recipe.

When considering the gravitational waves we can form a set of combinations of masses and calculate their waveforms. These are the ingredients and we'll call them e_i, where i can be anything between 0 and however many ingredients we have. We can then create any other waveform by adding a dash of e_1, a spoon-full e_2, a pinch of e_3, etc.

Finding the proper ingredients, or more appropriately called basis functions for gravitational waves is challenging. It gets more challenging the more parameters we add to the waveform. For testing general relativity we need additional testing parameters on top of the already parameter-heavy waveforms. In this thesis I describe the method by which we can overcome some of the difficulties involved in finding the proper e_i and demonstrate that we can make our tests of GR up to 300 times as efficient!

To give a sense of how we find these e_i, pretend once more that gravitational waves are only described by the masses of the two black holes that generated them. We begin by collecting lots of pairs of mass values. So if we have ten values for the first mass and ten for the other, we have one hundred possible combinations. We calculate the waveform for one of these combinations and call it e_1. We then compare this e_1 with the waveforms corresponding to every other mass combination. The combination that generates the waveform that is most different to e_1, we remember and call e_2. These two waveforms are now a basis. To return to the recipe analogy: Using only two ingredients e_1 and e_2 is just not enough to generate all the recipes we want, so we continue the process of finding more ingredients until we are happy with how accurately we can reproduce any recipe.

This is how we continue building the basis for our waveforms. At each step we compare all the onehundred waveforms with our current basis and remember the one that has the most to add. This process of finding basis functions e_i, that contribute the most to our current basis continues until we are happy with how accurately we can reproduce any waveform we want.

In my thesis I introduce a way to beat the curse of dimensionality: Using ten values for each mass gives one hundred possible combinations, but when we wish to include all parameters (two masses, six spin parameters and one testing parameter), this amount becomes huge with 10^9 possible combinations. That's a ten digit number. All this needs to either be stored in a computer's memory which can add up to well over 200 GB (2 TB when adding only a single additional parameter) or waveforms would need to be calculated over and over again for all these combinations. The latter would quickly result in a computation that takes a lifetime. By making use of existing bases for pure GR waveforms and carefully choosing ranges in parameter values I was able to generate bases for waveforms that also included testing parameters.

The title explained

I hope I have been able to convince the reader that the celebrated theory of general relativity still needs to be put to the test and that the universe may still have some

secrets in store for us. What we have seen of GR is just the tip of the iceberg. Binary black holes spiralling toward each other and collapsing into a single object while emitting gravitational waves is the perfect laboratory to perform the ultimate test of GR.

Black holes can be described by pure GR. As far as the outside observer is concerned there is no matter there, only curved space-time: Black holes way as well be voids to us. We substantiated[2] this void and thereby GR, by performing our first tests of the genuinely strong-field regime and concluding that Einstein's predictions still stand strong.

[2]Substantiate, verb: Provide evidence to support or prove the truth of.

A SPARK IN THE DARK

SCINTILLATION TIME DEPENDENCE AND NEUTRON-INDUCED SIGNALS IN DUAL-PHASE XENON TPCS

ACADEMISCH PROEFSCHRIFT

ter verkrijging van de graad van doctor
aan de Universiteit van Amsterdam
op gezag van de Rector Magnificus
prof. dr. ir. K.I.J. Maex
ten overstaan van een door het College voor Promoties
ingestelde commissie, in het openbaar te verdedigen
in de Aula der Universiteit
op vrijdag 8 maart 2019, te 13:00 uur

door

Erik Hogenbirk

geboren te Alkmaar.

SUMMARY

(OF: A SPARK IN THE DARK)

CHAPTER 1: EVIDENCE FOR DARK MATTER

We have never seen the most common material in the Universe. From many independent astronomical and cosmological observations, we know that 85 % of all matter must be *dark matter*, a mysterious form of matter that is not part of the Standard Model.[1] The nature of the particle responsible for dark matter remains one of the outstanding problems in modern fundamental physics.

One of the most precise measurements of the dark matter abundance comes from the observation of the cosmic microwave background (CMB) radiation. In the early Universe, density fluctuations were amplified by dark matter: it attracts gravitationally, but lacks the repulsive pressure of ordinary matter. The density fluctuations cause temperature fluctuations in the measured CMB map, which clearly bears the distinct fingerprint of the large amount of dark matter in the Universe.

There is one thing that cosmology and astronomy cannot do: tell us what *particle* dark matter consists of. Since dark matter is inferred from its gravitational interactions only, single particles cannot be observed.[2] The particle constraints from cosmology are therefore weak, so that many models exist that can solve the dark matter problem. One of these is the WIMP (Weakly Interacting Massive Particle) model. The WIMP has a mass of about 100 GeV and an interaction cross section of the order of the weak scale. One of its merits is that there is a very natural production mechanism in the early Universe, that predicts the right amount of dark matter that we observe. It is furthermore heavy enough to be 'cold', i. e. slow-moving dark matter, which is in agreement with simulations of large-scale structure formation. If WIMPs are supersymmetric particles, they could also solve the hierarchy problem in particle physics.

One of the ways WIMPs may be observed is through direct detection. WIMPs are moving through the Galaxy with typical speeds of about 200 km/s, and added to

1 In terms of energy density, there is even more *dark energy*, something even more puzzling than dark matter, but this is a discussion for another day.

2 Unless the dark matter 'particles' are extremely heavy, such as in the case of primordial black holes.

that comes the speed due to the motion of the Sun around the center of the Galaxy. This speed is high enough for WIMPs to produce a detectable signal if they collide with an atomic nucleus, transferring up to tens of keVs to the recoiling nucleus. The challenge of direct detection dark matter searches is to build large detectors capable of reaching this low energy threshold.

CHAPTER 2: DARK MATTER DETECTION WITH LIQUID XENON

In recent years, there has been a rapid increase in the sensitivity to low dark matter cross sections, mainly as a result of the success of dual-phase time projection chambers (TPCs) using liquid and gaseous xenon. Figure 1 schematically shows how dual-phase TPCs work. The cylindrical detector volume is partly filled with liquid xenon, cooled to $-90\,^{\circ}\mathrm{C}$, with a layer of gaseous xenon at the top. The top and bottom of the TPC are lined with sensitive light detectors, photomultiplier tubes (PMTs). When a particle interacts, it transfers (part of) its energy to a xenon nucleus or an electron, which creates a short track of excited xenon atoms (Xe^*), xenon ions (Xe^+) and electrons (e) (see panel 1a). The excited xenon atoms produce scintillation light that is detected by the PMTs as a short pulse, called S1. Some of the free electrons generated in the interaction are also measured. They are pulled up towards the gas layer by an electric field, generated by a high voltage applied on the cathode. At the liquid-to-gas interface, there is a stronger field from the anode, which pulls the electrons out of the liquid into the gas. The electrons gain energy in the gas and produce excited xenon atoms. This causes the emission of a second flash of light in the gas phase, which is detected by the same PMTs. This signal is called S2. The result from one initial interaction is therefore two measured signals, with a delay in between (see top panel in figure 1).

By combining information of the two signals, many properties of the interaction can be derived. The first is the position of the interaction. Since the velocity of the electrons in the liquid xenon is constant, the time between the S1 and the S2 (drift time) is directly proportional to the depth of the interaction. The other two coordinates in the plane are derived from the light distribution of the S2 across the top PMT array. A second property is the type of the recoiling particle, which can either be a xenon nucleus (nuclear recoil, NR) or an electron (electronic recoil, ER). Most of the backgrounds, such as those caused by beta and gamma radiation, will cause ER signals, while WIMPs are expected to only give observable interactions from NRs. Compared to ERs, NRs cause more excitations and fewer ionizations, resulting in a relatively large S1 signal and small S2 signal. This means that the recoil

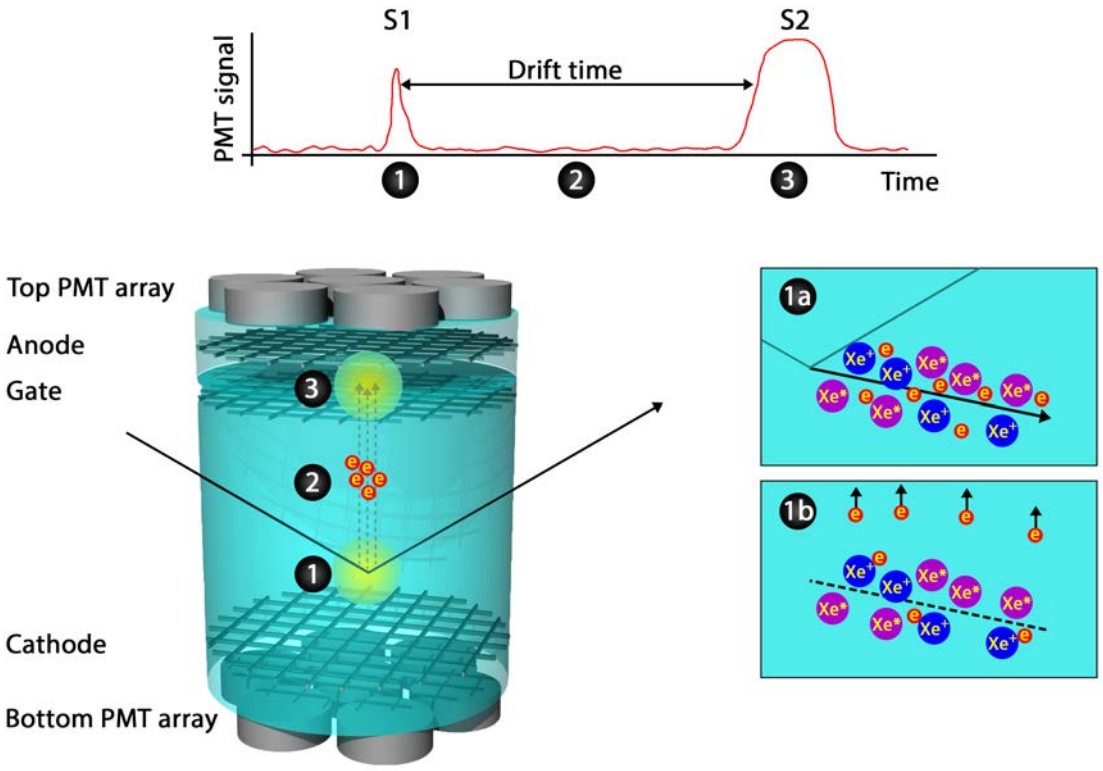

Figure 1: *Schematic showing the operational principle of dual-phase TPCs. A particle interacts in the liquid xenon, which causes excitations and ionizations (1a). The excitations decay and emit scintillation light (1), detected by the PMTs as a short pulse (S1). The electrons are pulled upwards by an electric field (1b) and travel through the liquid (2) until they arrive at the liquid-to-gas interface. A stronger field pulls them out of the liquid, causing secondary scintillation in the gas (3). This is the S2 signal.*

type can be determined experimentally from the ratio S2/S1. The combination of the interaction position and the recoil type gives the excellent background rejection required for dark matter searches.

There are several corrections and calibrations required for xenon TPCs. For instance, the size of the S1 signal is position-dependent due to varying light detection efficiency. The S2 signal size furthermore decreases with drift time due to electrons being trapped by impurities during their drift through the liquid xenon. Both of these are corrected with mono-energetic sources.

Another calibration is the energy calibration. Both the average S1 size and the S2 size increase with energy, so that they can both be used as a measure for the recoil energy. However, a superior energy resolution can be achieved by using a combination of both signals, because the S1 and S2 signal sizes are anti-correlated.

The electrons that are not extracted from the interaction site recombine with xenon ions, and in this process generate excited xenon atoms that contribute to the S1 signal, rather than to the S2 signal. This process is called recombination. By using a linear combination of S1 and S2, fluctuations in the signal size due to fluctuations in the fraction of electrons participating in recombination are canceled out. This anti-correlation can be resolved by using multiple mono-energetic sources, or with a combination of multiple field settings.

Finally, the S2/S1 ratio is mapped out using ER and NR sources with varying energies. XENON1T uses an internal ^{220}Rn source for its ER calibration, giving beta radiation going down to low energies. For the NR calibration, high-energy neutrons are used. Since they are neutral, they do not interact with the electrons but rather with the atomic nucleus, just as WIMPs are expected to do. XENON1T uses both a radiogenic neutron source (^{241}AmBe, through an (α, n) reaction) and a deuterium-deuterium fusion neutron generator, which is described in detail in chapters 7 and 8.

CHAPTER 3: THE XAMS SETUP

As the field of dual-phase xenon TPCs has progressed, the effort of R&D into the operational principles of these detectors has been growing too. Some of the research groups in the large collaborations that operate dark matter detectors have built their own small-scale TPCs. The purpose of these is to test new experimental techniques, research the processes leading to signal generation and to give us a more fundamental understanding of the dual-phase technology. XAMS is one of such setups in Amsterdam, featuring a TPC containing about 430 grams of liquid xenon in its active volume. The 10 cm tall, 4.5 cm diameter cylindrical volume is viewed from the top and bottom by two two-inch PMTs. Most systems function just as the systems of XENON1T, including the cooling, gas purification, data acquisition and data processing. In fact, XAMS has been the first real test case of the data acquisition and processing software of the XENON1T experiment.

Chapter 3 contains the first publication of the XAMS experiment, which marks its introduction into the scientific community as a fully functional setup. Measurements with a ^{22}Na gamma ray source revealed many of the operational parameters and provided essential calibration of the setup, giving the position-dependent light yield correction, the correction for electron loss of the S2 and the energy resolution. An unusual population of events was found, where the S2 size was up to about 80 % larger than the usual S2s. The strong temporal correlation of these events

leads us to the conclusion that these are caused by instabilities in the liquid level, which are in turn related to a xenon gas pump in the purification system. In later measurements, this effect could be mitigated by using a different gas flow setting.

Another result from the analysis is a new PMT calibration technique. Usually, pulsed LED light sources are used to calibrate the PMT response due to single photons. The approach used in chapter 3 is different: it uses single-photon signals found in small S2 signals. These S2s are caused by single electrons that are liberated within the TPC due to the UV scintillation light (photo-ionization). Since they consist of only a few photons spread out over a microsecond or more, the individual single-photon pulses can be resolved, which makes it possible to measure the PMT's single-photon response. The single-photon signals are small and therefore close to the electronic noise level, which means an amplitude-dependent acceptance corrections needs to be applied for this method. Nonetheless, there are several advantages: this method requires no special hardware or calibration measurements, and directly probes the response at the xenon scintillation light wavelength (which is difficult to do with LED light through fibers). This makes it an ideal method to study effects only occurring for the UV scintillation light. An example of this is the emission of two photoelectrons as a result of one photon, which causes signals twice as high as expected.

CHAPTER 4: CALIBRATION OF XAMS

Chapter 4 improves and extends upon the initial characterization of XAMS that is presented in chapter 3. The S1 and S2 correction factors are recalculated (with an improved method of selecting the mono-energetic peaks of ^{137}Cs and ^{22}Na), the energy reconstruction that combines the S1 and S2 signal is shown and the effect of diffusion is measured. It is shown that multiple S2s are separated for $\Delta z > 3\,\mathrm{mm}$, and merged multiple S2s are identified for $\Delta z \gtrsim 2\,\mathrm{mm}$. The electron lifetime reached values up to 0.81 ms, and the typical light detection efficiency of the S1 signal is approximately 10 %. Chapter 4 is a prelude to the next two chapters, since the calibration is used as the starting point of more complex analyses. In addition, this chapter gives a more detailed description of some of the analysis shown in the next chapters.

CHAPTER 5: THE SCINTILLATION PULSE SHAPE

One of the distinguishing features of XAMS is its excellent timing, which makes it suitable to measure the pulse shape of the S1 signal that happens on the timescale of a few nanoseconds. One of the reasons to investigate the scintillation pulse shape is because of its importance for pulse shape discrimination (PSD). This method exploits the difference in the pulse shape between ERs and NRs to improve the separation between these events, and thus reduce the (ER) background. The effectiveness of PSD depends on the precise pulse shape of ERs and NRs. For high-energy recoils, this has been measured and the difference between ERs and NRs is large enough for effective PSD. However, measurements of the pulse shape at the low energy relevant to direct detection dark matter experiments were lacking. The publication in this chapter fills the gap in our knowledge with measurements and analysis of the pulse shape at the energy and electric field relevant to dark matter detectors.

The scintillation pulse shape depends on the way that the scintillation light is produced. There are two main ways that this occurs: through direct excitation and recombination (see figure 2). In the case of direct excitation, the scintillation light is emitted only after the formation of an excited molecular state, called an excimer. While excimer formation is very rapid, the finite lifetime of the excimer causes a significant delay in the emission of scintillation light. There are two possible excimer states, the singlet and the triplet state (corresponding to the spin state of the excimer), with approximate lifetimes of 3 ns and 22 ns, respectively. The observed pulse shapes from these states follow an exponential function and are shown in figure 3.

Scintillation can also occur through electron-ion recombination. The mechanism of excimer formation and decay is the same as in the case of direct excitation, but this is preceded by the recombination process, which causes an additional delay. Depending on the electric field, energy and particle type, the recombination process can either be very fast, or cause a significant delay. Figure 3 shows the singlet and triplet recombination pulse shape in the latter case.

The total observed S1 pulse shape is a combination of all four previously mentioned components: the direct singlet and triplet states, and the singlet and triplet states due to recombination. For any S1 pulse, all of these are superimposed. A model of the scintillation pulse shape should in principle include all these components.

In practice, there are some difficulties with constructing a model like this. The summed pulse shape in figure 3 is rather featureless and depends on many pa-

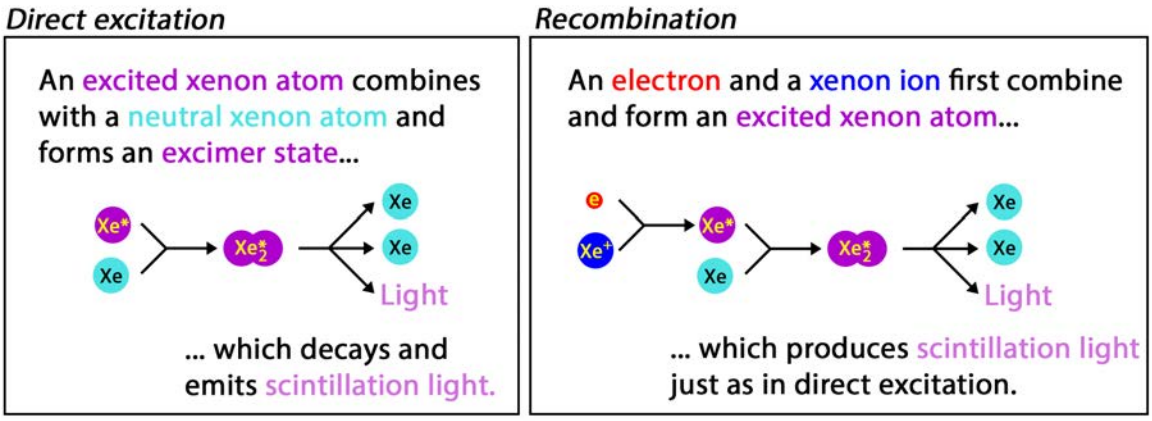

Figure 2: *The processes leading to scintillation light. Direct excitation (left panel) and recombination (right panel) first produce a molecular excited state (excimer), which then decays and emits scintillation light.*

rameters that are correlated when fitting a pulse shape model. In addition, the time behavior of recombination is not well known, and models are usually derived based on approximations that do not always hold. The model shown in figure 3, for instance, is based on high-energy electronic recoils at zero electric field. To counter these difficulties, an effective model is often used. In this model, the singlet and triplet times are allowed to vary to capture the slower tail of the observed pulse shape. We apply this model to data taken with XAMS, which includes ER and NR data going down to energies of a few keV, and at three different electric fields.

The results of the pulse shape measurements show a difference between ER and NR pulses that is smaller than expected, and decreases at the lowest energies. Essentially, the lower the energy gets and the higher the field gets, the smaller the difference between ER and NR pulse shapes. This makes the PSD performance worse than initially expected. Based on a pulse shape simulation, the increase in sensitivity using PSD corresponds to an effective increase in exposure of at most 6.8 % for large dark matter experiments, and only if the time resolution is improved. The minor increase in exposure likely does not justify the effort to improve the time resolution for the next generation of xenon-based dark matter detectors.

Apart from the gloomy conclusion about PSD, the measurements of chapter 5 tell us more: since the pulse shape depends on the dynamical behavior of electrons, it gives us information about the recombination process. For instance, the recombination time for low-energy ERs was previously assumed to be < 1 ns, but our results show an increase of the effective triplet time from 22 ns up to 25 ns, even when the field is relatively high. This suggests a recombination time that is at least approx-

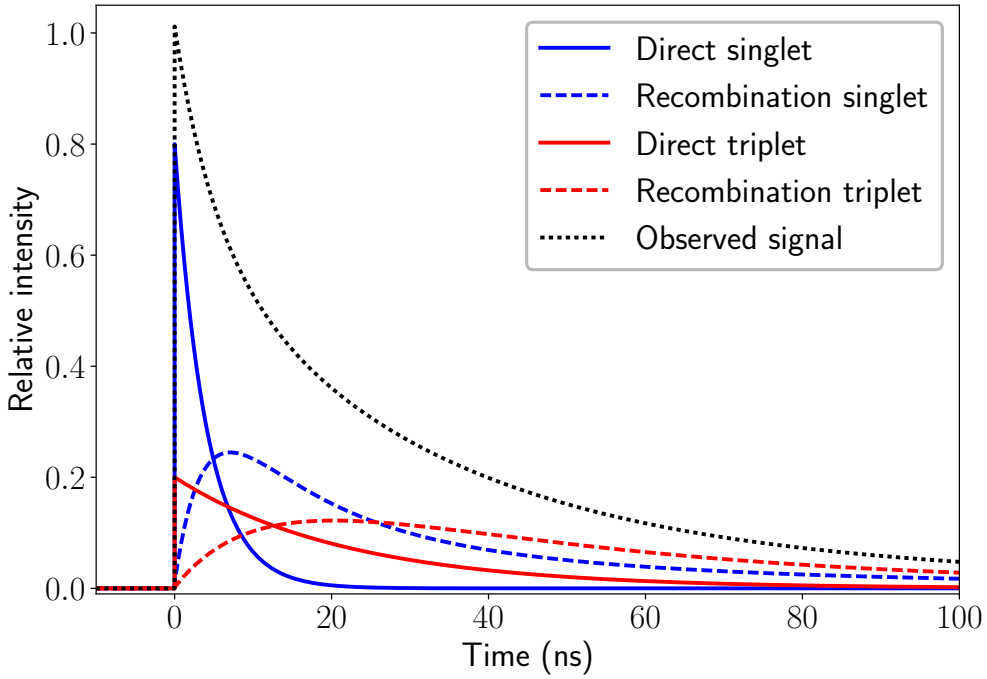

Figure 3: *The measured scintillation pulse shape is built up from several components, coming from the two possible excimer states with different lifetimes (3 ns for the singlet state, 22 ns for the triplet state) and from the delaying effect of recombination.*

imately 3 ns, and thus shows that the delay cannot be neglected. The dependence of pulse parameters on recoil energy further implies that there is a correlation with the linear energy transfer for both ERs and NRs. Research into the pulse shape thus opens a window into the physics happening on the microscopic distances and on the nanosecond scale.

CHAPTER 6: FIELD DEPENDENCE

In addition to pulse shape measurements, the XAMS setup has been used for measurements of the field dependence of the signals in dual-phase TPCs. As xenon dark matter detectors have become larger, the voltage V required to maintain the same electric field E rises according to $V = E \cdot L$, with L the detector drift length. Despite significant effort in high voltage engineering, the last dark matter experiments never reached their target field, but rather operated at lower fields than intended. The voltage was kept low to avoid discharges or electron emission from the cathode, which appear at higher voltage and make proper operation impossible. As a result, the electric field has decreased from approximately 500 V/cm down to

100 V/cm in the last years. If this trend persists, the field will become even lower for the next generation of TPCs.

At the current field of about 100 V/cm, we have reached a critical field strength, since many of the relevant properties of TPCs show a large rate of change for fields below this value. Because of this, small inhomogeneities in the field cause relatively large fluctuations in observed parameters. To counter this, one must do three things: design the field such that the inhomogeneity is minor, model the electric field, and correct for field dependence of the operational parameters of TPCs. The measurements and analysis of chapter 6 present a systematic study of recoils at fields ranging from 10 V/cm up to 500 V/cm and at zero field, going down to the low fields that are not commonly probed. We thus obtain a better knowledge of the low-field operation of dual-phase TPCs.

The results of this analysis show the variation of the drift velocity, electron lifetime, diffusion constant, and light and charge yields as a function of field. One of the lesser known quantities of these is the diffusion constant. This parameter indicates how much the electrons drift apart during their journey through the liquid xenon to the top of the TPC. Interestingly, at low fields, the diffusion constant rises rapidly. In combination with the lower drift velocity, this means that the electrons diffuse more due to a combination of a longer drift time (at fixed drift length) and more diffusion during this time. More diffusion means that the S2 signals become wider, since the electrons arrive at the gas layer at different times. This might pose a problem for the rejection of events with multiple interaction sites. Usually, these events cause multiple S2 signals, but if the S2s become wider, they might overlap, so that a single interaction is reconstructed. Since multiple interaction sites are a clear indication of background rather than a WIMP signal, the misidentification of multiple scatters as single scatters causes an increase in background. On the other hand, the width of the S2s is highly dependent on the local electric field in the TPC, which can be used to *reconstruct* the field given the dependence of the diffusion constant as a function of field. This method has already been applied in a preliminary study of the XENON1T field.

In addition to the aforementioned properties, the dependence of the scintillation pulse shape on field has also been determined. As the recoils measured here are 511 keV ER signals, this gives complementary information to the pulse shape measurements from chapter 5, which are performed at lower energy. The effective triplet time changes from 45 ns at low field down to 25 ns for the highest fields applied. The pulse shape in literature for high-energy (approximately 1 MeV) recoils is usually given as '45 ns decay for zero field and 27 ns with applied field'. While

the results from chapter 6 are consistent with this, it paints a more nuanced and detailed picture, showing the gradual change of pulse shape with increasing field.

CHAPTER 7: CHARACTERIZATION OF THE NEUTRON GENERATOR

As mentioned before, dark matter detectors need to be calibrated with sources of ER and NR events to enable the distinction between signal and background based on the recoil type. For XENON1T, a neutron generator is used for the NR calibration. This device allows a variable neutron flux, depending on the applied voltage and current. However, before its deployment as a calibration source for XENON1T, the device itself needs to be calibrated. The characterization of the neutron generator aims to answer three questions: how many neutrons are produced (what is the absolute flux), where are they going (what is the angular distribution), and what is their energy? All of this was determined after an extensive calibration campaign. Based on this, the paper shown in chapter 7 was published.

The angular distribution of the neutrons appears to be consistent with an isotropic distribution, if the internal geometry of the neutron generator is taken into account. The absolute flux was determined using measurements at different voltage and current settings, taking into account the internal geometry of the neutron generator and the experimental setup with a Monte Carlo simulation.

For the energy spectrum of the neutrons, measurements with a liquid scintillator detector were used. The observed energy deposition in the detector is not equal to the energy of the neutrons, because the energy deposition depends on the unknown scattering angle. This means that even for mono-energetic neutrons, a spectrum of observed recoil energies is possible. Rather than measuring the energy of the incident neutrons event-by-event, the observed recoil spectrum can be calculated from the incident neutron energy spectrum given the known detector response. In the analysis in chapter 7, there are two methods used to retrieve the neutron energy spectrum. First, the neutron energy spectrum at production in the neutron generator and at the liquid scintillator detector are calculated with a Monte Carlo simulation. Using the response function, the recoil energy spectrum is then calculated, which can be matched to the observed spectrum. Second, a method called deconvolution performs the inverse operation to convolution, so that the neutron energy spectrum at the detector can be computed. Both methods agree well. This thus gives us knowledge of the neutron energy spectrum. In the case of a plasma deuterium neutron generator, this is not equal to a single peak at the reaction neutron energy of 2.45 MeV, but is rather a spectrum with two peaks at 2.2 MeV and

2.7 MeV. This is because the fusion reaction does not occur in the same frame of reference as the lab frame, which gives an observed kinetic energy that depends on the reaction angle.

An unexpected result from the energy calibration of the neutron generator is the observation of neutrons with a much higher energy than the neutrons from deuterium-deuterium fusion. Using the Monte Carlo method described above, we reconstruct a neutron energy of roughly 14 MeV, consistent with neutrons from deuterium-tritium fusion. We attribute this to minor quantities of tritium produced in the deuterium-deuterium fusion reaction. Although the amount of tritium is small, the cross section of this fusion reaction is much higher, so that the contribution of these high-energy neutrons is around 3.5 %. This result illustrates the importance of a detailed calibration of neutron generators, since unknown effects like this can cause an overestimate of the signal yields in xenon if they remain unaccounted for.

chapter 8 and 9: neutron calibration and dark matter search

After the characterization of the neutron generator described in chapter 7, it was deployed as a calibration source for XENON1T. The results of this calibration are shown in chapter 8. The calibration of the neutron generator gives the input into Monte Carlo models, which are then matched to data from XENON1T. This gives essential information that is used for the dark matter search of XENON1T. In particular, the S2/S1 ratio required for background rejection is mapped out with this data. The nonhomogeneous spatial distribution of events is furthermore used to validate the position reconstruction.

In the year-long science run of XENON1T, no significant excess of events was found. Unfortunately, this means that dark matter has yet to be discovered. With the null result, XENON1T tightens the constraints on dark matter, excluding parameter space in the plane of mass and cross section, as shown in figure 4. The XENON1T limits are the strongest limits to date.

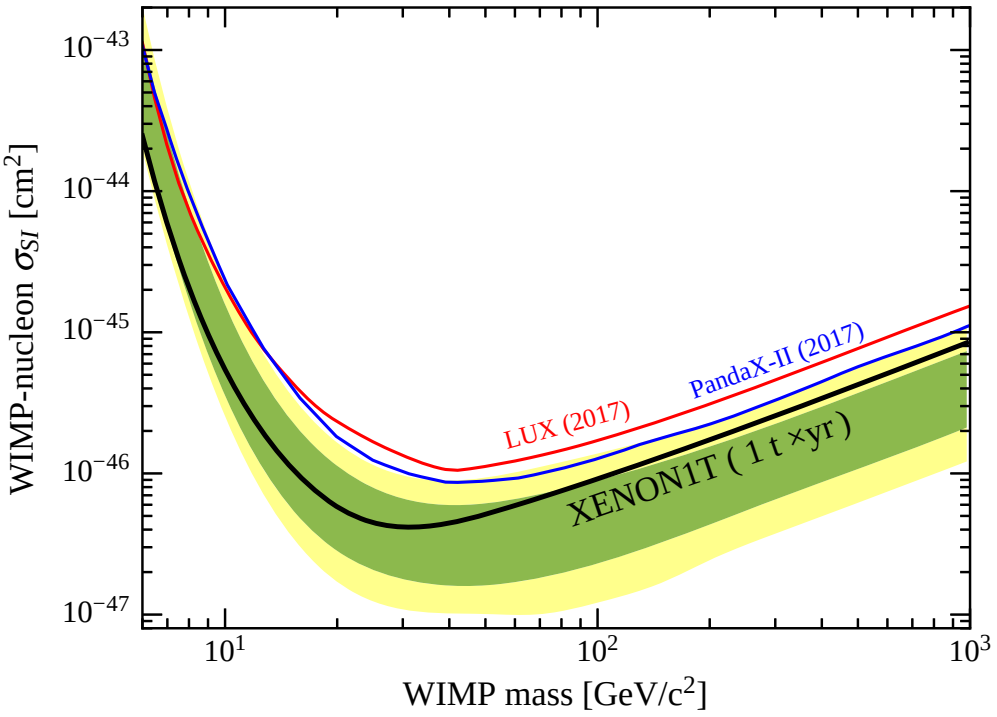

Figure 4: *The obtained exclusion limit from the 1 tonne-year exposure of XENON1T (solid black line). The red and blue lines show the results from LUX and PandaX-II. The green and yellow regions are the 1σ and 2σ sensitivity bands, respectively. Adapted from [5].*

The search for dark matter is not over yet; larger xenon-based experiments, such as LZ and XENONnT, are under construction and will likely start taking data in 2019. These experiments will be up to 10 times more sensitive to WIMPs than XENON1T due to the combination of a larger target mass and a lower background. It is impossible to say if these experiments will find dark matter. We just have to try hard and hope for the best. In any case, the next few years will be exciting, and I eagerly await the results from the next phase of xenon experiments, whether it is a null result or, finally, a detection.

Myth busting precision physics

Improving SM predictions with resummation, and the status of fine-tuning in SUSY

Proefschrift ter verkrijging van de graad van doctor
aan de Radboud Universiteit Nijmegen
op gezag van de rector magnificus prof. dr. J.H.J.M. van Krieken,
volgens besluit van het college van decanen
in het openbaar te verdedigen op

maandag 7 september 2020

om 13.30 uur precies

door

Melissa Corona van Beekveld

geboren op 2 oktober 1992

te Oss

SUMMARY

As a kid, I loved August, for which I had three good reasons. Firstly, I did not have to go to school in August, so I could play with my sister the entire day. Secondly, the Perseids meteor shower peaks around the 12^{th} of August, creating an incredible scene of shooting stars. And thirdly, it is *the* time for bats: when the night falls, these beautiful creatures numerously appear. Bats intrigued me for several reasons, one of which being that my mom was and remains terribly afraid of them, but also because of how they catch their prey. My dad explained to me that bats navigate by using echolocation: they send out a sound, and when it scatters off an object they can locate and identify this object. But I noticed one thing: the bats would eat moths but, to my grave disappointment, they would hardly ever eat the annoying mosquitoes!

It took some time, but in high school, I finally understood the reason for the bat's diet. As humans, we can observe and identify objects only if light can scatter from the object. This scattering does not take place if the wavelength of the light wave is smaller than the size of the object [1]. Analogously, the bat's echolocation works if the insect is larger than the wavelength of the sound wave of the bat's squeak. If the insect is smaller than this wavelength, it is simply invisible to the bat. We can estimate that the wavelength is around 0.75 cm if we assume that the frequency of the bat's squeak is around $40 - 50$ kHz [2]. The average size of a mosquito is around 0.5 cm, so it is just a bit too small to be easily spotted by the bat. To 'see' smaller insects, the bat would need to produce sounds with higher frequencies.

From bats to particle physics

Particle physicists study the smallest length scales of the universe: *fundamental particles*. A fundamental particle is anything that cannot be broken into even smaller pieces. Everything that we see around us is composed out of these particles. The bat story above illustrates that to explore the small length scales of fundamental particles, one needs high frequencies. High frequencies are equivalent to high energies. Naturally, *high energy physics* is often used as a synonym for particle physics: to study the smallest length scales of the universe, we need very high energies.

To probe the properties of fundamental particles, we smash them into each other with a tremendous amount of energy in a particle collider. The Large Hadron Collider (LHC), located near Geneva, is the world's most powerful collider. In the LHC, *hadrons* are smashed into each other, and particle detectors observe the collision products. Hadrons

[1] For example, with a light microscope, we can only see stuff that is larger than about 0.5 μm, which is roughly 200 times smaller than the width of a human hair.

[2] We take the speed of sound to be around $c = 340$ m/s. Denoting the frequency by f, the wavelength λ then becomes $\lambda = c/f \simeq 0.68 - 0.85$ cm.

(e.g. protons, which may be found inside atoms) may be seen as bound packets of fundamental particles. A particle collision is very different from any classical collision during which the colliding objects would break. Instead, in a particle collision, the two colliding particles form a *bundle of energy*, which then transforms into a collection of *different* fundamental particles. By measuring and analyzing these collision products, we have discovered that there are only a few *different* groups of particles.

The fundamental particles and their properties are mathematically described by the Standard Model (SM). This theory organizes particles into two groups. Matter forms the first group, and is further divided into leptons, such as the electron, and quarks, which are contained inside the hadrons. The second group is composed of the so-called *force carriers*, which allow for interactions/transitions between particles during e.g. a particle collision. The photon (light particle) is an example of such a force carrier, and is responsible for the presence of the *electromagnetic force*. Besides this force, the SM describes two additional forces: the *strong force* carried by the gluon, and the *weak force* carried by the W- and Z-bosons. Finally, the SM contains the *Higgs boson*, which does not belong to either of the two groups. Instead, this particle is responsible for the masses of the fundamental particles.

Theoretical particle physicists predict how often certain collision products will be measured at the LHC. These predictions are based on calculations performed within the SM. The outcome of these calculations can then be tested by experimentalists, who can tell us whether the SM indeed correctly describes the measured physics, making it a good (mathematical) description of nature. Using this two-step process, the particle physics community found that an astonishing amount of data, ranging from very small to very large distances, can be described accurately by the SM. However, there is also strong evidence that the SM is not complete. For example, a variety of astrophysical observations imply that there exists a new and unknown (not SM-like) form of matter, which is called dark matter. Without dark matter, we cannot explain why the universe can exist in its observed form, as it is required at every stage of the evolution of our universe: it is needed to form atoms, create galaxies, and account for the motion of galaxy clusters. The SM does not account for this form of matter. Such a shortcoming tells us that the SM is not a complete description of nature, therefore we expect its ability to describe experimental data to break at some point. This makes it absolutely necessary to test the validity of the SM in experiments. The availability of reliable theoretical predictions has a crucial and indispensable role in this.

Perturbation theory

So how does a theorist make predictions? Conventionally, a theorist would sit down and open the toolbox of *perturbation theory*. This technique may be understood as follows. Imagine that Sascha has never seen a cow in real life, and I aim to explain what this animal looks like. A first-order approximation of a cow would be:

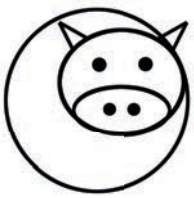

(a) *First-order approximation of a cow.*

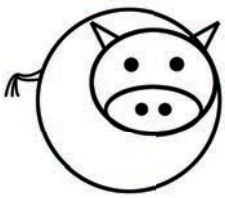

(b) *Second-order approximation of a cow.*

Figure S.1

The cow is roundish, has a head, ears, and a nose (Fig. S.1a).

I can now show Sascha a picture of, say, a car, and since it does not meet my descriptive model of the cow, she would respond with: definitely not a cow. But imagine I would show her a picture of a pig. This animal is also roundish, has a head, ears, and a nose. For Sascha to give a correct answer, I need to improve my description of the cow. Thus, I make a second-order approximation of the cow, for which I add:

The cow is roundish, has a head, ears, a nose, *and a fluffy tail* (Fig. S.1b).

Since the pig has a curly tail, it is definitely not a cow, and not identified as such by Sascha. This simple example shows that depending on the data (i.e. the pictures that I show her), Sascha needs a better description of the cow.

In perturbation theory, we follow a similar procedure. Theorists predict the number and/or characteristics of the observed collision products (or *observables* in short). A theoretical prediction is nothing more than to describe an observable with an equation that *follows* from the SM. Experimentally, an observable is a measurable number. Theorists then provide experimentalists with an *as-good-as-needed* mathematical description of their data. If the experimentalists cannot give a conclusive answer to the question 'does the SM describe these data?', it is the theorists' job to update the mathematical description, and more accurately predict what the observable should look like.

The calculations that are needed to make these predictions can be illustrated using *Feynman diagrams*. These intuitive pictures represent the equations that follow from calculations performed in a particle-physics theory such as the SM. Using Feynman diagrams, the particle-physics equivalent of the lowest-order cow description looks like:

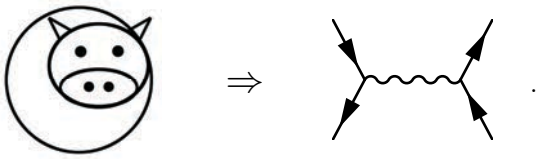

The Feynman diagram on the right illustrates the equation that belongs to the scattering of two quarks (represented by two lines with arrows on the left-hand side). This scattering is illustrated by a *vertex* where the two quark lines meet. Such a vertex pictorially

describes an interaction between particles, and shows up with the emission of a particle: the energies of the two quarks are bundled in one photon (the wiggly line). This bundle of energy then transforms into two leptons (the two lines on the right-hand side) [3]. This is a first-order approximation of the observable 'two leptons'.

We need to upgrade the prediction if the first-order approximation turns out to be insufficient. In perturbation theory, this amounts to dressing the first-order approximation with diagrams that have an *additional* vertex. This means that the particle-physics equivalent of a second-order description of a cow is

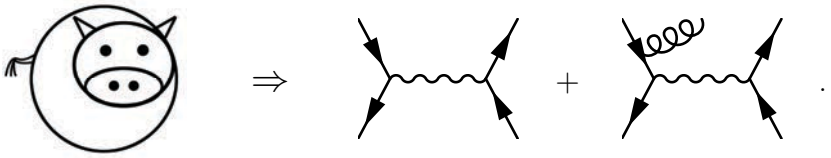

The order of a certain diagram is given by the number of additional vertices it has with respect to the first-order diagram. A second-order description can then be obtained by *adding* second-order diagrams to the first-order diagram. This process has to be repeated if a higher-order description is needed, leading to a more accurate description of the observable.

Why do we only provide the experimentalists with an as-good-as-needed description, and not just give the full higher-order description of the observable? We would certainly wish to do so, but unfortunately it is extremely difficult, if not impossible, to calculate all higher-order contributions. Luckily, higher-order contributions are often not necessary to provide an as-good-as-needed description of the data. There is a simple reason for this: every additional vertex comes with a factor of the *coupling* (α). Any n^{th}-order diagram is then proportional to α^n. This coupling represents the particle-interaction strength, and each force has its own coupling strength. The coupling of the strong force (α_s) has the highest value of all couplings in the SM (hence the name). The coupling strength needs to be smaller than 1 in perturbation theory. Indeed, if α_s is smaller than 1, then α_s^2 is smaller than α_s, etc, ensuring that higher-order diagrams with larger values of n can be neglected.

Resummation

However, there are some cases where this assumption fails. This happens because not only the size of α_s^n matters, but that of the coefficient c_n multiplying α_s^n. Every n^{th}-order diagram can be written as $c_n\alpha_s^n$, where c_n depends on the dynamics of the collision (for example the energies of the ingoing particles and collision products). If c_n grows 'too fast' when n increases, we enter a situation where we certainly cannot neglect higher-order contributions. An example of such a too-quickly growing c_n is shown by Fig. 2.3

[3] This equation may be seen in its full form on page 14, Eq. (2.2). The process represents the so-called Drell-Yan scattering process, see Chapter 2.

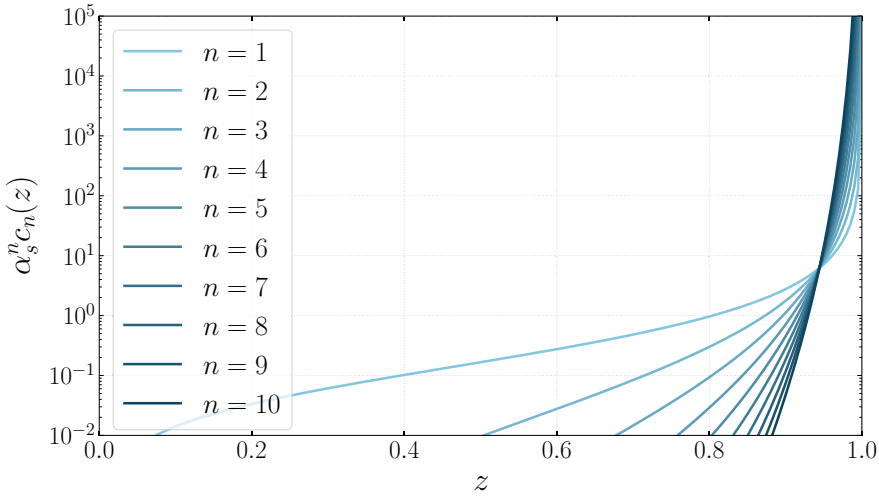

Figure S.2: *The product $\alpha_s^n c_n(z)$ for $n = 1 \ldots 10$ as a function of the threshold parameter z. A darker shade of blue indicates a higher value of n.*

on page 22, relabeled here in Fig. S.2. We show here the product $\alpha_s c_n(z)$ as a function of the *threshold parameter* z. This threshold parameter is a number between 0 and 1 that indicates how far we are from the *threshold region*, the region where a higher-order contribution is *larger* than a lower-order contribution. In the figure, it may be seen that for most values of z, the lines with a lower value of n lie on top of those with a higher value of n. This behavior turns around when z gets closer to 1. There, we end up in the threshold region where we no longer may neglect the higher-order contributions.
One might say that there is a simple solution to this issue: why not calculate c_n to arbitrary n? Unfortunately, as already mentioned above, this is technically not achievable. Therefore, to make a theoretical prediction in the domain where c_n grows with increasing n, we need to resort to a different toolbox.
The first part of this thesis is devoted to the development of such a new toolbox called

next-to-leading power
threshold
resummation.

We have already come across the word *threshold*. The region where the perturbative description of the observable fails is called the *threshold region*. The coefficient c_n is a sum of different contributions. *Power* is the term that is used to indicate how badly-growing each of these different contributions of c_n is in the threshold region. *Leading power* then constitutes those parts of c_n that cause its largest growth in the threshold region, while *next-to-leading power*, or NLP in short, indicates the 'next-to-largest'-growing parts of c_n.
The calculational technique that is used to make the theoretical predictions is called *re-*

summation. Instead of calculating the full form of c_n, for resummation one *only* considers the parts of c_n that cause its growth. We then sum *only* these parts for all values of n, which gives an accurate description of the observable in the threshold region. Resummation requires that one can identify and predict for all values of n only those contributions to c_n that cause it to grow. The leading-power contributions to c_n were unraveled around the 1980s, which allowed for the development of *leading-power threshold resummation*. This toolbox has proven to be crucial to accurately describe the experimental data.
Much less is known about NLP threshold resummation. In particular, it is unknown how we should predict c_n for all values of n at NLP. In Chapter 2, we analyze this problem. We find that the emission of quarks must be taken into account, while it was previously assumed that this source could be neglected. Another important result of this chapter is that we have succeeded in writing down a universal formalism that predicts the NLP contributions for any observable.
One might place doubts on whether the numerical size of NLP contributions is of importance to the measurements that are done at the LHC. To that end, we examine the numerical impact of NLP contributions in Chapter 4. There we consider the process where a single photon is created in an LHC collision. This process is of particular theoretical and experimental relevance since it is used to measure the size of the strong coupling, hence accurate and reliable theoretical predictions are needed for it. We find that the NLP contributions constitute a $10-20\%$ correction to the behavior of the observed photon, which is shown in Fig. 4.6 on page 138. That is, without taking into account the NLP contributions, the theoretical prediction would be off by $10-20\%$. This confirms the necessity to further develop the toolbox of NLP threshold resummation, such that we can optimally test the SM at colliders.

The fine-tuning problem

The second topic explored in this thesis is the *fine-tuning problem*. This problem *may* arise in the construction of a beyond the SM theory (BSM). Such a theory is necessary to, for example, accommodate for dark matter, but in general to account for the shortcomings of the SM. The fine-tuning problem is a problem of the Higgs boson, which is discovered in 2012 but predicted long before that. We knew that many of the fundamental particles are massive, and without the Higgs boson, there is no way to explain the presence of those masses in the SM. Hence, it is often quoted that the Higgs boson 'gives' mass to the other SM particles. Particle masses are expressed in units of 'GeV', where 1 GeV is equal to the mass of the proton. The mass of the Higgs boson is measured to be 125 GeV. As for any other observable, theorists can express this observed mass in terms of an equation. By doing so, one finds that the *observed* Higgs boson mass is a sum of the *theory parameter* that represents the Higgs boson mass, plus the masses of *all* other fundamental particles [4]. The terms in the sum that results in the

[4] This is represented by Eq. (6.3) on page 171.

measurable Higgs boson mass *must* equate to 125 GeV. Each term in this sum is a 'free' theory parameter (a freely tunable knob of the theory). However, these parameters have to be tuned such that the observed Higgs boson mass of 125 GeV comes out. We speak of a fine-tuning problem if 'considerable' tuning of the theory parameters is required to obtain the observed Higgs boson mass.

Particle physicists use a percentage to represent the amount of fine-tuning. This *fine-tuning number* indicates with what percentage the theory parameters need to vary to induce a change of $\mathcal{O}(100\%)$ in the observed Higgs boson mass. A *small* fine-tuning number means that there is a *large* fine-tuning: the theory parameters need to be tuned considerably to get out the observed Higgs boson mass in case of small fine-tuning numbers. Note that there is no consensus on how much tuning is 'considerable' fine-tuning. Here, we assume that fine-tuning numbers below 1% are too low and result in too much fine-tuning.

The SM does not have a fine-tuning problem with this definition. This is because the heaviest particle in the SM has a mass of 175 GeV, which is of the same order of magnitude as the Higgs boson mass itself. We may naively estimate the fine-tuning number to be around $\mathcal{O}\left(\frac{125}{175}\right) = \mathcal{O}(100\%)$, which is much higher than 1%. By constructing a BSM theory, we introduce new particles whose masses then enter in the equation for the observed Higgs boson mass. Let the mass of a new particle be 1000 GeV. When we now change the mass of this particle by $\mathcal{O}(10\%)$, the mass of the Higgs boson changes by $\mathcal{O}(100\%)$, as 100% of the Higgs boson mass is of the same size as 10% of 1000 GeV. We then say that the fine-tuning number is around 10%. The fine-tuning gets worse (and the fine-tuning number gets smaller) for increasing BSM masses: suppose we introduce a particle of 10^6 GeV. In this case, the mass of the observed Higgs boson would change by $\mathcal{O}(100\%)$ if the mass of the BSM particle changes by only $\mathcal{O}(0.01\%)$!

We find fine-tuning unsound, and the reason for it is that we assume that the effects of physics that take place on widely different mass scales do not affect one another. This assumption does not seem to hold in case of severe fine-tuning, as then the Higgs boson mass is extremely sensitive to the mass scale of new BSM particles. We may therefore use fine-tuning as a constraint on a BSM theory by demanding that the induced fine-tuning number does not get below 1%.

How then can one construct a BSM theory with a fine-tuning number above 1%? This question is analyzed in Chapter 6 in the context of the popular BSM theory *supersymmetry* (SUSY). SUSY introduces a collection of new fundamental particles, of which one is a candidate for dark matter. SUSY *can* result in fine-tuned scenarios depending on the masses of these new particles. Unfortunately, none of the newly predicted SUSY particles have been observed at the LHC. This causes concern in the particle physics community, and makes many believe that the non-observation of new SUSY particles necessarily results in a severely fine-tuned theory.

Chapter 6 busts this myth: there, we carefully examine what the masses of the new SUSY particles should be such that SUSY results in fine-tuning numbers above 1%. We

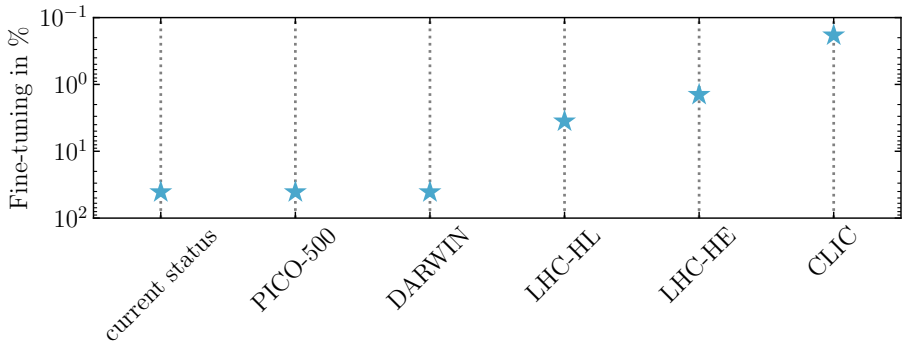

Figure S.3: *Fine-tuning number of the current situation, and that in case of a non-observation in various future experiments.*

implement all world-wide constraints on the SUSY-particle masses and interactions, and show that SUSY scenarios with high fine-tuning numbers (i.e. those above 1%) are actually *untested* by our current experiments. The myth is therefore busted: the current experiments cannot say whether SUSY exists without severe fine-tuning. This conclusion is shown in Fig. 6.20 on page 215, of which a simplified version is presented in Fig. S.3. Because our current experiments do not see any signs of SUSY, they constrain the fine-tuning number of SUSY to about 33%. In this figure, we also show which experiment may best be build to discover SUSY with fine-tuning numbers above 1%. PICO-500 and DARWIN are proposed future dark matter detection experiments. The LHC-HL and LHC-HE are upgrades of the LHC, whereas CLIC is a proposed new future collider. We see that CLIC has the highest sensitivity, and the figure shows that the fine-tuning number drops to 0.2% if we do *not* find any SUSY-signal at CLIC. This would make SUSY fine-tuned, but there is no reason for concern just yet.

In this thesis we have tackled two aspects of the search for physics beyond the SM: on the one hand, we have improved the predictions that follow from the SM, and on the other hand, we have studied where we should look for signs of BSM physics. Will we see any signs of it at the LHC or future experiments? Only time will tell. For now, we are like hungry bats: we just cannot spot the BSM mosquito.

VRIJE UNIVERSITEIT

Seismic and Newtonian noise modeling for Advanced Virgo and Einstein Telescope

ACADEMISCH PROEFSCHRIFT

ter verkrijging van de graad Doctor of Philosophy
aan de Vrije Universiteit Amsterdam,
op gezag van de rector magnificus
prof.dr. V. Subramaniam,
in het openbaar te verdedigen
ten overstaan van de promotiecommissie
van de Faculteit der Bètawetenschappen
op dinsdag 9 februari 2021 om 15.45 uur
in de aula van de universiteit,
De Boelelaan 1105

door

Maria Karolina Margit Bader

geboren te München, Duitsland

English summary

For centuries, humans have been curious to understand the nature of the Cosmos surrounding us. Not only do we aspire to understand the underlaying laws that hold the Universe together, even more so do we hope to reveal the mystery behind its origin. The quest that gravitational wave science is set upon is nothing less than gaining deeper understanding of the composition of the Universe.

What are gravitational waves?

Gravitational waves have been predicted as a consequence of Einstein's Theory of general relativity, that has been formulated in 1916. General relativity describes how mass, such as planets, stars or black boles, curves spacetime in our Universe and how this curvature in turn affects the motion of the masses. Masses that are accelerated induce "ripples" in the fabric of spacetime (see Fig. 2). These ripples are called gravitational waves. In general, all kinds of accelerated masses can produce gravitational waves. However, the fabric of spacetime is very stiff and only the most violent events in the Universe emit waves that are large enough to be measurable with our detectors on earth. Such events are for example the collision of heavy objects such as stel-

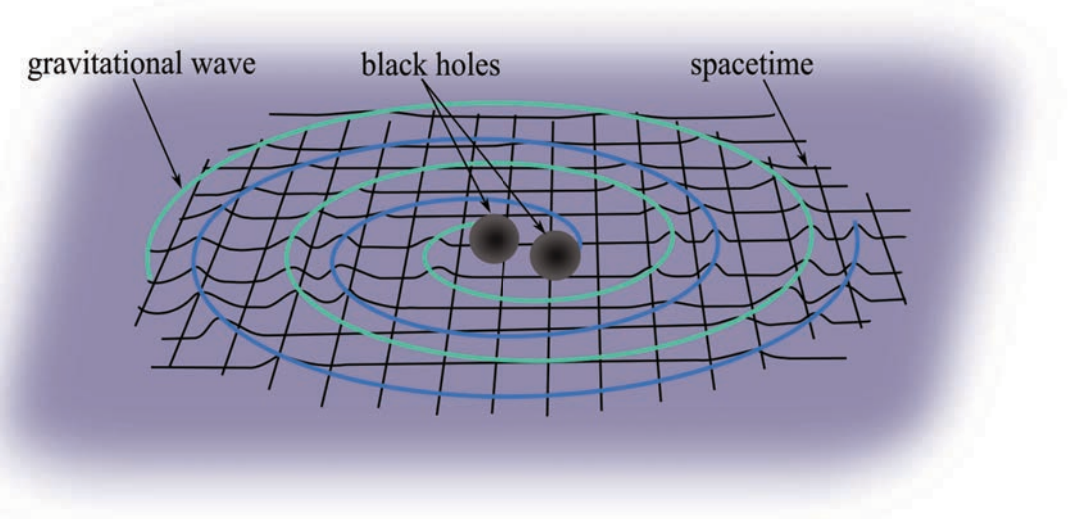

Figure 2: *Spacetime can be imagined like a rubber band. Heavy objects that move in an accelerated motion, such as colliding black holes, cause ripples in spacetimes. These ripples are called gravitational waves and they travel through the Universe at the speed of light.*

lar mass black holes, asymmetric rotating neutron stars or burst events of new, undiscovered objects. Numerous events from colliding black holes and two events from binary neutron star mergers have been reported since the very first detection of gravitational waves in 2015. Gravitational wave measurements of neutron star mergers complement electromagnetic observations from telescopes and give new information on the structure of neutron stars and on cosmological parameters such as the Hubble parameter.

How do we measure gravitational waves?

On Earth gravitational waves are measured with laser interferometers, which are based on the design of a Michelson interferometer. Advanced Virgo is a laser interferometer in Italy, where a laser beam is split with a beam splitter into two 3 km long paths (see Fig. 3, left panel). At the end of each arm the laser beam is reflected back towards the center and both beams are recombined at the beam splitter. The intensity of the resulting laser beam is then investigated with a photo diode.

If no gravitational wave is present, the lengths of both arms are almost the same and are tuned such that the recombined beams interfere destructively. As a result, almost no light is detected at the photo diode. If a gravitational wave passes, it stretches one arm, while the other one is compressed. Now one laser beam travels a longer distance than the other one and they are out of phase when they are recombined. As a result a time dependent signal can be measured with the photo diode (see Fig. 3, right panel). The strength, duration and shape of this signal depends on the type of source that emitted the gravitational wave. It allows to distinguish between different

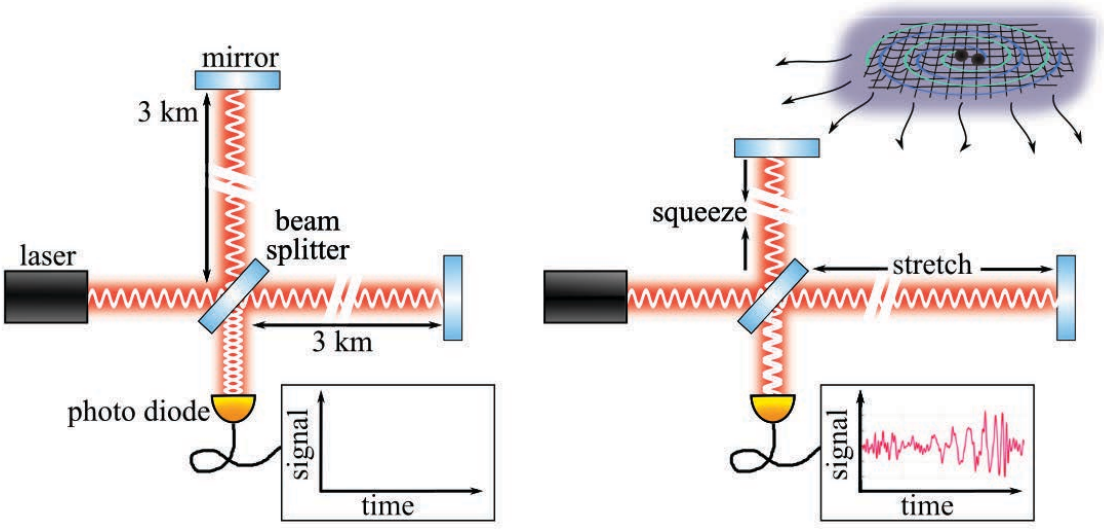

Figure 3: *Left: Gravitational waves are measured with laser interferometers, where a laser beam is split into two arms of several kilometers length. At the end of the arms, mirrors reflect the laser beam back towards the center, where both beams are recombined and measured with a photo diode. If no gravitational wave is present, then the arm lengths are tuned such that the laser beams interfere destructively and no signal is visible at the photo diode. Right: If a gravitational wave passes, one arm is compressed and the other one is stretched. The recombined laser beams do not interfere destructively anymore and as a result a signal is measured at the photo diode. The shape is characteristic for each gravitational wave source type. Note that in reality this effect is much smaller than depicted here.*

types of events and gives valuable information on the mass composition and distance of the gravitational wave source.

Performance limitations of gravitational wave detectors

Gravitational wave signals are very faint, for instance the loudest event measured so far only lead to a variation in arm length of about 0.000 000 000 000 000 01 m, which is a small fraction of the radius of the atomic nucleus. On Earth, many noise sources disturb the detector and thereby limit its performance. Seismic motion, driven by oceanic and human activity, couples directly and indirectly to the mirror motion and is the main cause of the noise sources discussed in this dissertation. The interaction of the mirrors with the seismic motion of the soil is suppressed by suspending the mirrors from a system of springs and pendula such that they can be assumed to be freely floating across almost the full frequency range of the detector (see Fig. 4, left panel). However, at very low frequencies, the suspension system is not sufficient anymore, and an active feedback control loop is in place to correct the mirror motion (see Fig. 4, central panel). In this work the performance of the angular control system that is in place at Advanced Virgo is briefly discussed and its performance during the third observation run is evaluated. Another important aspect is that seismic motion couples directly to the mirrors, which are attracted to denser regions in the seismic field via gravitational attraction (see Fig. 4, right panel). Modeling this so called *Newtonian noise*, depending on seismic fields that are characteristic for the detector site, is the main topic of this thesis.

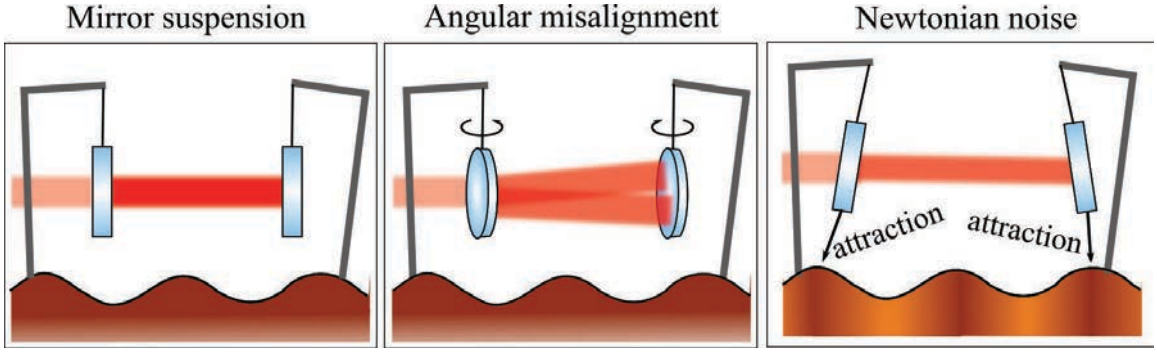

Figure 4: *Left: To reduce the interaction between the mirror and the ground motion, the mirrors are suspended by a system of pendula. They can be assumed to be freely floating across almost the full frequency range. Center: At low frequencies, the seismic motion is not sufficiently suppressed by the suspension system and the mirrors suffer from residual angular motion. Active angular feedback control loops are in place at Advanced Virgo to keep the mirrors aligned during operation. Right: Direct interaction between the mirrors and density fluctuations in the seismic field induce the so called Newtonian noise.*

Seismic models for site-based Newtonian noise

Current models that estimate Newtonian noise at gravitational wave detectors assume surface detectors and rely on a soil that consists of a single material in which only one specific wave type propagates. However, realistic geologies are multilayered and the seismic field consists of a complex composition of surface and body waves, which are excited by seismic sources. Such sources can for example be traffic on roads or over bridges or wind shaking buildings. In

addition, the prospective construction of Einstein Telescope, a next generation European gravitational wave detector that will be installed 100 to 300 m underground, gives rise to the necessity for realistic seismic and Newtonian noise models. From a scientific point of view, the selection of the location for Einstein Telescope will be set in an area that favors low Newtonian noise levels.

Recently, the subsurface composition at Advanced Virgo in Italy and at the Belgian-German-Dutch (BGN) Einstein Telescope candidate site in the Netherlands have been determined by using large arrays of seismic surface sensors. The geology at Advanced Virgo has been found to consists of nine soft soil layers. The most dominant seismic sources are more than 1 km away and originate from road bridges of a nearby highway and a distant wind park. The geology at the BGN site has been found to consist of five subsurface layers, which consist of soft soil down to about 35 m laying on a thick layer of hard rock. Noise sources in this region are local and within a few hundred meters up to 1 km distance from the sensor array. For both detectors a seismic model that is based on the measured geology and that reproduces seismic conditions such as

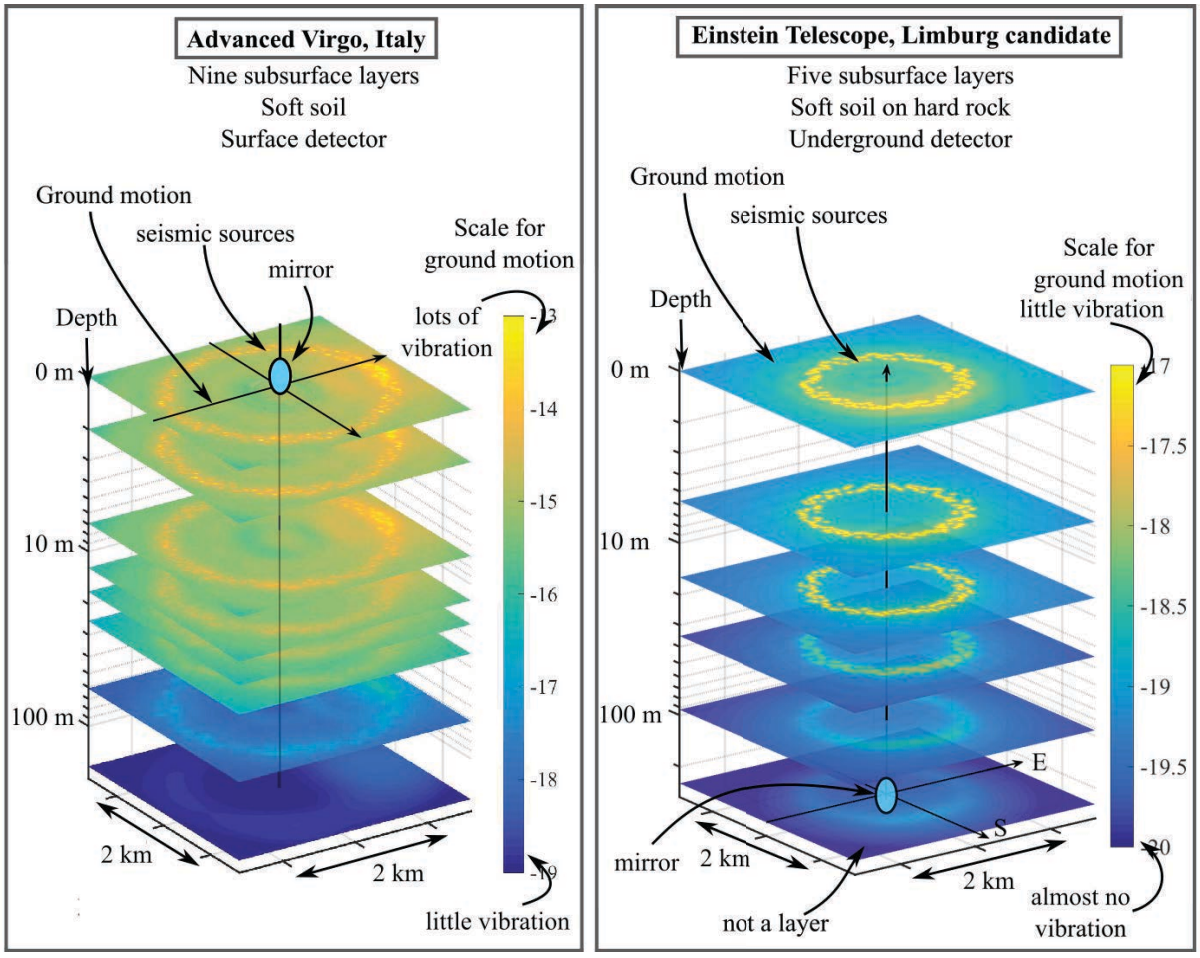

Figure 5: *Schematic drawing of the seismic model that is based on the geology and source locations as measured at the Advanced Virgo detector in Italy (left) and at the Einstein Telescope candidate site in Limburg (right). The color indicates the strength of the ground motion and each colored sheet represents the seismic motion at the start of a new subsurface layer. It is visible that the seismic motion is strongest on the surface and attenuates further underground. Note that at Advanced Virgo the mirror is on the surface while for Einstein Telescope it is* 250 m *underground.*

surface wave speeds and seismic spectra has been derived (see Fig. 5). From these seismic models, site-based Newtonian noise has been calculated for both detector sites by numerically integrating the seismic field in the vicinity of the mirrors.

Where do we go from here?

The research that has been presented in this dissertation has lead to a better understanding of how local seismic conditions such as the geology and the seismic field affect Newtonian noise at a given gravitational wave detector. We have also learned that additional factors such as the detector depth as well as the shape and size of the cavern have a strong influence on Newtonian noise. Future research is therefore recommended to elaborate on the one hand on the geology models, for example by including complex three-dimensional subsurface structures, and on the other hand on a detailed understanding of the influence of cavern geometries on the Newtonian noise of underground gravitational wave detectors.

In this work a detailed understanding of the site-based Newtonian noise at a given detector site is obtained. However, Newtonian noise cannot be suppressed and at times it may limit the detector performance during operation. It is therefore of the utmost importance that future research encompasses the development of online subtraction schemes based on permanent seismic sensor arrays that constantly monitor the seismic field around the detector and cross-correlate it to the detector output. First steps towards the development of an online subtraction scheme are taken at Advanced Virgo, where a permanent sensor array is currently being installed and integrated into Virgo's online-monitoring system for environmental noise.

Quantum Effects on a Planetary Scale
The First Neutrino Oscillation Measurement with KM3NeT/ORCA

ACADEMISCH PROEFSCHRIFT

ter verkrijging van de graad van doctor
aan de Universiteit van Amsterdam
op gezag van de Rector Magnificus
prof. dr. ir. K.I.J. Maex
ten overstaan van een door het College voor Promoties ingestelde commissie,
in het openbaar te verdedigen in de Aula der Universiteit
op woensdag 8 juni 2022, te 11.00 uur

door Lodewijk Jurriaan Nauta
geboren te AMSTERDAM

English Summary

Oscillation (noun): movement back and forth in a regular rhythm
—Oxford English Dictionary

Setting the Stage: the Standard Model

Neutrinos are strange, very strange particles. In order to understand what this dissertation is about we will first have to discuss the properties of these strange particles.

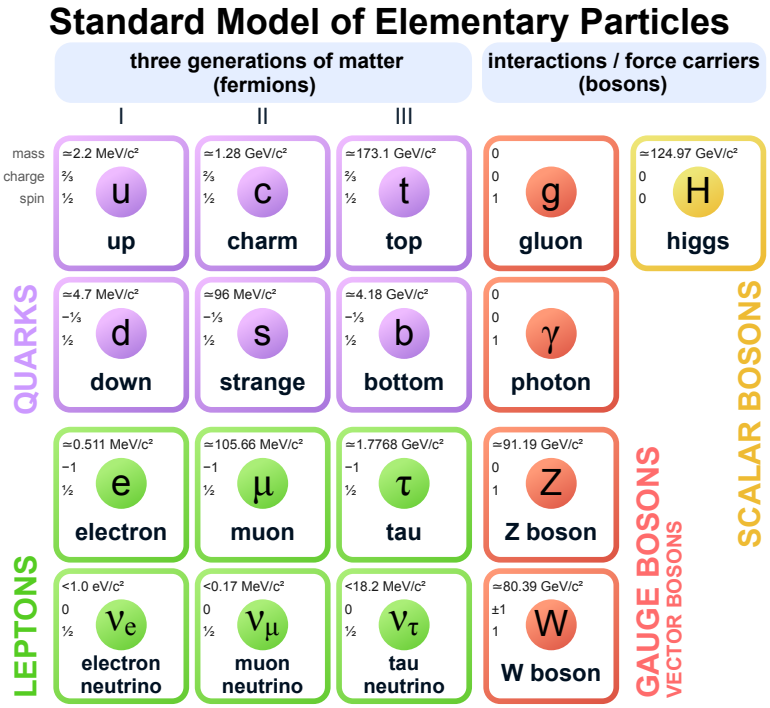

Figure S.1: Overview of the fundamental particles in the Standard Model of particle physics. On the left the three generations of matter (fermions) are shown, for both the quarks and leptons. On the right the particles that carry the forces are shown (bosons). Adapted from [110].

Neutrinos (indicated by the symbol ν) are fundamental particles in the SM. There are 3 neutrino *flavours*, one in each generation with the same flavour as the charged leptons: the electron-neutrino, the muon-neutrino and the tau-neutrino. But in many aspects they are unlike any of the other particles in the SM. For example, neutrinos have no electric charge, the other matter particles do. The *quarks* that make up protons, neutrons, and

more exotic forms of matter all carry electric charge. The other particles in the *lepton* family, called electrons, muons and tauons, also carry charge. Moreover, neutrinos have a very small mass compared to the other fundamental particles. The *sum* of the masses of the three neutrinos is at least a million times smaller than the electron mass, the lightest of the charged leptons. This is true even more so for the quarks, which are generally heavier than the lepton of the same generation.

Besides being extremely light and electrically neutral, the strength of the interaction that governs the neutrinos, the *weak force*, is 1.000 times weaker than the *electromagnetic force*, which governs charged particles, and 1.000.000 times weaker than the *strong force*, which is the force that ensures quarks stick together to form protons, neutrons, and other more exotic forms of matter. The result of the feebleness of the weak force is that even though trillions and trillions of neutrinos pass right through you and me every *second*, the number of neutrinos that will interact with your body over the course of your life can be counted on one hand. In particular, the weak force brings about nuclear fission and nuclear fusion reactions. Neutrinos are created in these processes, and in the decay of unstable particles. Neutrinos are instrumental in nuclear fusion in our Sun, which provides our planet with the energy to sustain life. While neutrinos are an important part in the reactions that allow for life on our planet, they are by far the hardest to measure of all the particles that make up matter in the SM, and because of this, they are also the least understood.

Neutrino Flavour Oscillations

Because neutrinos have so few interactions, making precise measurements to find the properties of these elusive particles is a challenge physicists have been struggling with for over 70 years. For the first 50 years after their discovery, it was thought that neutrinos were massless. One of the most surprising discoveries about neutrinos is that they do have mass. Especially in the SM, one of the best tested scientific models we have today, neutrinos *can not have* a mass. This is because neutrinos are always found to be *left-handed*, meaning the spin they carry is always in the same direction relative to their velocity. However, one of the most basic equations describing fundamental particles, called the Dirac equation, breaks down for *massive* neutrinos. This equation describes all matter particles (or *fermions*), like the leptons and the quarks. This equation requires the existence of both left- and right-handed massive particles. But if we want to describe only left-handed neutrinos in the SM, their mass needs to be zero. As a result, neutrinos are massless particles in the Standard Model.

How do we know neutrinos to be massive, if they have such a low mass, and are so hard to measure? This discovery was made by measuring a property of neutrinos called *flavour oscillation*, which is the main topic of this thesis. This flavour oscillation means that when you start with a neutrino of an initial flavour, say ν_e, and you measure at some later point in space and time what the state of this particle is, it is not guaranteed to be ν_e. You could measure a different neutrino flavour, ν_μ or ν_τ, or indeed the same ν_e. The flavour of the neutrino *oscillates* between e, μ and τ as it travels. This peculiar property of the neutrino is only present when neutrinos *have mass*, and the *mass states* and the *flavour states* of the neutrinos are not the same states.

Neutrino Sources

Neutrino oscillation experiments are designed to probe these flavour oscillations. In such experiments, knowing the travel distance L and energy E of the neutrino are vitally important, as these quantities govern the frequency and size of the oscillation. By studying a well-known source of neutrinos, the distance and the starting neutrino flavour[†] are already known.

Neutrino sources are generally a nuclear reactor core, the Sun, a particle accelerator or the atmosphere of the Earth. These different sources are all used to measure different neutrino oscillations parameters. For all these cases, the distance is known: for reactors, the detector can be placed metres to kilometres away, for accelerator we know where the beam hits a target that creates neutrinos, and for the Sun we also know the location and distance very well.

For the atmosphere it is slightly more complicated: high-energy particles from outer space called Cosmic Rays (CR) hit the particles that make up the atmosphere. From these interactions, unstable daughter particles are created that decay into neutrinos and other particles at about 15 km high. And since neutrinos interact extremely rarely, they move in a straight line through the Earth! As the atmosphere covers the whole Earths surface, the incoming angle of a particle in a detector indicates where in the atmosphere the neutrino was created and thus the distance L that the neutrino travelled through the atmosphere and the Earth. Using atmospheric neutrinos we can probe a value of L of up to $\sim$ 12.000 km, i.e. the diameter of Earth.

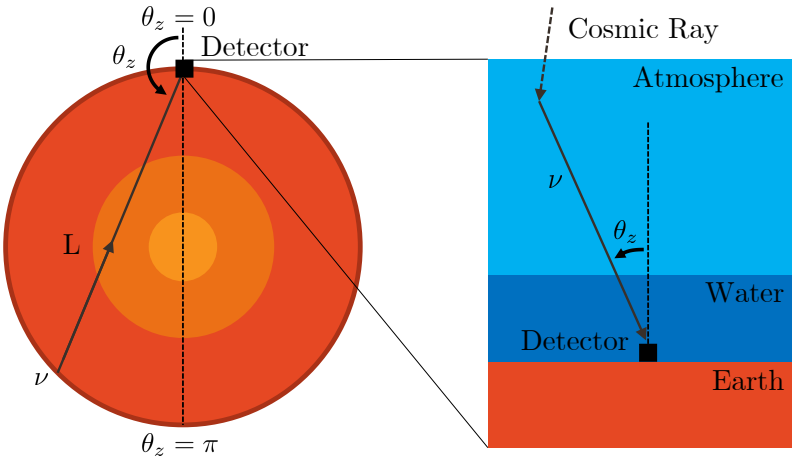

Figure S.2: Overview of Earth, the path a neutrino travels from the atmosphere to the detector and the relation between path length L and incoming angle θ_z. On the left a large overview of the Earth and an incoming neutrino with $\theta_z > 90°$ and on the right a zoomed in view where a neutrino is produced from a cosmic ray in the atmosphere and enters the detector under an angle $\theta_z < 90°$.

Now, we need to measure the energy and travelled distance of the neutrino and we can start measuring oscillations.

[†]For some experiments also whether the neutrino is a particle or anti-particle is known. This detail is omitted for brevity.

The KM3NeT/ORCA Detector

Since neutrinos interact so rarely, there are two approaches to get enough data for a good analysis. One is to create a detector with a clear signal which is shielded very well, to suppress any backgrounds that may show up in the few neutrino events captured. The other is to build a very large detector so that the detection rate scales with the large volume.

KM3NeT is a research infrastructure that uses both these approaches in its design. KM3NeT is comprised of two detectors deployed at the bottom of the Mediterranean Sea. To perform neutrino physics research two large grids of light sensors will be deployed that each make up a detector. The ARCA detector is built to do astrophysical neutrino research, while the ORCA detector is built for neutrino oscillation research. The main goal of the completed ORCA detector is to do a precision study of neutrino oscillations, where it will be determined which of the neutrino masses is the largest. This is called the Neutrino Mass Ordering problem.

The water shields the detector from a lot of the backgrounds that reach the surface of the Earth. In the case of ORCA, this grid of sensors will cover a volume of about 7 million tonnes of water when the detector is finished. Because of the large detector size, hundreds of neutrino events will be captured each day. With a complete detector, ORCA will be at the forefront of neutrino physics. At the time of writing, out of the 115 *Detection Units* (DUs) that KM3NeT/ORCA plans to deploy, 10 have been deployed. This detector is called ORCA-10, being roughly 9% of the full size. The oscillation research presented in this thesis was done when ORCA was made up of 6 DUs, called ORCA-6.

Each of these DUs is a vertical line containing 18 *Digital Optical Modules* (DOMs) with a 9m vertical spacing between them in ORCA. Each DOM is a glass sphere containing 31 light sensors called *Photo-Multiplier Tubes* (PMTs) looking in different directions. The multi-PMT setup combined with the nanosecond timing of the light sensors allows for great reconstruction of the events. Even this partial detector can already detect and study neutrino oscillations.

Su

Figure S.3: Left: A KM3NeT photo multiplier tube (PMT).
Right: A KM3NeT digital optical module (DOM). The light sensitive areas of the PMTs are visible as the yellow circles inside the DOM.

Neutrino Interactions and Detection Mechanism

While neutrinos do not interact often, when they do, the neutrino can be transformed into the charged lepton of the same generation[†]. That means that a ν_e becomes an e, a ν_μ becomes a μ and a ν_τ becomes a τ.

[†]The neutrino can also transfer some energy-momentum and escape, but these details are omitted here.

Water is a good detection medium as Cherenkov light is created when these charged daughter particles travel through it at high speeds. This light is then detected by the sensors. From the detected light pulses, you can reconstruct the energy and direction of the through-going particle, and count the events for the different neutrino signatures.

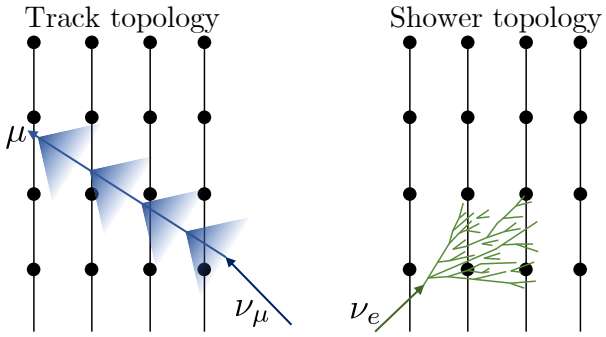

Figure S.4: A schematic overview of the difference between the track and shower topology. The lines are the DUs and the solid dots are the DOMs that contain the PMTs. **Left**: The track pattern provides a linear path through the detector through the little scattering of the muon and the emitted radiation, when the light sensors are hit. **Right**: The shower pattern provides a more sphere-like, localised shape in space, when the light sensors are hit. The differences between different types of showers and different decay channels of τ are neglected here.

The flavours can not be exactly identified by a unique signature, and that is because the e, μ and τ particle interactions can induce similar patterns. The pattern that is most easily identified comes from a muon, that travels in a straight line, from which light is emitted in a cone-like shape. This pattern is called a *track*. The electron and tau that appear, and other types of events, all create a cascade of secondary particles when they are present in the medium, called *showers*. Now we can count the number of tracks and showers and this is the basis of our physics experiment.

Measuring Flavour Oscillations

Shortly after the discovery of neutrinos in 1956, flavour oscillations were predicted in 1957. In the decades thereafter, it became more and more clear that neutrinos exhibit flavour oscillation. The experiment that provided the breakthrough measurement, found the evidence by investigating two different interaction channels in solar neutrinos. From solar fusion reaction models the amount of neutrinos created in the Sun during the fusion process is predicted. By measuring the neutrino flux - that is the number of particles per time per area of the sky - in different *channels* coming from the Sun, it became clear that some change was happening in the transit from the Sun to the Earth. By counting the total flux, and simultaneously counting the number of neutrinos of a specific flavour in another channel, the only conclusion could be that neutrinos have oscillated from one flavour channel to another flavour channel. And so, the fact that neutrinos have oscillated means that neutrinos are massive particles. The discovery does not fit into the SM, so by definition, neutrino oscillation physics is *Beyond the Standard Model* (BSM) physics.

The oscillation prediction also provided us with a model that describes the neutrino oscillation in terms of several physics parameters, called the *mixing angles* $\theta_{12}, \theta_{13}, \theta_{23}$,

the *mass-squared differences* $\Delta m^2_{21}, \Delta m^2_{31}$ and Δm^2_{32} and *CP-violating phase* δ_{CP}. The mass states contribute different amounts to each flavour state, and the mixing angles describe how much each of the mass states contribute to each flavour state. The mass-squared differences is the difference between the masses squared: $\Delta m^2_{ij} = m^2_i - m^2_j$. These Δm^2_{ij} drive the oscillation frequency, which means that for a given E, the mass-squared difference determines how fast the flavour oscillates as the neutrino travels over distance L. Finally, δ_{CP} provides a possible difference between particle and anti-particle interaction rates.

Given the model of neutrino oscillations, we now want to perform a measurement to find the oscillation parameters. If we know the original neutrino flux we can compare it to the oscillated neutrinos that enter the detector. For ORCA, the neutrino source is our atmosphere, and the atmospheric neutrino flux has been measured and modelled by other experiments.

Now we measure the travel distance L and the energy E of the neutrino, *and* the interaction pattern (track or shower) of the particle. With this information we can calculate which oscillation parameters describe our measurements best. Especially if we measure many neutrinos that have travelled over different distances, carrying a range of energies, and being of various flavours, we can get a more precise answer for the oscillation parameters because of the increased statistics.

This is exactly what I have done in this thesis: we took data with our detector, fitted a model to the data, and extracted the oscillation parameters θ_{23} and Δm^2_{31}. Combining the oscillation model and our neutrino counting experiment, we can find the parameters that here best describe the neutrino oscillations.

Results for Determining the Neutrino Oscillation Parameters

The analysis performed in this thesis is the first study of neutrino oscillations with the ORCA detector, using 6 detection lines for data taking. Over one year of data was used, containing 280 million events. From simulated data, it is estimated that about 20 thousand of these events are due to neutrinos interacting in the water and depositing light in the detector. The remainder of the events are background. It seems appropriate to say that we are *looking for a needle in a haystack* at this point.

Su

By investigating event characteristics, how the events are reconstructed and where they end up in the detector, a set of neutrino candidate events is selected and almost all of these hundreds of millions of initial events are rejected. Ultimately, 1237 events survive the selection criteria, and according to simulated data, around 31 of these may still be background.

The neutrino oscillation model predicts how many events should be measured on average in the detector, where the prediction depends on the energy of the reconstructed event, the angle in the detector (θ_z in figure S.2) and the pattern that the particle left behind in the detector. Currently we are only looking at *tracks*, the pattern corresponding to muons passing through.

The neutrino oscillation model is fitted to the data and the result provides the neutrino oscillation parameters that are most likely to describe what was measured in the detector. The result is:

$$\boxed{\begin{aligned} \theta_{23} &= 45.4^{+5.6}_{-5.7}\ \text{(stat.)}\ \pm 0.3\ \text{(syst.)}\ [\text{deg}] \\ \Delta m^2_{31} &= 1.95^{+0.24}_{-0.21}\ \text{(stat.)}\ \pm 0.17\ \text{(syst.)}\ [10^{-3}\text{eV}^2] \end{aligned}} \tag{S.1}$$

The *NuFIT* analysis combines measurements from multiple experiments to get even more accurate parameter estimations for neutrino oscillations than the individual experiments that are part of NuFIT. For comparison purposes, NuFIT has found:

$$\boxed{\begin{aligned} \theta_{23} &= 49.0^{+1.1}_{-1.4} \quad \text{(stat.)} \ [\text{deg}] \\ \Delta m^2_{31} &= 2.514^{+0.028}_{-0.027} \ \text{(stat.)} \ [10^{-3}\text{eV}^2] \end{aligned}} \tag{S.2}$$

where the normal neutrino mass ordering is assumed.
Three observations from my ORCA-6 result can be made:

- The θ_{23} value is compatible with NuFIT within statistical errors.
- The Δm^2_{31} value is about 2.3σ (standard deviations) away from the NuFIT value. The result is preliminary as some aspects are still under investigation.
- The systematic uncertainties of ORCA-6 are smaller than the statistical uncertainties. Meaning that with current statistics the impact can be neglected, but with more statistics the systematics will need further investigation to constrain them.

Visualising the Observed Neutrino Oscillations

In figure S.5 the neutrino oscillation pattern is visualised for a simulation containing only muon-neutrinos (left) and the fitted model as well as the data in ORCA-6 (right).

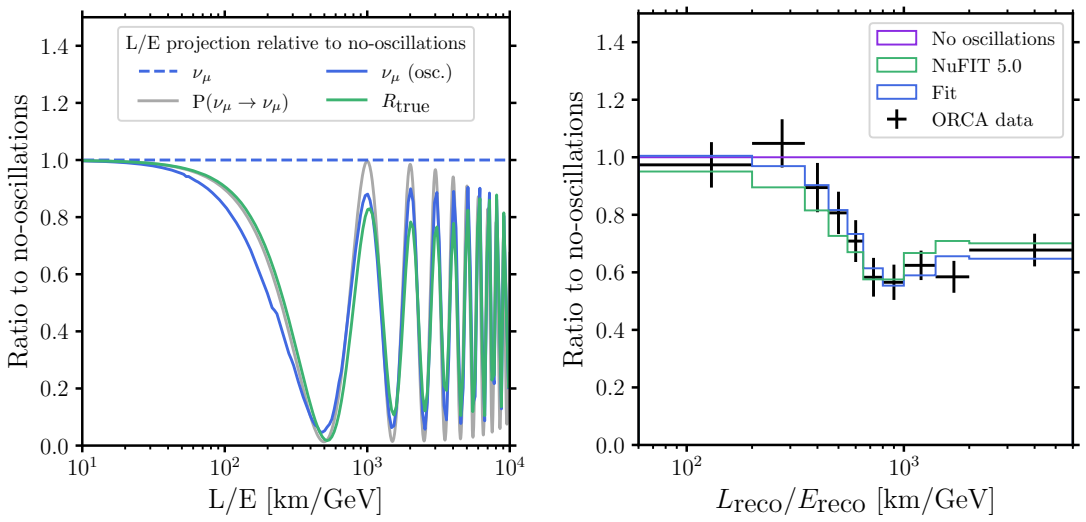

Figure S.5: Left: The (oscillated) atmospheric neutrino flux (blue), detection rate (green) and oscillation probability (grey) for the *muon-neutrino channel* as function of the neutrino energy, relative to the 'no oscillation' hypothesis. All channels depict information as it happens, not as it is measured by the detector. **Right**: Oscillation pattern as measured by ORCA-6, measured data (black) and the fit result (blue). The NuFIT (green) and no-oscillation (purple) curves without systematic effects are also shown.

The left part of figure S.5 shows the ratio for the expected neutrino oscillations compared to no oscillations of the neutrino flux, oscillation probability and detection rate in the detector. It is shown for a channel that contains only ν_μ induced events that create a track-like event.

The finite resolution of the detector is not included, and the resulting curves contain what is called *true information*: what actually happens in the detector volume. The effect of the neutrino oscillations in the oscillated ν_μ flux and the interaction rate R is clear. The shape of this oscillating pattern can be used to find the relevant oscillation parameters in real data.

On the right in figure S.5, the measurement with ORCA-6 is displayed. The measurement contains a mixture of all neutrino channels: we can not distinguish the different flavours that end up in the selected track events. The use of the track reconstruction introduces a bias towards selecting muon-neutrino induced events, because it is built to reconstruct muon tracks and the event selection uses this reconstruction information. For this reason the muon channel is shown on the left, as the analysis has a strong preference towards selecting muon-neutrino events. The first oscillation minimum can still be seen in real data, but due to the finite detector resolution all subsequent oscillations average out.

Although these neutrino oscillation patterns provide a good visual confirmation, statistical tests are used to determine how well we can see the oscillations quantitatively. The hypothesis that there are no neutrino oscillations can be rejected with a confidence level of 6.4σ. This 6.4σ can be interpreted as the chance of the measurement being a statistical fluctuation being 1 in 6.5 *billion*. We therefore conclude that **ORCA-6 has successfully measured neutrino oscillations**.

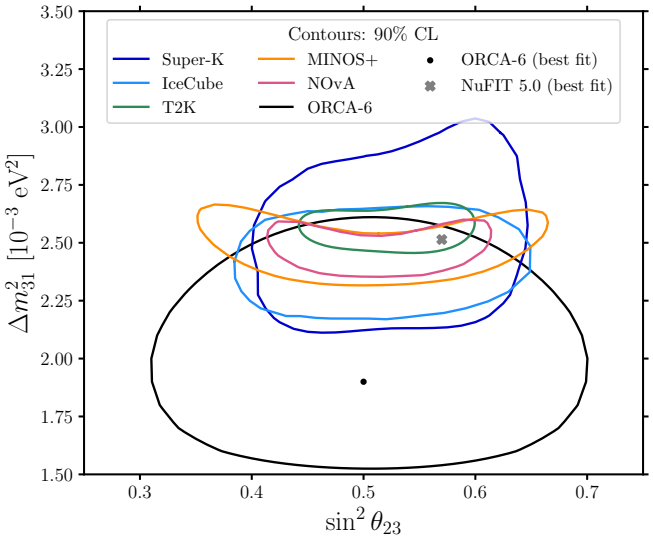

Figure S.6: The 90% confidence level contour of ORCA-6 compared to other experiments as a function of $\sin^2\theta_{23}$ and Δm^2_{31}. The 90% CL of other neutrino oscillation experiments as well as the NuFIT result are shown for comparison.

In figure S.6 the 90% confidence level (CL) contours are shown as a function of the measured oscillation parameters θ_{23} and Δm^2_{31}. These contours depict the part of the parameter space that we are 90% certain to contain the physics parameters based on the taken data.

It can be seen that the NuFIT best result is included in the ORCA-6 contour, meaning that the ORCA-6 results are compatible at 90% CL. Also the ORCA-6 contour is only slightly larger than other experiments. Keep in mind that this analysis uses 1 year of data with *only 6 DUs and only track reconstruction*, and conservative cuts to suppress as much of the the background as possible. Given all this and the resulting contour, the result is extremely promising and suggests that future ORCA results will be competitive with other experiments.